Investigation of ZnSe/ZnO Nanocomposite constructed as an electro-catalyst and photo-catalyst for Enhanced Supercapacitor and photo catalytic dye degradation application.

A thesis submitted towards partial fulfilment

of the requirements for the degree of

Master of Engineering / Technology in Nanoscience and Technology

Submitted by

SOUMILI KAR

ROLL NO.: M4NST24015

Under the guidance of

Dr. SOURAV SARKAR

School of Materials Science and Nanotechnology

Jadavpur University

Course affiliated to

Faculty of Interdisciplinary Studies, Law and Management

Jadavpur University

Kolkata, India

2024

M.Tech. (Nano Science and Technology)

course affiliated to

Faculty of Interdisciplinary Studies, Law and Management

Jadavpur University Kolkata, India

CERTIFICATE OF RECOMMENDATION

This is to certify that the thesis entitled "**Investigation of ZnSe/ZnO Nanocomposite constructed as an electro-catalyst and photo-catalyst for Enhanced Supercapacitor and photo catalytic dye degradation application.**" has been carried out under our guidance by Soumili Kar during the academic session 2023–24 in partial fulfilment of requirement for the award of degree of Master of Technology in Nano Science and Technology at School of Material Science and Nanotechnology, Jadavpur University, Kolkata- 700032. In our opinion the work fulfils the requirement for which it is submitted. It is further certified that the materials obtained from other sources have been acknowledged in the thesis.

THESIS ADVISOR

Dr. Sourav Sarkar

School of Materials Science and Nanotechnology

Jadavpur University, Kolkata-700 032.

DIRECTOR

School of Materials Science and Nanotechnology

Jadavpur University, Kolkata-700 032.

DEAN

Faculty Council of Interdisciplinary Studies, Law and Management

Jadavpur University, Kolkata-700 032.

M.Tech. (Nano Science and Technology)

course affiliated to

Faculty of Interdisciplinary Studies, Law and Management

Jadavpur University Kolkata, India

CERTIFICATE OF APPROVAL

The forgoing thesis is hereby approved as credible study of an engineering subject carried out and represented in a manner satisfactorily to warrant its acceptance as a prerequisite to the degree for which it has been submitted.

It is to be understood that by this approval the undersigned does not necessarily endorse or approve any statement made, opinion expressed or conclusion drawn therein but approved the thesis only for the purpose for which it has been submitted.

Final Examiners for Evaluation of thesis

Signature of the Examiners

1._____

2._____

3._____

Date _____

DECLARATION OF ORIGINALITY AND COMPLIANCE OF ACADEMIC ETHICS

I hereby declare that this thesis contains literature survey and original research work by the undersigned candidate, as part of his **Master of Technology (Nanoscience and Technology)** studies during academic session 2023-2024.

All information in this document has been obtained and presented in accordance with academic rules and ethical conduct. I also declare that, as required by this rules and conduct, I have fully cited and referred all material and results that are not original to this work.

NAME: SOUMILI KAR

ROLL NUMBER: M4NST24015

THESIS TITLE: Investigation of ZnSe/ZnO Nanocomposite constructed as an electro-catalyst and photo-catalyst for Enhanced Supercapacitor and photo catalytic dye degradation application.

DEDICATED TO MY BELOVED PARENTS FOR THEIR ENDLESS LOVE, SUPPORT AND ENCOURAGEMENT

Acknowledgement

The work described in this thesis entitled "**Investigation of ZnSe/ZnO Nanocomposite constructed as an electro-catalyst and photo-catalyst for Enhanced Supercapacitor and photo catalytic dye degradation application**". was started in the Thin Film & Nanoscience Laboratory, Jadavpur University in June 2022 and would not have been what it is today without the support and advice of others. First of all I would like to take this oppurtunity to sincerely express my earnest gratitude to my thesis advisor, **Dr. Sourav Sarkar** for giving me the opportunity to work under his esteemed guidance leading to thesis submission and motivating me thoroughly throughout my scientific and research endeavours. I am grateful to you for guiding me during the entire course of research work with your valuable suggestions. Thank you also for the amicable environment conducive to extensive research work at Thin Film and Nanoscience Lab, in which you have welcomed me.

I am also indebted to Dr. C.K. Ghosh, Dr. M.G. Chowdhury, and Prof. K.K Chattopadhyay for their valuable suggestions and constructive criticism during the course of my M. Tech program. Their enthusiasm provided me a helpful and effective way of learning which in turn inspired me to follow the research project with great vigour.

Finally, I owe my heartiest gratitude to Ankita Di, research fellow at Thin Film and Nanoscience Lab for providing me her immense support with rich scientific ideas and encouragement to work hard. All these provided me great support during my project, which I do not think I would have completed it otherwise.

Abstract

Energy crisis and depleting energy resources have triggered into plentiful efforts for the development alternative ways to cope up with the energy deficiency. Supercapacitor is one such energy storage device that plays an essential role in constant energy supply. Transitional metal selenides and their composites have undergone research in the recent times as potential candidates of supercapacitor devices due to their astounding physical, chemical and electrical properties. Selenium possesses an electronegativity lower than that of oxides and sulfur. This makes the chemical bond between the atom and the binding electrons weaker resulting in higher electrochemical activity that metal oxides or hydroxides. A ZnSe/ZnO composite has been synthesized by a facile hydrothermal method and investigated as a potential supercapacitor electrode in this work. The phase purity and morphology of the synthesized materials were examined through basic characterization techniques such as XRD, FESEM, FTIR etc. The composite material ZnSe/ZnO delivered high specific capacitance that is 155 at 0.3A/g in the charge-discharge profile and stable long cycle life retaining 95.5% over 3000 cycles. It also shows high specific capacitance that is 126.95 in 5mV/s. Moreover, the composite structure ZnSe/ZnO enhances electrochemical performance by offering additional electrolyte ions and electron mobility. Therefore ZnSe/ZnO composite can be utilized as a promising candidate for supercapacitor applications. The ZnO/ZnSe heterostructures showed significantly increased deep-level emission together with a comparatively decreased UV emission at ambient temperature. Furthermore, the heterostructure demonstrated impressive photo-catalytic abilities by degradation of organic azo dyes which are harmful for the environment and thereby helping in water purification.

CONTENTS

- Title Page
- Certificate by the Supervisors
- Certificate of Approval
- Declaration
- Acknowledgement
- Abstract

Chapter1 : Introduction to Nanotechnology 1-12

1.1. NanoScience & Technology 2

1.2. History..... 2-4

1.3. Synthesis……..…….……4-5

1.4. Applications..…….…...6-10

Reference

Chapter 2: Introduction to II-VI Semiconductor, Its Properties and Applications……17-47

2.1. II-VI Semiconductor 14

2.2. Crystal Structure…….....14-16

2.4. Chemical Bonding of II-VI Semiconductor……...16-17

2.5. Physical Properties of II-VI Semiconductor……..17-18

2.6. Size Effect on Semiconducting Property……..……..18-21

2.7. Synthesis Process…….……..21-23

2.8. Applications……...…24

2.8.1. Introduction to Supercapacitor…….……..……24-30

2.8.2. Introduction to Photocatalysis……...…….31-34

References…….……35-37

Chapter 3: Literature Review…….……...38-51

3.1. Introduction……...39-40

- ❖ Different properties of ZnO……....40-42
- ❖ Different phases of ZnO……..42-43
- ❖ Synthesis Methods of ZnO…….....44
- ❖ Different properties of ZnSe……45-47
- ❖ Synthesis Methods of ZnSe…….....47-48
- ❖ References……49-51

Chapter 4: Instruments and Apparatus……..…53-68

- Characterization techniques

4.1 Morphological Analysis

4.1.1 FESEM……..……..53-56

4.1.2 EDS/EDX……..……..56-57

4.1.3 HRTEM……..…….57-59

4.2 Crystal Structure Analysis:…….……..……..…59-62

4.3 Bond Structure Analysis

4.3.1 FTIR……62-64

4.4 Optical Property Analysis

4.4.1 UV-VIS near Infrared Spectroscopy…….……..64-67

4.5 Cyclic Voltammetry…….……67-68

Chapter 5:Synthesis, Characterization of ZnSe/ZnO Nanocomposite..70-79

5.1 Introduction…….……..70-71

5.2 Experimental Section

5.2.1 Synthesis……71-72

5.3 Characterizations

5.3.1 XRD (X-ray diffraction)……..……..73-74

5.3.2 FESEM analysis…….75-76

5.3.3 FTIR analysis…….77

References……..……..78-79

Chapter 6: Electrochemical Study of ZnSe/ZnO Nanocomposite…..…85-94

Details of 3-electrode setup…….…..81

- ❖ CV Performance of ZnSe, ZnSe/ZnO, ZnO coated Ni electrode……81
- ❖ Z350 electrode performance and different capacitance ……..…..82-83
- ❖ Z400 electrode performance and different capacitance……..…83-84
- ❖ Z450 electrode performance and different capacitance…….…..…85-87
- ❖ Charge Discharge Characteristics……..…87-91
- ❖ EIS……..…92-93

References……94

Chapter 7:Application of ZnSe/ZnO Nanocomposite In PhotoCatalysis….

……..…96-101

5.3.4 UV-VIS spectroscopy……..……..…96

- ➢ Photocatalytic Test……..96-97
- ➢ Bandgap Calculation of Z450, Z4255, Z400, Z375, Z350…….…..98
- ➢ UV light driven Photocatalysis……..99-100

References…….101

Chapter 8: Conclusion & Future Scope…….……102-104

8.1. Conclusion……..……103

8.2. Future Scope…….…….103-104

CHAPTER 1:

Introduction to Nanotechnology

1.1. Nano Science & Technology:

On 29th December of 1959, Nobel Laureate Richard P. Feynman presented a talk at the annual meeting of the American Physical Society at the California Institute of Technology which has converted one of the 20th century's classic science lectures, named "There's Plenty of Room at the Bottom". The personoffered a technological vision of extreme miniaturization several years before the word "chip" converted part of the lexicon. He told on the difficulties of monitoring and manipulating things on a small scale. Generalizing from known physical laws, a technology was envisioned by Feynmanto cover the extreme toolbox of nature which cancreatenano objects using molecule by molecule or atom by atom. The word "nanoscience" is themixture of nano, from the Latin "nanus"(Greek "Nanos"), the meaning of which is "Dwarf", and "Science" means knowledge.Up to 70-85 µm can be seen by persons stripped eyes, this is impossible to see anything in nano range without usingmicroscope. Nanotechnology is probable to have a profound impact on our society and economy in the early 21stcentury, similarly to that of information technology, semiconductor technology, molecular and cellular biology. Nanotechnology is described by a wide spectrum of different technologies that are based on various biological, physical, chemical processes on nano level.Nano Science and Technology has the potential to breakthroughs in this areas as materials, healthcare and medicine, biotechnology, nano electronics,information technology, energy and national security.

1.2. History:

- The Professor of 'Californian Institute of Technology' named Mr. R Feynman, gave a lecture on "There is a lot of space down there" in 1959.
- Arthur and Cho. devoted Molecular Beam Epitaxy in 1968.
- In 1974 the word "nanotechnology" was presented for the first time into a scientific world by N. Taniguchi in an international conference on industrial production in Tokyo University for describing the super thin processing of materials with nano meter accuracy and also the creation of nano sized mechanism.
- Rohrer and Binnig established Scanning Tunnelling Microscope (STM) in 1981.
- In 1985, fullerenes and C60 were established by Harry Kroto, Robert Curl and Richard Smalley.

- The first page of Charles Dickens's novel "A tale of Two Cities" was written by Top Newman with a reduction factor of 25000 using Electron Beam Lithography(EBL) in 1985.
- Atomic Force Microscopy(AFM) was developed by Binning and Co-workers in 1986.
- Magnetic Force Microscopy was discovered by Wickramasinghe and Martin in 1987.
- From the second half of 80's to the early 90's a number of important discoveries and inventions were completed, which created annecessary impact on the further development of nanotechnology.
- In 1988, the ideas of nanotechnology were developed by E. Drexler in his book named "Vehicles of Creation: the arrival of nanotechnology era".
- In 1990, E.K Schweizerused and D.M Eigler an STM to exhibit atomic scale positioning of separate Xenon atoms on a Nickel surface at the low temperature(4K) forwriting IBM.
- Sumio Ijima discovered CNT(Carbon Nanotube) in 1991.
- The first nanotechnological program of "National Scientific Fund" was started in USA in 1991.
- Single walled carbon nanotubes were grown by Ichihashi and Ijima in 1993.
- In 1996,Gimzewski,Cuberes, and Schilitter established room temperature locating of individual C60 fullerenes with an STM to produce the "C60 abacus".
- Anusree Roy and Umar Mohideen restrained the Casimirforce using AFM at distances scales down to 90 nm.
- Steve Lamoreaux measured the Casimirforce at submicron distances in 1997.
- Presidential Council on Science and Technology (PCAST) supported IWGN conclusions and recommendations in 1999.
- A special department on nanotechnology under the auspices of the Industrial and Technical Committee was organised by the Japanese Economic Association in 2000.
- In 2001, the National Nano technological Initiative of the USA was accepted. The principal idea of the program: NNI defined the strategy of interaction between federal departments of the USA for the determination of prioritizing nanotechnology development, which should provide a basis for the economy and national security of the USA in the first half of the 21st century.
- The framework plan of nanotechnology research was developed in 2001.
- In 2001, Postma and co-workers established single electron transistor operation using Carbon Nano Tube.

- In 2002, Brusentov and co-workers accomplished regression of tumour in mouseusing magnetic nanoparticle thermia.
- The first human clinical trials of magnetic nanoparticle hyperthermia as a cancer treatment were conducted in 2007 by Johanseen and his colleagues.
- In England, The Council of Physics & Technology and National Physics Laboratory controlled the development of nanotechnology.
- In Germany, research in nanotechnology was sustained by Ministry of Science, Education, Research and Technology.

Thus the nanotechnology paradigm was made at the turns of 1960's, while the 1980's and 1990's were the start togrow of nanotechnology in its own right.

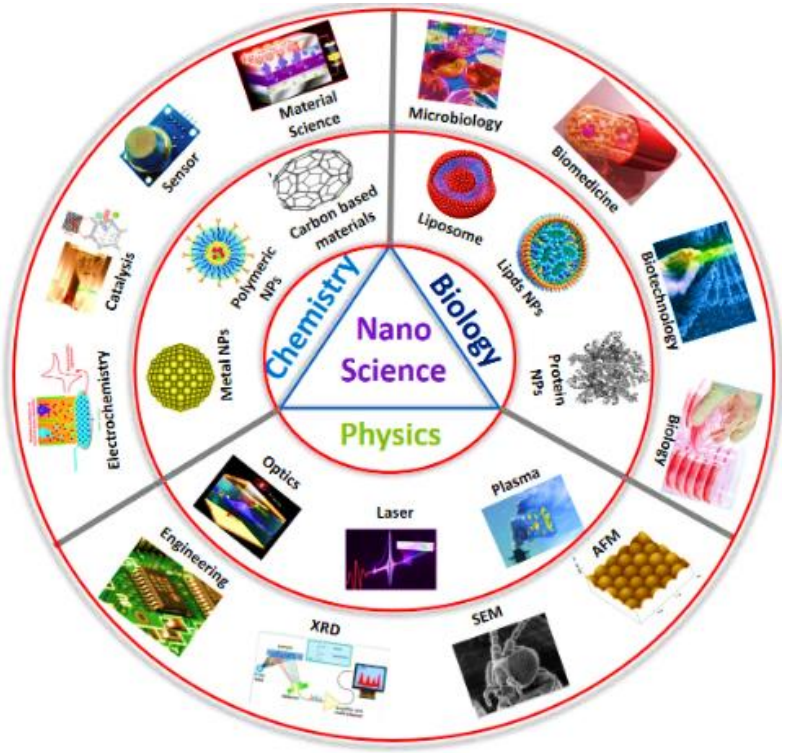


Figure 1.1 Materials in Nanoscale

1.3 Synthesis of nanomaterials

There are various ways to manipulate matter on the nanoscale. The two most are bottom-up and top-down methods.

According to the bottom-up method, structures are created molecule by molecule or atom by molecule via supramolecular or covalent interactions, much like bricks are put together to

build a house. Conversely, the top-down approach centers on achieving the necessary tiny structural designs by the etching away of bulk materials, often through lithographic processes. This procedure might be likened to shaping a stone block into the desired shape. Both strategies play a major role in contemporary industry and perhaps in nanotechnology as well. These approaches both have benefits and drawbacks. A common top-down technique in the synthesis of nanoparticles is milling or attrition; in contrast, a good example of a bottom-up approach is colloidal dispersion [20].

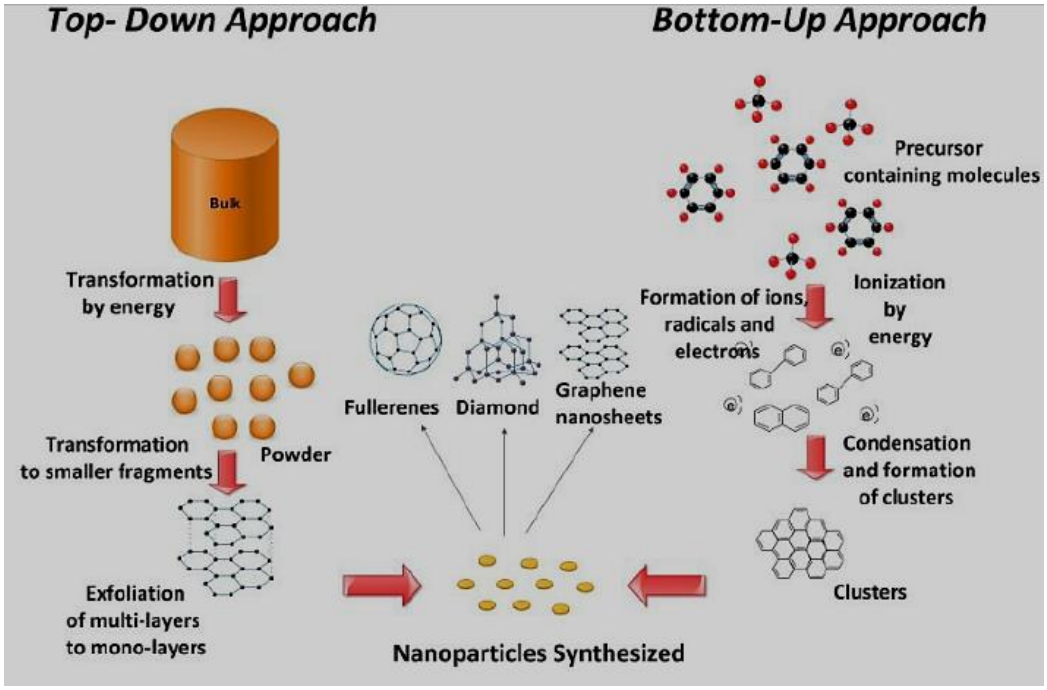


Figure1. 2 Top-Down and Bottom Up Approach

Self-assembly:

Natural systems frequently engage in self-organizing processes, which can range from molecular (like protein folding) to even more distant (like galaxies) and planetary size (like weather systems). Designing the components necessary for self-assembly into desired patterns and functionalities is the key to using self-assembly as a direct and controlled production method. Self-assembly is a reflection of information encoded in certain components, such as shape, charge, magnetic dipole, surface features, polarizability, etc. These attributes dictate the interactions between the components.

1.4. Application:

Nano systems are estimated to discoverseveral unique applications. Nanostructured materials are formed with unique nanostructures and properties. This field is expected to open new areas in science and technology. Due to the permitting nature of the systems, and because of these significant influence they can have on the viable and defencepresentations, venture capitalists, industry, as well as the federal government hasoccupied a special interest in nurturing growth in this field. Nano and microsystems arereasonable step in “silicon revolution.”

When a particle is contracted to nano scale, various properties of the material convertedaccording to size. That’s why it provides new presentations in several fields. As the surface to volume ratio increases due to the size, it creates large surface area for reacting. Several mechanical and optical properties are also dependent on the diameter of the particlesize.

1.4.1. In Medical Science:

It has several applications in nano biotechnology, biomedical nanotechnology and nano medicine. The size of the nanomaterial is close to that of most biological molecules and structures, so nanomaterial can be valuable in vitro and vivo medical research and applications. The combination of nanotechnology with biology has caused in growth of diagnostic devices, analytical tools, contrast agents, physical therapy applications and drug delivery cars [21-23].

1.4.1.1.Tissue Engineering:

Nanotechnology helps for duplicating and healing damaged cell. “Tissue engineering” can procedure artificially enthused cell production by using appropriate nano material-based skeletons and growth factors. For example, bones can be grown insincerely on CNT skeletons. Tissue engineering might swap today’s conventional treatments like artificial implants or organ transplants.

1.4.1.2. Diagnostic:

Nanotechnology-on-a-chip provides one more measurement of lab-on-a-chip technology. Multi color optical coding for biological analyses has been attained by implanting different-sized quantum dots into polymeric microbeads. Gold nanoparticles, marked with short sections of DNA, can be used to detect of genetic sequence in biological samples. Nanopore technology renovates strings of nucleotides straightly into electronic signatures for analysis of nucleic acids.

1.4.1.3.Drug Delivery:

Nanotechnology has been a new way for the medical area to deliver drugs to desired cells consuming nanoparticles. An example of drug delivery can be found in nano porous materials and other example is to use block co-polymers which create micelles for drug encapsulations. They can grip small drug molecules totransport them to the preferred location.

1.4.2. Information and Communication:

The critical length scale of integrated circuits is already within 50 nm and below regarding the gate length of transistors of CPU and memory device.

1.4.2.1. Novel Semiconductor Device:

In 1999, the eventual CMOS device was established in the laboratory of Electronics and Information Technology in Grenoble of France. The limits principles of MOSFET transistor (with diameter of 18 nm) was tested by them, that means approximately 70 atoms are placed side by side. This was almost one tenth size of the smallest industrial transistor.

1.4.2.2. Display Technology:

In display system the low energy consumption can be accomplished by using CNT. It is conductive and they can be used as field emitters due to their small diameter. For this reason it is used in Field Emitter Display. The working principle is equivalent to CRT display but it is in a small length scale.

1.4.2.3. Memory Storage:

Electronic memory design is dependent on transistors. Still, crossbar switch dependent electronics has offered a different using reconfigurable between horizontal and vertical wiring arrays for creating ultra-high density memory.

1.4.2.4.Quantum Computers:

It is a new method in the industry of computer. It has quantum bit memory, called qubit for some computations at the same time. It progresses the facility of the older system.

1.4.3. Environment applications:

1.4.3.1.Energy:

The most advanced nanotechnology correlated works are on conversion, storage, energy saving, manufacturing improvements, process rate and enhancement of renewable energy sources. Solar cells have layers of numerous semiconductors arranged to absorb light at different energies but they can manage only 50 % of solar energy. Nanotechnology can rise the energy proficiency of light conversion by using nano structured material with a continuum of band-gap.

1.4.3.2.Filtration:

A strong inspiration of photochemistry on air purification, waste-water treatment is there. One class of filtration methods is the use of membranes with appropriate holes, whereby the liquid is forced through the membrane. Nanoporous membranes are appropriate for mechanical filtration with pores which are smaller than 10 nm. Magnetic nanoparticles also propose an operative and reliable technique for removing heavy metal pollutants from waste water by using magnetic separation techniques.

1.4.4. Heavy Industries:

1.4.4.1. Catalysis:

Chemical catalysis has an opposite impact in the nano range due to its high surface to volume ratio. This catalyst is used in photocatalytic devices, fuel cells, and catalytic converters. An essential step in the production of chemicals is catalysis. The catalyst is used in photocatalytic devices, fuel cells, and catalytic converters. Although it is not appropriate to include toxicity in this research, nano filtration is a significant presentation in this subject.

1.4.4.2. Aerospace:

Stronger and lighter materials are used in aircraft manufacturing. Spacecraft will be helpful, where weight is themain factor. Nanotechnology helps to decrease the size of equipment and reduces fuel consumption which isessential to get it airborne.

1.4.4.3.Construction:

Nanotechnology has potential to construct cheaper, faster, and safer construction materials. Nanotechnology has an adversarial effect in the field of glass, coatings, steel, fire protection and detection, vehicle manufacturing etc.

1.4.5. Consumer Goods:

Nanotechnology has a great impact in the field of consumer goods from easy to clean to scratch resistant surfaces. Clothes have converted smart and entrenched with wearable electronics. Modern textiles are strain repellent and wrinkle resistant. In the field of cosmetics also, nanotechnology has a vast effect.

1.4.5.1.Household application:

Self-cleaning is the most effective application of nanotechnology in the household.

1.4.5.2. Textiles:

The combination of contrived nano fiber in clothes creates the clothes wrinkle free, water and strain repellent. Nano technological finished textiles can be washed less frequently at lower temperatures.

1.4.5.3. Agriculture:

Applications of nanotechnology can change the entire agriculture sector and food industry from production to conservation, processing, packaging, transportation, and even waste treatment.

1.4.5.4. Foods:

Some examples of nanotechnology in this field are bacteria identification and food quality nursing using intelligent, biosensors, smart and advance food packaging systems. Nano composite coating progresses the food packaging by placing anti-microbial agent openly on the surface of coating. They can recover the mechanical and heat resistant property and lower the O_2 transmission rate.

References

1. Klabunde, Kenneth J. "*Introduction to nanotechnology." Nanoscale Materials in Chemistry* (2001): 1-13
2. Romig, Alton D., et al. "An introduction to nanotechnology policy: Opportunities and constraints for emerging and established economies." *Technological Forecasting and Social Change* 74.9 (2007): 1634-1642.
3. Chan, Chih-Chieh, et al. "Efficient and stable photocatalytic hydrogen production from water splitting over Zn x Cd 1–x S solid solutions under visible light irradiation." *International Journal of Hydrogen Energy* 39.4 (2014): 1630-1639.
4. Asiyanbola, Bolanle, and Winston Soboyejo. "For the surgeon: an introduction to nanotechnology." *Journal of surgical education* 65.2 (2008): 155-161.
5. Poel, I. "The introduction of nanotechnology as a societal experiment." *Technoscience in progress. Managing the uncertainty of nanotechnology* (2009):129.
6. Jeon, H., et al. "Low threshold pulsed and continuous-wave laser action in optically pumped (Zn, Cd) Se/ZnSe multiple quantum well lasers in the blue-green." *Applied physics letters* 59.11 (1991): 1293-1295.
7. Chelikowsky, James R., and Mark A. Ratner. "Guest Editors' Introduction: Nanoscience, Nanotechnology, and Modeling." *Computing in Science & Engineering*3.4 (2001): 40-41.
8. Owens, Frank J., and C. P. Poole. "*Introduction to nanotechnology*." (2003).
9. Cuixing, Meng. "APPLICATION OF NANOTECHNOLOGY IN MODIFICATION OF POLYMER [J]." *New Chemical Materials* 2 (2001): 000.
10. Evans, Philip, Hiroshi Matsunaga, and Makoto Kiguchi. "Large-scale application of nanotechnology for wood protection." *Nature nanotechnology* 3.10 (2008): 577-577.
11. Postek, Michael T., and Andras E. Vladár. "Helium ion microscopy and its application to nanotechnology and nanometrology." *Scanning* 30.6 (2008): 457-462.
12. Hu, A. W., and Z. H. Fu. "Nanotechnology and its application in packaging and packaging machinery." *Packaging Engineering* 24 (2003): 22-24.
13. Sahaym, Uttara, and M. Grant Norton. "Advances in the application of nanotechnology in enabling a 'hydrogen economy'." *Journal of Materials Science*43.16 (2008): 5395-5429.
14. Seeman, Nadrian C. "DNA engineering and its application to nanotechnology." *Trends in biotechnology* 17.11 (1999): 437-443.

15. Cai, Weibo, et al. "Applications of gold nanoparticles in cancer nanotechnology." *Nanotechnology, science and applications* 2008.1 (2008).
16. Wang, Shu, et al. "Application of nanotechnology in improving bioavailability and bioactivity of diet-derived phytochemicals." *The Journal of nutritional biochemistry* 25.4 (2014): 363-376.
17. Hickernell, Fred S. "The piezoelectric semiconductor and acousto-electronic device development in the sixties." *Frequency Control Symposium and PDA Exhibition Jointly with the 17th European Frequency and Time Forum, 2003. Proceedings of the 2003 IEEE International*. IEEE, 2003.
18. Singhal, Sunil, Shuming Nie, and May D. Wang. "Nanotechnology applications in surgical oncology." *Annual review of medicine* 61 (2010): 359.
19. Zhu, W., P. J. M. Bartos, and A. Porro. "Application of nanotechnology in construction." *Materials and Structures* 37.9 (2004): 649-658.
20. Parvez Iqbal, Jon A. Preece, and Paula M. Mendes, Nanotechnology: ―The Top-Down and Bottom-Up Approaches‖, Supramolecular Chemistry: From Molecules to Nanomaterials, 2012.
21. Frietas RA Jr, "Current status of nanomedicine and medical nanorobotics". J Comut Ther Nanosci.(2005);2:1–25.
22. Boisseau P, Loubaton B "Nanomedicine, nanotechnology in medicine". ComptesRendus Physique 12 (2011): 620-63
23. Minchin R "Nanomedicine: Sizing Up Targets With Nanoparticles". Nat Nanotechnoly 3(2008): 12-13.
24. Nassar, Nashaat N., Azfar Hassan, and Pedro Pereira-Almao. "Application of nanotechnology for heavy oil upgrading: Catalytic steam gasification/cracking of asphaltenes." Energy & Fuels 25.4 (2011): 1566-1570.

CHAPTER 2:

Introduction to II-VI Semiconductors Its Properties & Applications

2.1 II-VI Semiconductor:

II-VI semiconductors (like Cadmium Chalcogenides: CdS, CdSe, CdTe and Zinc Chalcogenides: ZnTe, ZnS, ZnO, ZnSe, etc) are the class of materials which are considered widely in the field of catalysis and optoelectronics etc. Due to their quantum efficiency and high sensitivity they are accepted as optoelectronic devices. II-VI compounds were the first to be considered and used as phosphors for the applications on Cathode-Ray Tubes (CRT) displays. The range of wide bandgap is 3.9eV – 2.4 eV which gives theopportunity to work on various wave lengths in optoelectronics application. At ambient temperature, ZnO has a substantial exaction binding energy of 60 meV and a direct band gap of 3.37 eV, making it a substantial semiconductor in the II–VI group [1], which is appropriate for a variety of applications related to photocatalysis, supercapacitors, photoelectronic, photovoltaic, photosensors and others. A heterostructured semiconductor has synergistic effects, such as improved light garnering, improved the photostability, efficient charge separation, and has accelerated electron–hole transfer through heterojunction, which renders it beneficial to improved photocatalytic performance equated to a single phase semiconductor [2–5]. Since zinc selenide (ZnSe) and zinc oxide (ZnO) are well matched and have a band gap of 2.67 eV, so Zinc Selenide is the perfect material to employ to generate ZnO-based heterostructures. Additionally, ZnSe exhibits environmentally beneficial qualities [6–9].

2.2. Crystal Structure:

Group II-VI compounds are made up of a comparable number of atoms from each of the elements in the VI column and the element from the periodic table's II b column. The crystallisation of almost all group II–VI compounds places one fundamental atom in the centre of a regular tetrahedron with atoms of additional elements covering its edges.

(a) The sphalerite (cubic) type

(b) The wurtzite (hexagonal) type.11

2.2.1. The sphalerite type:

Zinc-sphalerite (ZnSe) crystallises in the cubic F∨43m space group and has a zinc-blende structure. Zn^{2+} forms corner-sharing $ZnSe_4$ tetrahedra when it is linked to four comparable Se^{2-} atoms. Every Zn-Se bond has a length of 2.45 Å. Corner-sharing $SeZn_4$ tetrahedra are formed when four equivalent Zn^{2+} atoms are connected by Se^{2-}.

Zinc oxide (ZnO) is a zinc-lead sphalerite crystal with a cubic F∨43m space group structure. Corner-sharing ZnO_4 tetrahedra are formed when Zn^{2+} is coupled to four identical O^{2-} atoms.

2.2.2. The wurtzite type:

ZnSe crystallises in the hexagonal $P6_3mc$ space group and has a Wurtzite geometry. Zn^{2+} forms corner-sharing $ZnSe_4$ tetrahedra when it is linked to four comparable Se^{2-} atoms. Zn-Se bond lengths come in three shorter (0.245nm) and one longer (0.246nm) varieties.

ZnO crystallises in the hexagonal $P6_3mc$ space group and has a Wurtzite structure. Corner-sharing ZnO_4 tetrahedra are formed when Zn^{2+} is attached to four comparable O^{2-} atoms. Zn-O bond lengths come in three shorter (0.197nm) and one longer (0.198nm) varieties.

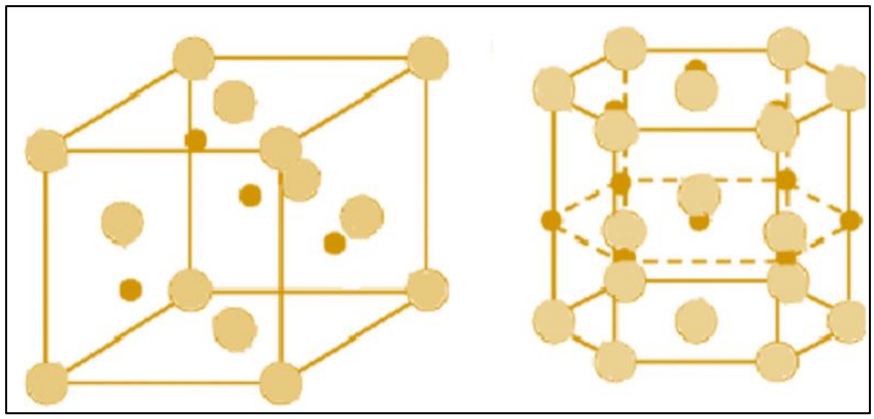


Figure 2.1 i. Sphalerite ZnSe Structure ii. Wurtzite ZnSe Structure

❖ **Lattice (Conventional)**

a	0.56 nm
b	0.56 nm
c	0.56 nm
α	90 º
β	90 º
ɣ	90 º

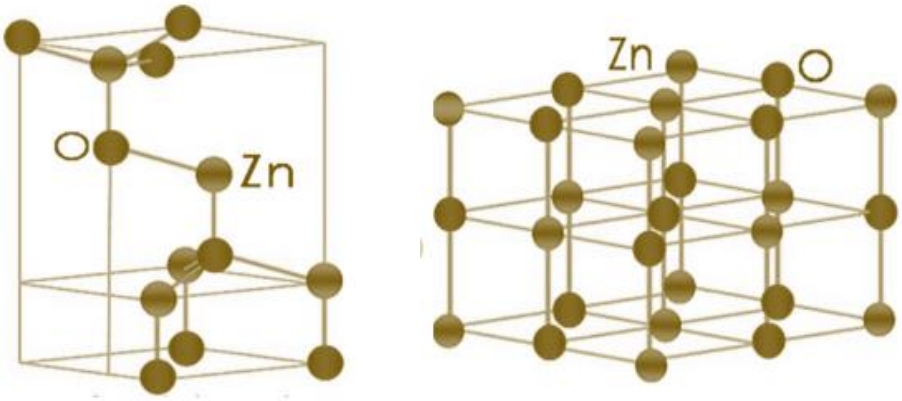


Figure 2.2 i. Sphalerite ZnO Structure ii. Wurtzite ZnO Structure 12

❖ Lattice (Conventional)

a	0.456 nm
b	0.456 nm
c	0.456 nm
α	90 º
β	90 º
ɣ	90 º

2.3. Chemical Bonding II-VI Semiconductor:

Group II atoms contain two electrons in the outermost shell (s^2), while oxygen subgroup atoms have six electrons in their s and p shells (s^2p^4). An octahedral coordination structure (of the NaCl type) and positively charged ions with a filled p shell are generated when metal atoms possess strong enough electropositive characteristics to give up two outer shell electrons to non-metal atoms. Two electron clouds move from group II elements to group VI elements because group VI elements have more electro negativity than group II elements. As a result, the II-VI compounds display characteristics similar to both forms of binding, and their binding is partially covalent and partially ionic.

With high melting temperatures, nearly all zinc compounds are wide band-gap semiconductors. High temperatures are necessary for the development of these chemicals. These substances are exclusively available in sphalerite or wurtzite formations.

2.4. Physical Properties of II-VI semiconductor:

Six binary substances that have potential as semiconductors are produced by combining zinc from group II-A with sulphur and oxygen from group VI-A of the periodic table. Electrical characteristics, thermal conductivity, Debye temperature, density, flexibility, magnetic susceptibility, optical value of the prohibited bandwidth, etc. are some of the compounds' primary physical characteristics. Some important physical properties of group II-VI compounds are arranged in table. The values of elastic constants and optical properties have been defined by Berlincourt et al. and Moss.

Material	**ZnSe**	**ZnO**
Refractive Index(ZB/WZ)	2.61(550nm	2.0
Dielectric Constant ($\varepsilon_0/\varepsilon_a$)	8.6	9.34
Exciton Binding Energy(meV)	60	68.3
Band Gap(eV) (ZB / WZ)	2.7	3.37
Melting point(K)	1798.15	2248.15
Bond length (um)	0.000245	0.000189
Lattice Constant (ZB) (nm)	0.5668	0.325

Electron effective mass(m*/ m0)	0.613	0.215
Young's modulus	67.2 GPa	140 GPa
Thermal Conductivity (W m^{-1} K^{-1})	18 W m^{-1} K^{-1} at 298K	4.5 W m^{-1} K^{-1} at 300 K
Thermal Conductivity (W m^{-1} K^{-1})	18 W m^{-1} K^{-1} at 298K	4.5 W m^{-1} K^{-1} at 300 K

2.5. Size effect on semiconducting material:

2.5.1. Melting Point:

The temperature at which a substance transitions from a solid to a liquid is known as its melting point. It is the energy required to separate atoms sufficiently to change their state from solid to liquid. Cohesive energy (Ec) and melting point temperature are intimately correlated. The quantity of surface atoms rises as the material shrinks from bulk to nanoscale. There are less nearby atoms for surface atoms. Therefore, less energy is needed to dissolve this bond. As Cohesive energy falls, the temperature at which the melting point occurs also drops.

$$\frac{T_{mp,nano}}{T_{mp,bulk}} \propto \frac{1}{R}$$

2.5.2. Bandgap (Eg):

The single energy level of every atom gets divided into an energy band made up of extremely closely spaced levels of slightly different energies when a large number of atoms are brought close together to create a solid. Quantum theory has demonstrated that the energy of a bonded electron in an atom is quantized, meaning that the electrons can only take on discrete energy

values. The likelihood of detecting an electron at a specific distance from the nucleus is represented by a probability density function, from which the position of the electron is derived. Pauli's exclusion principle states that when two atoms are brought closer together, their wave functions overlap and the discrete single energy level in the overlapping region splits into two levels due to the interacting potential, allowing each electron to occupy a different quantum state. The word "valance band" refers to the energy band that contains an atom's outermost electrons, or valance electrons. It is the band that is most occupied. Electrons can either entirely or partially fill it. The conduction band is the next permitted the band higher. Electrons can flow freely in this area. The term "bandgap" refers to the prohibited space where no electrons exist between the valance band and conduction band.

The energy gap in a semiconductor is quite small, measuring about 1 eV between the full and empty bands. There are gaps in the higher valance band caused by electrons jumping from states in the upper valance band to the lower conduction band. Thus, when an electric field is applied, a finite number of electrons are available at the conduction band for conduction. Because there are fewer free electrons and holes in the energy bands than there are in metals, the electrical conductivity is therefore substantially lower. This conductivity is a function of bandgap and temperature. Since resistance decreases with temperature, the semiconductor has a negative temperature coefficient of resistance.

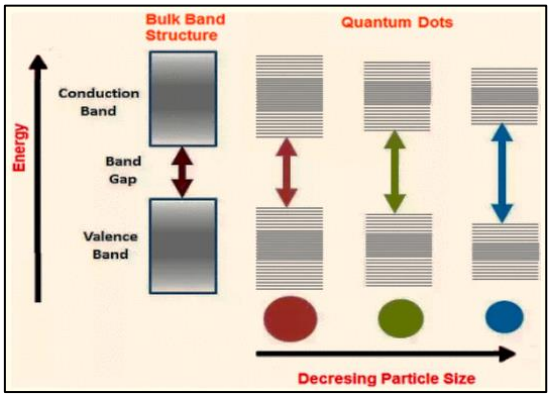


Figure 2.3 Band gap Variation with Size

An electron must have energy equal to or more than the bandgap energy that causes the valance band hole to open up in order to leap from the bandgap to the conduction band. The electron moves from a higher VB to a lower CB when a photon's energy exceeds the bandgap, and the extra energy is dissipated in inelastic collisions. Through the process of electron hole recombination, which releases a photon with energy equal to the bandgap or the reduction of particle size from bulk to nano, the electron returns to the valance band. This

allows the energy levels to gradually broaden and become more distinct. The lowest unoccupied molecular orbital (LUMO), which is at the bottom of the conduction band, and the highest occupied molecular orbital (HOMO), which is at the top of the valance band. The bandgap widens when the material's size decreases. Due to the limited space available to electrons, holes, and excitons in structures resembling nanocrystals, only specific energy bands can be moved. As a result, the valance band and conduction band continuum of states is divided into discrete energy states with gapping that is inversely proportional to the crystalline radius. Thus, there is a blue shift in optical absorption.

$$E_g \propto 1/L^2$$

2.5.2.1. Effect of doping:

When metallic impurities are inserted inside particles, the energy band diagram's new energy level is created, changing the particle's conductivity in line with it. Both n-type and p-type doping produce new levels of acceptor and donor, respectively, just above and below the valance band and below the conduction band. Therefore, the addition of dopant also causes a change in the bandgap can be seen here.

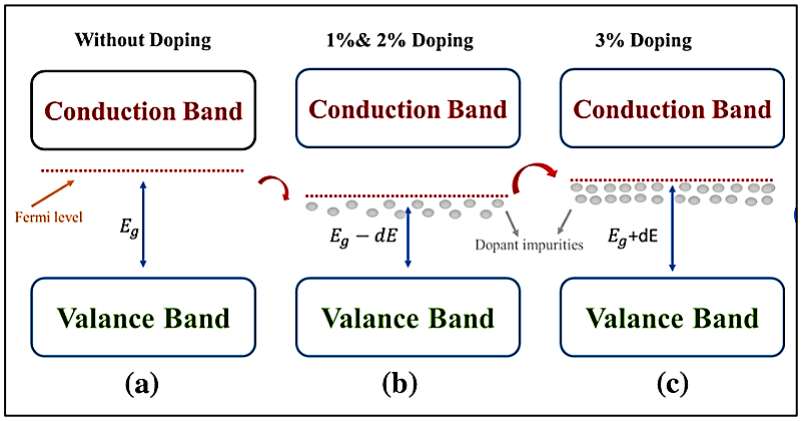


Figure 2.4 Effect of Doping in Bandgap

2.5.3. Specific heat:

The quantity of heat needed per unit mass to raise the temperature by one degree Celsius is known as specific heat. It is preferable for the temperature to stay constant while energy levels rise. Thus, the focus is on specific heat, or the transition from bulk to nanoscale range.

$$C_V \propto Q/\Delta\Theta$$

Where, Q= thermal energy, $\Delta\Theta$=Change in temperature.

Delocalized electrons and localised nuclei absorb external energy, or heat. Localised nucleus vibrates with energy around its equilibrium point, whereas delocalized electrons absorb and increase kinetic energy.

When there is atomic vibration, it is simple to ascertain the location of the atom for macroscopic particles with arbitrary precision. However, for minuscule particles, the likelihood of discovering the particle determines its position. As ω is the frequency of atomic vibration, then it's inversely proportional to the size of the particle and C_V is directly proportional to the fourth power of frequency of atomic vibration i.e.

$$C_V \propto 1/d^4$$

Where, d is the size of particle.

A particle's surface area and atomic count both rise when its size is reduced to the nanoscale. Because surface atoms may absorb more energy, the specific heat increases.

2.5.4. Work Function:

The variation in energy between the vacuum and Fermi levels is known as the work function. The energy level of an electron when it is completely free, that is, when it is outside the metal surface, is measured by the vacuum level. Because the doping concentration can alter the location of the Fermi energy level, the work function for a particular material is not constant. The difference between the discrete energy levels for nanoparticles increases as

$$E_n \sim E_{n+1} \propto 1/L^2$$

If the particle size decreases from bulk to nano range then the Fermi energy level rises and becomes closer to the reference energy level.

2.6. Synthesis Process:

2.6.1. Solvothermal process:

A technique for creating a range of materials, including metals, semiconductors, ceramics, and polymers, is called solvothermal synthesis. In order to promote precursor contact during synthesis, a solvent operating at moderate to high pressure (1 atm to 10,000 atm) and temperature (100 °C to 1000 °C) is used in the process. The process is known as "hydrothermal synthesis" if water is utilised as the solvent. Under hydrothermal conditions,

synthesis is typically carried out below the water's supercritical temperature of 374 °C. Thin films, single crystals, bulk powders, and nanocrystals can all be produced using this method. Chemical concentration, kinetic control, and solvent super saturation can all be adjusted to modify the crystals' shape. The process can be used to create novel materials that are difficult to generate through existing synthetic pathways, as well as thermodynamically stable and metastable states. Kinetic control over the phases is an advantage of the solvothermal process, but an initial prediction of the material is a drawback. Solvothermal processes are any heterogeneous chemical reactions that occur in a closed system, with a solvent present, and at a temperature higher than the solvent's boiling point. This is a pressure and mineralizer that I made on my own. The element known as the mineralizer forms compounds with the reactants to aid in their dissolution. In this case, the solvent is heated in a sealed vessel to a pressure that is significantly higher than the surrounding air. This instantly causes the solvent's effective boiling point to rise. In fact, this method is widely employed to prepare inorganic solids, especially zeolite compounds.

2.6.2. Historical Development:

1845: K.E. von Schafhäutl formed quartz crystals with the use of Papin's digestor.

1848: R. Bunsen formed Sr, Ba carbonates in thick-walled glass tubes.

1851: Glass tubes were employed in autoclaves by H. de Sérnamont to create quartz, carbonates, steel tubes, sulphates, and sulphides. In the geosciences, he is credited with founding hydrothermal fluoride synthesis.

1873: Au lining was employed by K. von Chrustschoff to stop corrosion.

1890: Doetler found a Cu washer for mineral recrystallization and an Ag-lined steel tube mineral that was sealed with a screw cap.

1892: Industrial hydrothermal bauxite leaching with sodium hydroxide at 170-180°C is credited to C.J. Bayer.

1914: The conventional Morey-type autoclave was discovered by G.W. Morey.

1948: Zeolites were first synthesised by R.M. Barrer.

1949: Tuttle invented cold seal and test tube autoclaves.

1950-1960: Analysis is done on phase diagrams for natural systems.

1960-1980: Technological material synthesis: the creation of novel inorganic substances lacking natural counterparts or synthesised prior to discovery.

1980-1990: The method is important for studying the physical chemistry of hydrothermal solutions in materials science.

1985: Hydrothermal synthesis was characterised by Rabenau as heterogeneous processes in aqueous mediums over 100°C and 1 bar. In his research paper, Lobachev described it as a class of techniques where high pressure crystallisation is achieved from superheated aqueous solutions. According to Roy et al., water is used as a catalyst and occasionally as a component of solid phases in hydrothermal synthesis, which occurs at high temperatures (>100°C) and pressures (>a few atmospheres).

1992: Any heterogeneous reaction in an aqueous medium that is conducted at room temperature and at a pressure greater than 1 atm is referred to as hydrothermal synthesis by Byrappa. "...reactions occurring under the conditions of hightemperature high-pressure (>100°C, >1 atm) in aqueous solutions in a closed system," according to Yoshimura's definition.

2001: K. Byrappa defined a hydrothermal reaction as "any heterogeneous chemical reaction in the presence of a solvent (whether aqueous or non-aqueous) above room temperature and at pressure greater than 1 atm in a closed system" in the "Handbook of Hydrothermal Technology."

2.6.3. Autoclave:

Autoclaves are employed as reaction vessels in hydrothermal procedures to hold extremely corrosive solvents at high temperatures and pressures for extended periods of time. Teflon, a non-reactive material, is used in the construction of most autoclaves because it has a higher coefficient of thermal expansion than metal, the material that encloses the liner. This means that Teflon will expand and contract significantly more during heating and cooling cycles than the enclosure material.

Parameters for choosing autoclave -

- It must withstand high temperatures and pressures for an extended period of time.
- It has the ability to change inert into bases, acids, and oxidising agents.
- Its capacity should be adequate to achieve the required temperature differential.
- At the appropriate pressure and temperature, it ought to be leak-proof.

2.7. Applications:

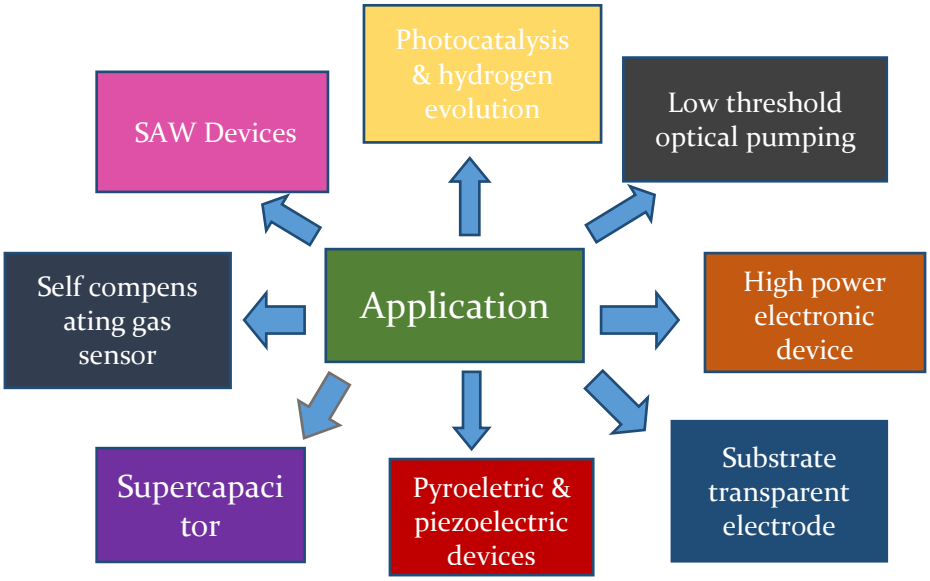


Figure 2.5 Applications of II-VI semiconductors in various domains

2.7.1. Supercapacitor:

2.7.1.1. Introduction to Supercapacitor:

The major international powers and the scientific community have turned their attention primarily to energy as a result of the shifting global environment. The creation and improvement of more effective energy storage technologies has attracted a lot of interest. Supercapacitors are one such gadget that has developed dramatically over the past 10 years and has the potential to enable substantial advancements in energy storage.

Supercapacitors, often referred to as ultracapacitors or electrochemical capacitors, are capacitors with capacitances many orders of magnitude greater than regular capacitors. They achieve this by using thin electrolytic dielectrics and high surface area electrode materials [15-19]. By doing this, supercapacitors are able to achieve higher energy densities without sacrificing the high power density that distinguishes traditional capacitors.

Energy density and power density are crucial metrics for describing the operational characteristics of energy storage systems. The quantity of energy that a substance can hold in a specific volume of weight is known as its energy density. The total energy that may be stored in a device per unit of time is known as its power density. Thus, both a high energy density and a high power density are desirable in a storage device. Batteries have a low power

density but a high energy density. The lowest power consumption and highest energy efficiency are found in fuel cells. Supercapacitors, in comparison, have the ability to have a high power density and a notably higher energy density. Other names for supercapacitors include electric double-layer capacitors (EDLC), ultracapacitors, super condensers, and pseudo capacitors.

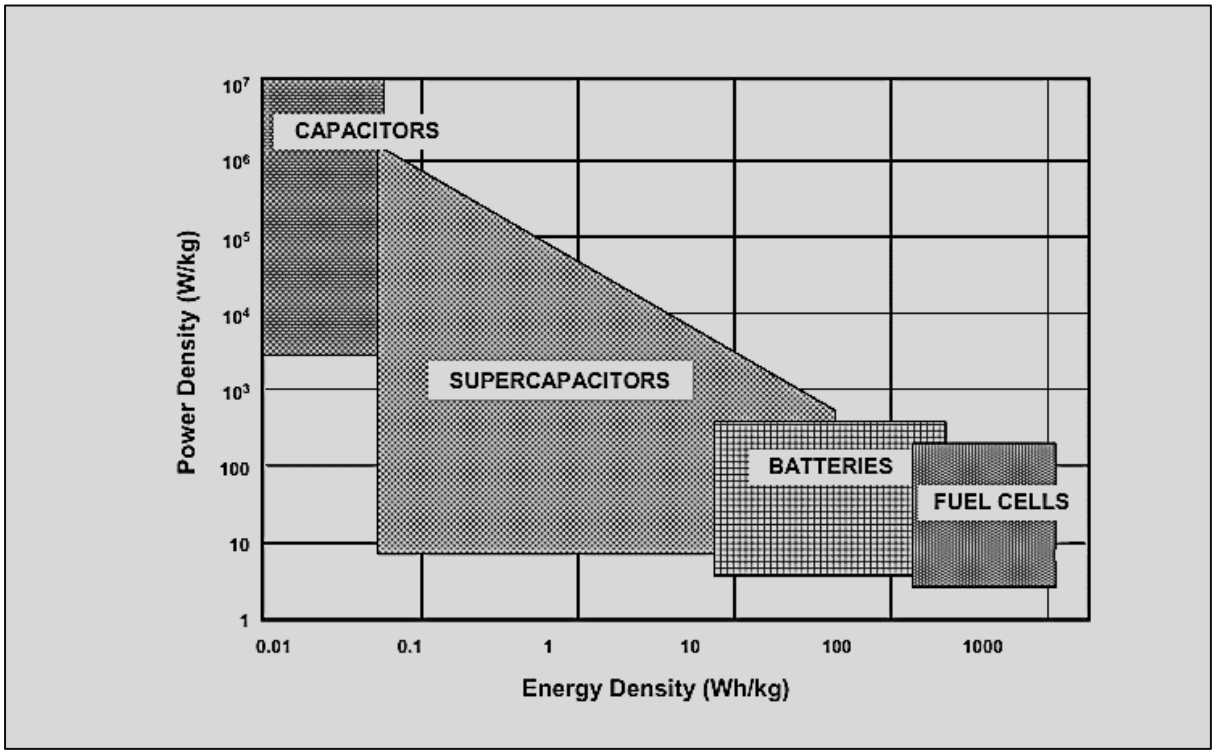


Figure 2.6 Ragone plot of various energy storage devices (adopted from webpage)

2.7.1.2. Classification of Supercapacitors:

Based upon present situations, supercapacitors can be separated into three general classes:

- Electrochemical double-layer capacitors
- Pseudo capacitors
- Hybrid capacitors

Each class is characterized by its unique mechanism for storing charge. These can be classified as non-Faradaic, Faradaic, or a mix of the two. Charge transfer between the electrode and electrolyte occurs during faradaic processes like oxidation-reduction reactions. In contrast, a non-Faradaic mechanism doesn't rely on a chemical one. Instead, physical processes rather than the formation or breaking of chemical bonds are responsible for the distribution of charges on surfaces. A graphical taxonomy of the different classes and subclasses of supercapacitors is presented in the below figure.

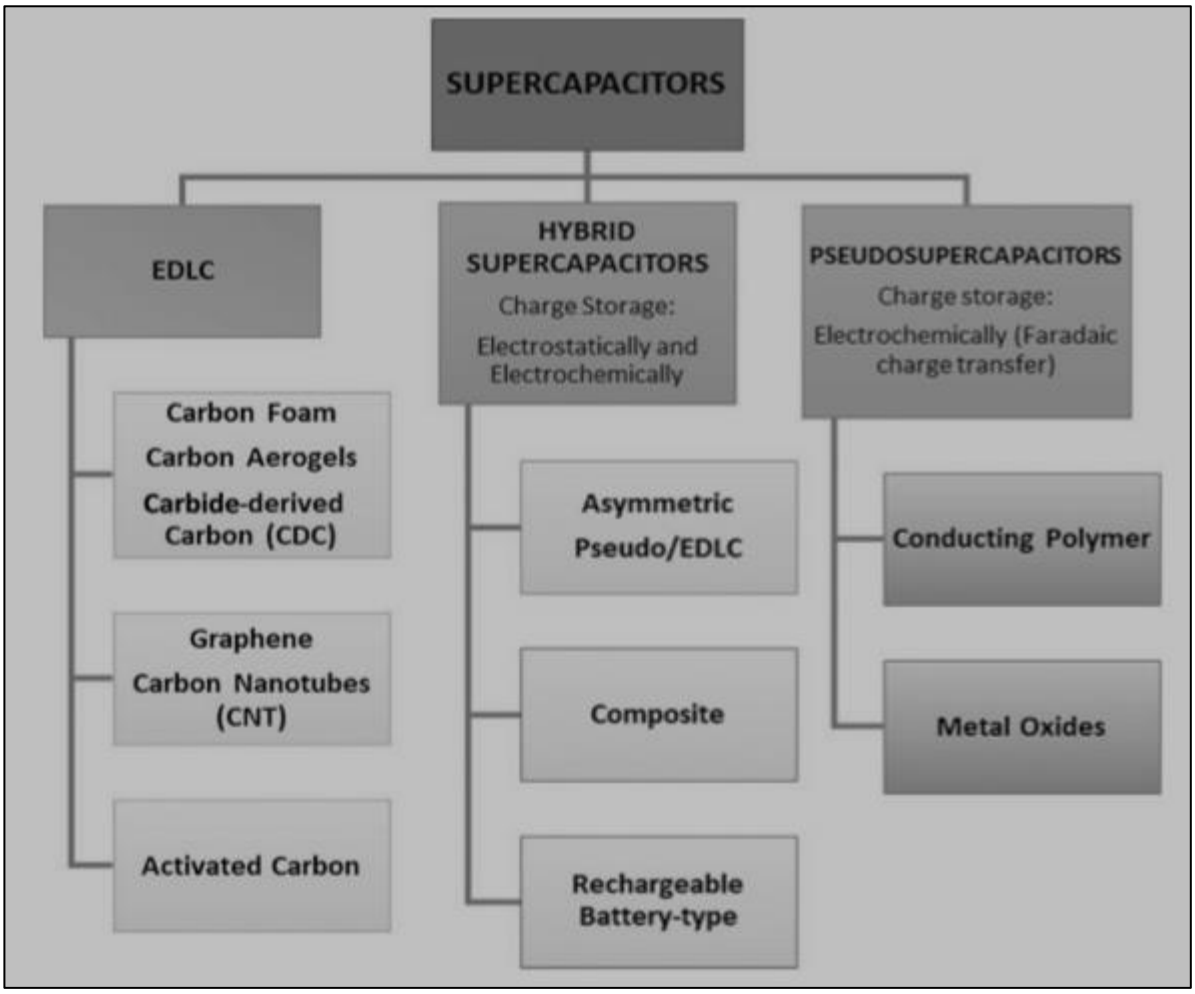


Figure 2.7 Classification of supercapacitors (adopted from webpage)

- **Electrochemical double-layer capacitors (EDLC):**

An electrochemical double-layer of charge is used by EDLCs to store energy. On the electrode surfaces, charge builds up as voltage is applied. Ions in the electrolyte solution permeate past the separator and into the pores of the electrode with the opposite charge due to the attraction of dissimilar charges. On the other hand, the electrodes are designed to stop the ions from recombining. As a result, each electrode produces a double layer of charge. Because of these double-layers, EDLCs are able to attain higher energy densities than traditional capacitors by increasing surface area and decreasing the distance between electrodes [15-18].

The absence of charge transfer between the electrode and electrolyte means that non-Faradaic reactions do not result in any changes to composition or chemistry. Because of this, EDLCs have extremely reversible charge storage, enabling them to attain

extremely high cycling stabilities. Typically, EDLCs exhibit consistent performance traits over an extended period of charge-discharge cycles, up to 106 cycles in some cases. However, the typical cycle life of an electrochemical battery is only roughly 103. EDLCs are ideally suited for applications involving non-user serviceable locales, including deep sea or mountain conditions, due to their cyclical stability [15-18,20].

Changing the electrolyte composition can alter the performance of an EDLC device. An EDLC can use either aqueous or organic electrolytes. Aqueous electrolytes, such H2SO4 and KOH, typically have lower ESR and minimum pore size requirements than organic electrolytes like acetonitrile. However, aqueous electrolytes have lower breakdown voltages. When deciding between aqueous and organic electrolytes, it's important to examine the tradeoffs between capacitance, ESR, and voltage. The electrolyte used in a supercapacitor is often determined by its intended application due to tradeoffs involved [15-18,21].

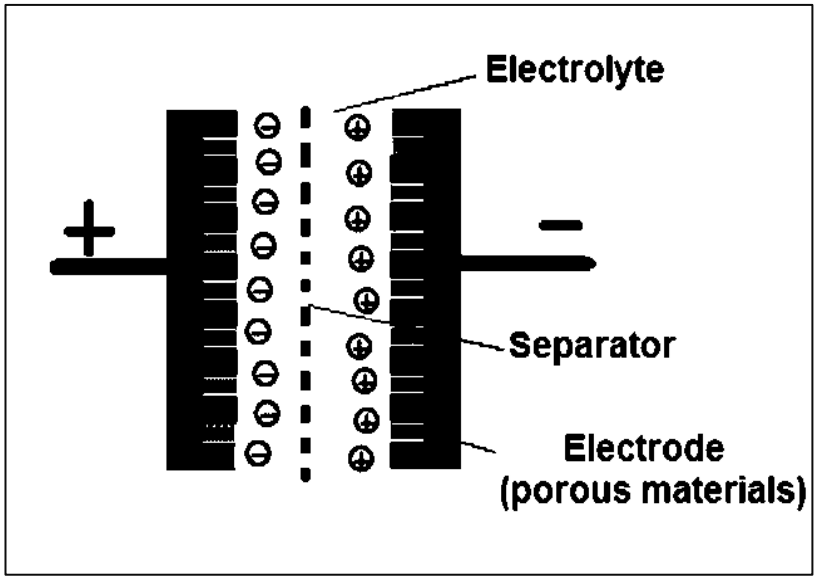


Figure 2.8 Schematic diagram of EDLC (adopted from webpage)

- **Pseudo-capacitor:**

Pseudocapacitors, sometimes known as faradaic supercapacitors, are non-EDLC devices. This capacitor's electrodes contain redox-active materials that store electrical energy through a different method than EDLCs. When an external voltage is applied to this capacitor, rapid and reversible redox processes on the electrode occur, including charge transfer between the

electrode and the electrolyte. The charge and discharge mechanisms of this capacitor are similar to those of electric batteries.

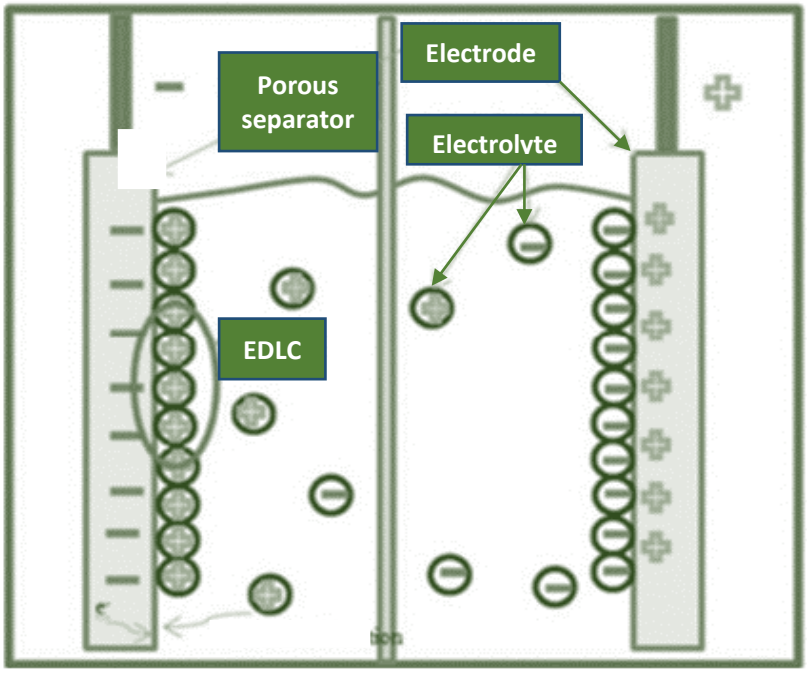


Figure 2.9 Schematic diagram of pseudo capacitors (collected from web page)

- ## Hybrid Capacitors:

  In order to achieve improved device performance, hybrid capacitors aim to take advantage of the relative benefits and minimise the relative drawbacks of EDLCs and pseudocapacitors. Hybrid capacitors, which use both Faradaic and non-Faradaic methods to store charge, have outperformed EDLCs in terms of energy and power density while maintaining the cycling stability and cost-effectiveness that have hindered the growth of pseudocapacitors. Three distinct forms of hybrid capacitors composite, asymmetric, and battery-type that are identified by their electrode configurations have been the subject of research.

2.7.1.3. Application of Supercapacitor:

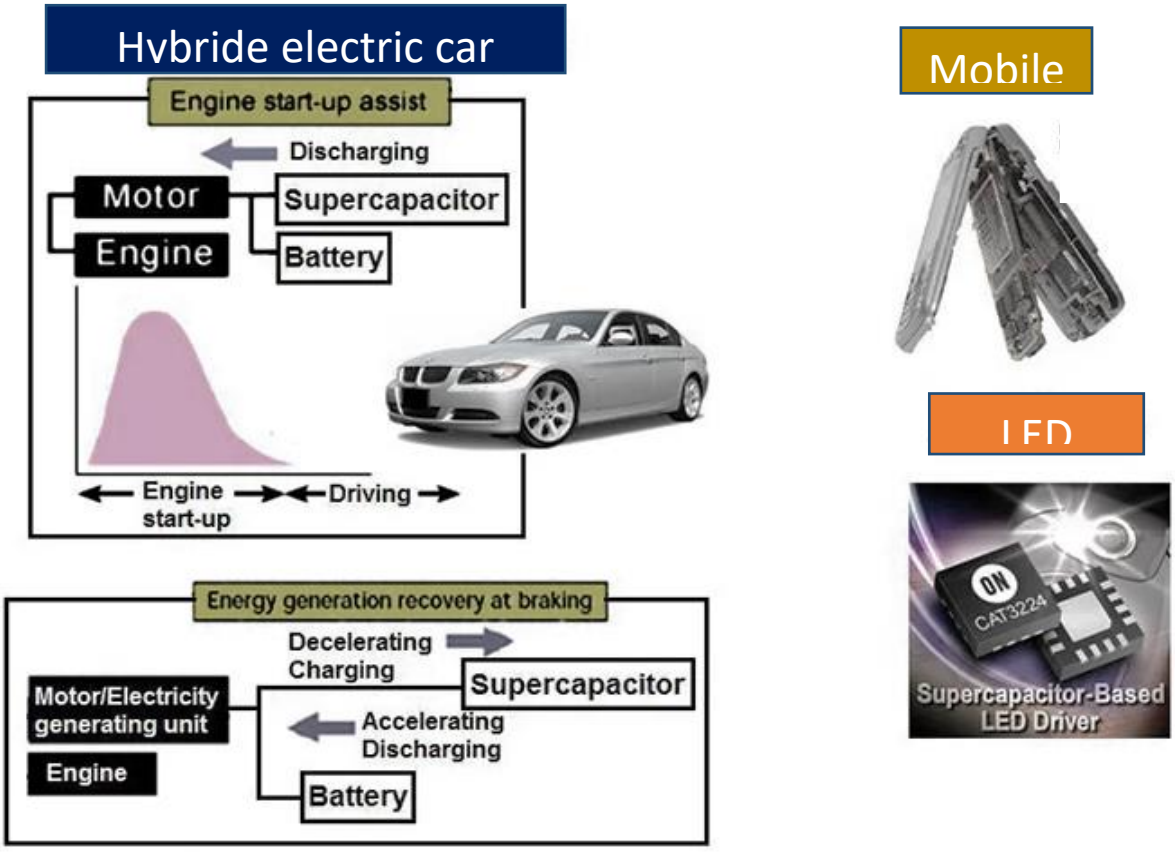


Figure 2.10 Application of Supercapacitor

- **Voltage stabilization:**

Supercapacitors function as dampers to stabilise voltage fluctuations for powerlines. The supply fluctuates in wind and solar systems due to gusts or clouds, which supercapacitors can quickly rectify in milliseconds.

- **Micro-Grid:**

Energy sources that are clean and renewable typically power micro networks. However, the majority of this energy generation fluctuates throughout the day and typically falls short of the demand. Supercapacitors can be utilised for micro grid storage to store energy in the opposite situation and instantly inject power when demand is high and production is temporarily low. They are helpful in this situation since capacitors may be used in both DC and AC applications, and micro grids are providing more and more DC power. Chemical batteries are the ideal combination for supercapacitors to operate with. Their fast rate of

charge and discharge, along with an active control mechanism, allows them to operate as an instantaneous voltage buffer to quickly adjust to changing power loads [23,24.

- **Energy harvesting:**

Supercapacitors are useful short-term energy storage components for systems that capture solar energy. Energy is gathered from ambient or renewable sources, such as mechanical motion, light, or electromagnetic fields, and transformed into electrical energy in an energy storage device, in energy harvesting systems. For instance, it was shown that energy from radio frequency (RF) fields may be collected and stored in a printed supercapacitor by employing an RF antenna as a suitable rectifier circuit. After that, an application-specific integrated circuit (ASIC) was powered for more than ten hours using the gathered energy [25.

- **Batteries:**

The UltraBattery combines a supercapacitor and a lead-acid hybrid rechargeable battery. Its cell structure consists of a standard positive electrode for lead-acid batteries, a standard sulphuric acid electrolyte, and a specifically made negative electrode made of carbon that uses double-layer capacitance to store electrical energy. In high rate partial state of charge use, the supercapacitor electrode changes the chemistry of the battery and provides significant protection against sulfation, which is the usual failure mode of valve regulated lead-acid batteries used in this manner. The resultant cell has improved efficiency, performance, cycle life, charge and discharge rates, and overall features that go beyond those of a lead-acid cell or a supercapacitor.

- **Mobile Devices:**

Supercapacitors can be used in smaller, thinner versions by taking on various physical shapes. A built-in xenon flash allows the camera on certain modern smartphones and other gadgets to take high-quality pictures in low light. This flash needs a lot of power quickly. A mobile device that can handle this kind of power consumption would need to be unduly large and weighty; otherwise, the battery life would be limited. Some mobile industry brands have found a solution to this problem by employing supercapacitors to supply surged power using voltage from the current battery. This lowers the load on the main battery while maintaining the overall load at its prior level.

2.7.2. Photo-catalysis:

2.7.2.1. Introduction to Photo-catalysis:

The acceleration of a photoreaction in the presence of a catalyst is known as photocatalysis. Light is absorbed by an absorbing substrate in this process, and the activity depends on the catalyst's capacity to form electron-hole pairs, which produce free radicals (OH) that can undergo secondary reactions. Chlorophyll is a natural example of a photocatalyst. By absorbing sunlight, it converts CO2 and water into O2 and glucose. TiO2 was used to discover photocatalysis in a practical setting. The advanced oxidation process (AOP) is the name of the commercially available method. The advanced oxidation process can be transported by a variety of methods, such as the use of UV radiation or TiO2. The generation and use of the OH radical is typically the distinguishing characteristic.

2.7.2.2. Types of Photo catalysis:

- Homogeneous Photo catalysis
- Heterogeneous Photo catalysis

Homogeneous Photo catalysis:

A collection of soluble molecular catalysts, comprising a light-absorbing system (photosensitizer), sites of catalysis for oxidation and reduction processes, and more, are assembled into a single form (solution) in homogeneous photocatalysis. Due to their appropriate stability and electronic band gap for homogeneous photocatalysis, transition metal complexes are frequently used as homogeneous photocatalysts26. Homogeneous photocatalysts often employ the ozone and photo-Fenton processes (for example, Fe^{+} and Fe^{+}/H_2O_2 systems). These reactions are the next step in the ozone process that produces OH radicals.27

$$Fe^{2+} + H_2O_2 \rightarrow HO^{\bullet} + Fe^{3+} + OH^{-}$$

$$Fe^{3+} + H_2O_2 \rightarrow Fe^{2+} + HO_2^{\bullet} + H^{+}$$

$$Fe^{2+} + HO^{\bullet} \rightarrow Fe^{3+} + OH^{-}$$

Heterogeneous photo catalysis:

In heterogeneous photocatalysis, the reactant and catalyst are in separate phases. A wide range of reactions include water detoxification, gaseous pollutant removal, dehydrogenation,

hydrogen transfer, deuterium to alkane isotopic exchange, and moderate or complete oxidants. The most widely used heterogeneous photocatalysts are semiconductors, transition metal oxides, and sulphides due to their distinct properties. Semiconductors, in contrast to metals, contain a void energy zone where no energy levels are available to encourage the recombination of an electron and hole created by photo activation in a solid. A light source, a semiconductor material utilised to start the photoreaction, and a catalyst system that can concurrently carry out an oxidation and reduction reaction using long wavelengths, such as UV and solar light, are examples of the two or more systems that are needed. A positive hole is created in the valance band when an electron is driven from the valance band to the conduction band by a photon that has energy equal to or greater than the semiconductor's bandgap. The energy obtained from the excitation of the electron can be released via the recombination of the electron with the hole. Recombination, however, is not at all desired when it comes to photocatalysis. Both the produced hole and the reductant will react to produce an oxidised product, as well as an excited electron and an oxidant to form a reduced product.

Oxidative Reaction:

$$h^+ + H_2O \rightarrow H^+ + \cdot OH$$

$$2h^+ + 2H_2O \rightarrow 2H^+ + H_2O_2$$

$$H_2O_2 \rightarrow \cdot OH + \cdot OH$$

Reductive Reaction:

$$e^- + O_2 \rightarrow \cdot O_2^-$$

$$\cdot O_2^- + 2 \cdot OH + H^+ \rightarrow H_2O_2 + O_2$$

$$H_2O_2 \rightarrow \cdot OH + \cdot OH$$

Both processes ultimately result in the generation of hydroxyl radicals. These radicals have a redox potential, are highly oxidative by nature, and are not selective.

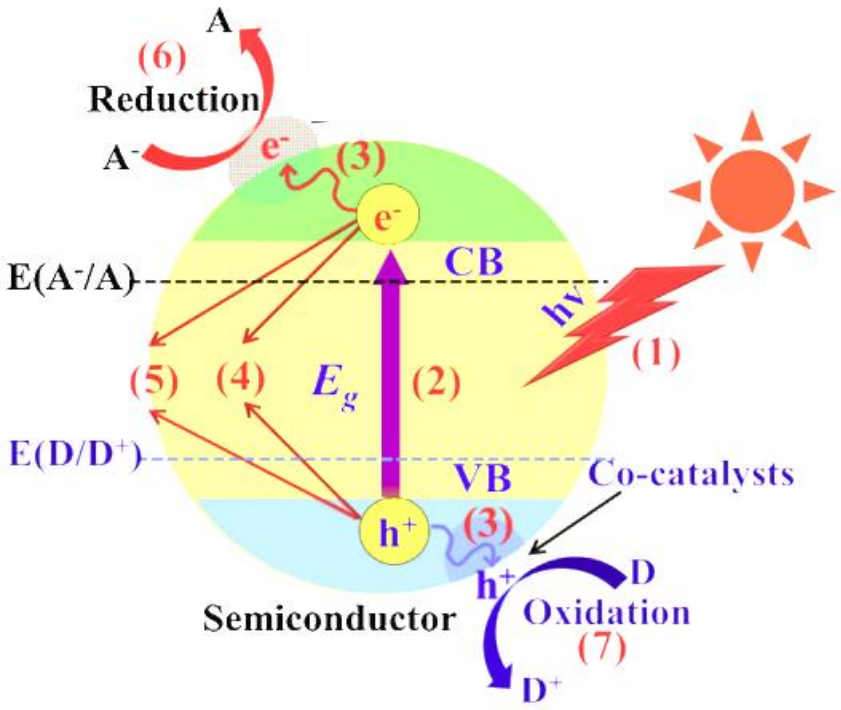


Figure 2.11 Fundamental mechanism of heterogeneous photocatalysis (adopted from webpage).

$$catalyst + energy > E_g \rightarrow e^- + h^+$$

$$H_2O + h^+ \rightarrow H^+ + \cdot OH^-$$

$$\cdot OH^- + organicpollutant \rightarrow CO_2 + H_2O$$

$$O_2 + e^- \rightarrow O_2^-$$

$$O_2^- + organicpollutant \rightarrow CO + H_2O$$

$$O_2^- + H^+ \rightarrow \cdot OOH$$

$$\cdot OOH + \cdot OOH \rightarrow O_2 + H_2O_2$$

$$\cdot OOH + organicpollutant \rightarrow CO_2 + H_2O$$

2.7.2.3. Applications of Photocatalysis:

There are many fields where photocatalysis is applicable:

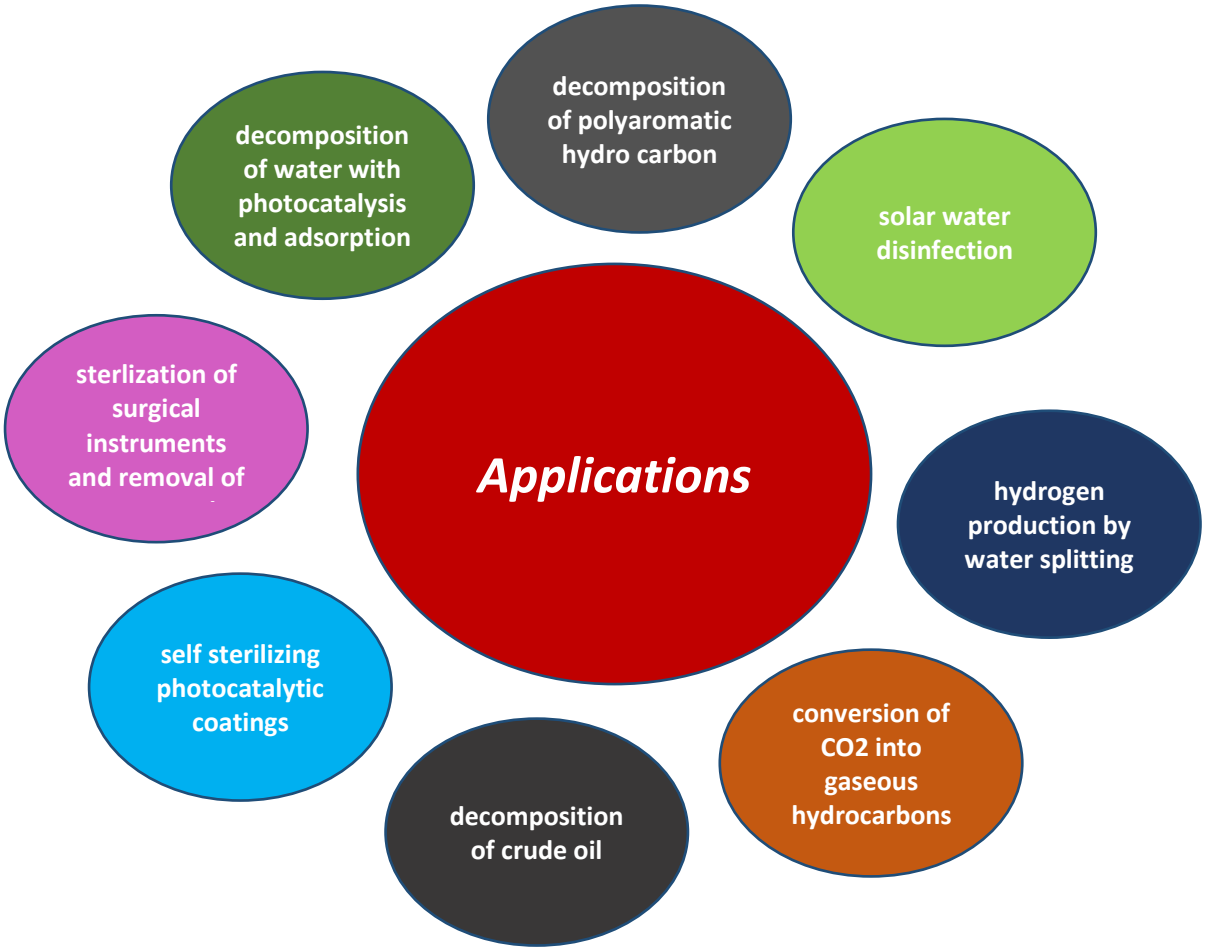


Figure 2.12 Applications of Photocatalysis

References:

1. C. Pacholski, A. Kornowski, H. Weller, Angew. Chem. Int. Ed. Engl. 43 (2004) 4774–4777
2. Burapat Inceesungvorn, Thidarin Teeranunpong, J. Nunkaew, Sarunya Suntalelat, Doldet Tantraviwat, Catal. Commun. 54 (2014) 35–38.
3. N. Boonprakob, N. Wetchakun, S. Phanichphant, D. Waxler, P. Sherrell, A. Nattestad, J. Chen, B. Inceesungvorn, J. Colloid Interface Sci. 417 (2014) 402–409.
4. M.D. Hernández-Alonso, F. Fresno, S. Suárez, J.M. Coronado, Energy Environ. Sci. 2 (2009) 1231–1257.
5. X. Guo, H.J. Zhu, Q. Li, Appl. Catal. B: Environ. 160–161 (2014) 408–414.
6. W. Chen, N. Zhang, M.Y. Zhang, X.T. Zhang, H. Gao, J. Wen, CrystEngComm 16 (2014) 1201–1206.
7. D. Lee, K. Yong, Mater. Chem. Phys. 137 (2012) 194–199. [15] Z.M. Wu, Y. Zhang, J.J. Zheng, X.G. Lin, X.H. Chen, B.W. Huang, H.Q. Wang, K. Huang, S.P. Li, J.Y. Kang, J. Mater. Chem. 21 (2011) 6020–6026.
8. J.J. Zheng, Z.M. Wu, W.H. Yang, S.P. Li, J.Y. Kang, J. Mater. Res. 25 (2010) 1272–1277.
9. Seungho Cho, Ji.-Wook Jang, Jungwon Kim, Jae Sung Lee, Wonyong Choi, Kun-Hong Lee, Langmuir 27 (2011) 10243–10250.
10. Liu, Xiaoyan, et al. "Facile fabrication and photocatalytic properties of ZnO nanorods/ZnSe nanosheets heterostructure." *Superlattices and Microstructures* 83 (2015): 447-458.
11. Mehta, Vimal, et al. "Temperature effect on properties of chemical induced nanocrystalline ZnSe thin films." *Journal of Materials Science: Materials in Electronics* 29.10 (2018): 8801-8808.
12. Razak, K. Abdul, N. Mohamad Nor, and Nur Syafinaz Ridhuan. "Metal Oxide nanostructure-modified Electrode for glucose biosensor." *Advanced Materials and their Applications: Micro to nano scale, One Central Press (OCP), United Kingdom* (2017): 31-68.
13. Mehta, Vimal, et al. "Temperature effect on properties of chemical induced nanocrystalline ZnSe thin films." *Journal of Materials Science: Materials in Electronics* 29.10 (2018): 8801-8808.
14. Wang, Huimin, et al. "Low thermal conductivity of monolayer ZnO and its anomalous temperature dependence." *Physical Chemistry Chemical Physics* 19.20 (2017): 12882-12889.
15. Conway, B. E. (1999). Electrochemical Supercapacitors : Scientific Fundamentals and Technological Applications. New York, Kluwer-Plenum.

16. Burke, A. (2000). "Ultracapacitors: why, how, and where is the technology." Journal of Power Sources 91(1): 37-50.
17. Kotz, R. and M. Carlen (2000). "Principles and applications of electrochemical capacitors." Electrochimica Acta 45(15-16): 2483-2498.
18. Aricò, A. S., P. Bruce, et al. (2005). "Nanostructured materials for advanced energy conversion and storage devices." Nature Materials(4): 366-377.
19. Chu, A. and P. Braatz (2002). "Comparison of commercial supercapacitors and highpower lithium-ion batteries for power-assist applications in hybrid electric vehicles I. Initial characterization." Journal of Power Sources 112(1): 236-246.
20. Amatucci, G. G. (2006). Private communication.
21. Frackowiak, E. and F. Beguin (2001). "Carbon materials for the electrochemical storage of energy in capacitors." Carbon 39(6): 937-950.
22. Chumphongphan, Somwan. "Physical and Electrical Property of TiO2 Nanotube Arrays for Supercapacitors." *Key Engineering Materials* 798 (2019): 91-96. Chumphongphan, Somwan. "Physical and Electrical Property of TiO2 Nanotube Arrays for Supercapacitors." *Key Engineering Materials* 798 (2019): 91-96.
23. Crispo, Rick; Brekken, Ted K. A. (2013). "A motor-generator and supercapacitor based system for microgrid frequency stabilization". *2013 1st IEEE Conference on Technologies for Sustainability (Sus* Tech*)*. pp. 162–166.
24. Inthamoussou, F. A.; Pegueroles-Queralt, J.; Bianchi, F. D. (September 2013). "Control of a Supercapacitor Energy Storage System for Microgrid Applications". *IEEE Transactions on Energy Conversion*. **28** (3): 690–697.
25. Lehtimäki, Suvi; Li, Miao; Salomaa, Jarno; Pörhönen, Juho; Kalanti, Antti; Tuukkanen, Sampo; Heljo, Petri; Halonen, Kari; Lupo, Donald (2014). "Performance of printable supercapacitors in an RF energy harvesting circuit". *International Journal of Electrical Power*. **58**: 42–46.
26. [22] M. Mrowetz, et al., Oxidative power of nitrogen-doped TiO2 photocatalysts under visible illumination, J. Phys. Chem. B 108 (45) (2004) 17269–17273.
27. Tahir, Muhammad Bilal, et al. "Nanomaterials for photocatalysis." *Nanotechnology and photocatalysis for environmental applications*. Elsevier, 2020. 65-76.
28. Arai, Takeo, et al. "Cu-doped ZnS hollow particle with high activity for hydrogen generation from alkaline sulfide solution under visible light." Chemistry of Materials 20.5 (2008): 1997-2000.

29. Xing, Chanjuan, et al. "Band structure-controlled solid solution of Cd1-xZnxS photocatalyst for hydrogen production by water splitting." International Journal of Hydrogen Energy 31.14 (2006): 2018-2024.
30. Bao, Ningzhong, et al. "Facile Cd-thiourea complex thermolysis synthesis of phase-controlled CdS nanocrystals for photocatalytic hydrogen production under visible light." The Journal of Physical Chemistry C 111.47 (2007): 17527-17534.
31. SUBRAHMANYAM, M., VT SUPRIYA, and PRAM REDDY. "PHOTOCATALYTIC Hz PRODUCTION WITH CdS-BASED CATALYSTS FROM A SULPHIDE/SULPHITE SUBSTRATE: AN EFFORT TO DEVELOP MgO-SUPPORTED CATALYSTS."
32. Fujishima, Akira, Tata N. Rao, and Donald A. Tryk. "Titanium dioxide photocatalysis." Journal of Photochemistry and Photobiology C: Photochemistry Reviews 1.1 (2000): 1-21.

CHAPTER 3:

Literature Review

3.1. Introduction:

In a variety of industries requiring high energy throughput (hybrid electric cars) and stable energy throughput (sensitive automation, computer chips, and portable electronic devices), supercapacitors have come out as promising candidates in line with recent technological advancements in electric-powered devices in terms of cycle life, charge time, and specific power. High-power throughput power systems can already use supercapacitors, though not always to their full potential as energy storage devices [1]. The usage of supercapacitors in energy backup devices is limited because they are unable to store the full amount of power. With regard to cell voltage, specific power, and operating cost, supercapacitors fill the gap left by power sources in comparison to conventional dielectric capacitors, which are well-suited for rapid power storage and release systems [2]. These capacitors can deliver and absorb up to 196 kW kg^{-1}, or 10–100 times the energy density of electrolytic capacitors, in a matter of seconds [3], [4], [5]. Reliable power throughputs are also facilitated by the appealing features of supercapacitors, which include faster charge and discharge times and better power densities. A pulse current system or supercapacitor, is utilized to meet requirements for high current and specific power (10,000 W kg −1) for shorter than one minute. As a result, SCs can provide increased power efficiency and cycle life for applications including hybrid cars, cranes, trains, and elevators when used alone or in conjunction with another energy storage option (i.e., batteries) [6], [7], [8]. The first patent for a prototype SC was published and granted in 1957 [8]. Outside of the realm of hybrid electric vehicles, there was little demand for SC technology until the 1990s. The goal of current, comprehensive SC technology development is to improve electrode materials' electrical performance [9]. Different kinds of SCs are already being utilized in drive systems that draw power from a voltage source to meet the power requirements for initiating and recovering braking energy [10]. Consequently, SCs are a good choice for a variety of energy storage applications, such as serving as backup power sources to guard against interruptions in power [11].

Solid solutions of semiconductors are disordered systems with fluctuating crystal potential due to composition changes and broadened exciton lines. II-VI semiconductors play a significant role in modern semiconductor physics and technology. They have strong radiative recombination efficiency, a high absorption coefficient, and direct bandgaps. These

systems provide a continuous spectrum of solid solutions, allowing for smooth control of physical properties and optimization of structural and optical features through molar composition. Binary II-VI nanocrystals are the most extensively studied semiconductor materials.

ZnSe nanostructure, one of the most important Zn-based II-VI semiconductors, has the potential for use in light-emitting devices, blue-green light laser diodes, and optical sensors due to its wide band gap (2.67 eV) and strong exciton binding energy (21 meV). ZnSe nanostructures with various morphologies have been synthesized using a variety of processes, including hydrothermal, chemical vapor deposition (CVD), sol-gel, and solvothermal. In other hand ZnO is semiconductor with a wide band gap energy of 3.37 eV, has been the subject of much research due to its inexpensive cost and comparatively high photocatalytic activity when compared to other semiconductor photocatalysts. As we know, the applications of nanoscale ZnO or ZnSe be contingent sturdily on their morphologies [12],[13].

❖ Different properties of ZnO:

Fundamental properties of ZnO:

ZnO is considered to be the most capable semiconductor for various applications, despite its peculiar direct band gap semiconductor (~3.4 eV) and enormous exciton binding energy of 60 meV [28], [29]. These features are particularly interesting for various optoelectronic device improvements. The fact that oxygen has the highest ionization energy of any element in the sixth group of the periodic table confirms many of the unique properties of ZnO and leads to the strongest orbital relationship between Zn (3d) and O (2p) [30]. Because of its excellent biocompatibility, low toxicity, and affordability, zinc oxide (ZnO) is a multifunctional material that has been used in a wide range of applications, including UV absorption, antibacterial treatments, sunscreen lotions, catalysts, photocatalysis, and biological uses. Zinc oxide (ZnO) finds application as an addition in a growing range of industrial products, including paint, rubber, cosmetics, and coatings. ZnO nanostructures are intriguing for liquid crystal displays and solar cells as well. Large electromechanical coupling effects in the piezoelectric and pyroelectric properties, which can be used in piezoelectric sensors and mechanical actuators, are caused by the defective symmetry of ZnO's wurtzite structure.

Physical Parameters	Values
Stable phase at 300 K	Wurtzite
Lattice Constants	a = b = 0.32495 nm and c = 0.52069 nm
Melting Point	1975 °C
Density	5.66 g/cm^3
Refractive Index	2.01
Band Gap	3.4 eV, Direct
Electron effective mass	0.24
Hole effective mass	0.59
Exciton binding energy	60 meV
Static dielectric constant	8.656

Table 1. The basic physical parameters of ZnO structure.

Optical properties of ZnO:

The interaction of a material with light is the subject of optical studies. Semiconductor materials have given rise to a wealth of information on a variety of physical characteristics, including the existence and kind of faults and impurities, as well as their electrical and vibrational states. Its intrinsic and extrinsic characteristics are related to semiconductors. The interaction between holes in the valence band (VB) and electrons in the conduction band (CB), as well as excitonic effects from the Coulomb interaction, are the foundations of a semiconductor's intrinsic features. The dopants or imperfections induced in the semiconductor that create discrete electronic states between VB and CB determine the extrinsic optical properties [30]. Various approaches, including photoluminescence (PL), transmission, optical absorption, reflection, and cathode luminescence, have been employed to study an optical transition in ZnO semiconductors. Out of all these techniques, the PL technique has been used a lot to understand ZnO structure optical behavior. The PL spectra of the various ZnO nanostructures show UV emission as well as one or two bands of visible emissions caused by vacancies, complicated defects, interstitials, and antisites. At ambient temperature, ZnO exhibits a band gap of 3.37 eV and a greater exciton energy of 60 meV.

Below low excitation energy, it exhibits efficient exciton emission at room temperature due to its greater exciton energy value (25 meV) than GaN. In the blue-UV range, ZnO is therefore one of the most promising photonic materials [32]. In PL research at room temperature, ZnO nanorods exhibit a broad band emission associated with deep level defects and a near-band edge (NBE) for UV emission. In ZnO nanorods with reduced impurity concentrations, deep level emissions (DLE) have been seen, and a single emission has been observed at UV emission (from 3.236 to 3.307 eV).

❖ Different phases of ZnO:

Wurtzite phase:

Because ZnO is ionic and lies precisely on the boundary between covalent and ionic materials, it is thermodynamically stable in the wurtzite phase. It's located at the "ionic extreme" of tetragonally coordinated compound semiconductors, which are categorized as covalently bound bulk materials due to their cubic and hexagonal geometries. Thus, ZnO is the tetragonally coordinated ionic semiconductor prototype. Because Wurtzite ZnO's piezoelectricity originates from the P63mc space group, the ZnO material lacks a center of inversion symmetry. Electric fields E and/or displacement field vectors $\bar{D}$, with $\bar{D}=K\bar{E}_0 + 4\bar{P}$, where $K=1+4\eta$ and η is the susceptibility, are produced in principle by the strain-induced polarization P. $\bar{P}=\tanh(\Delta\bar{E}/ 2kBT)$, where $\Delta\bar{E} = g\mu_B\bar{B}$, is a straightforward representation of the polarization $\bar{P}$, which ultimately aids in the quenching of excitonic characteristics in the wurtzite materials. For ZnO material, there are, in principle, three different piezoelectric strain coefficients: d_{15}, d_{31}, and d_{33}, with corresponding values of -10×10^{-12}, -5×10^{-12}, and 12×10^{-12} m/V, respectively.

Zincblende phase:

Wurtzite ZnO epitaxy has been the subject of several investigations, and the basic characteristics of metastable zincblende ZnO development have been the subject of a few theoretical and experimental works. Each Zn or O has four nearest neighbors in the zincblende and wurtzite formations; the in-plane bonds are stronger than the out-of-plane bonds, as shown by a larger electron density. In the rocksalt structure, each Zn or O has six nearest neighbors, in contrast to the zincblende/wurtzite structures. increased doping efficiencies, reduced carrier scattering, and other benefits are anticipated for zincblende II-VI materials for device applications because to the increased crystalline symmetry in the

zincblende structure[16]. With its maximum symmetry and ability to support piezoelectric polarization under strain in the (001) directions, the zincblende phase presents an appealing and straightforward platform for investigating the characteristics of excitonic systems in the absence of a perturbation field. In addition, it has technological benefits including simpler laser cavity manufacturing along the (110) directions in conjunction with the substrate, which goes hand in hand with evidence of increased optical gain. Furthermore, the long-running argument over whether the valance band in ZnO should be ordered normally or inverted can be resolved with the help of zincblende ZnO epitaxy.because it is challenging to compute the valence band dispersion in the wurtzite structure using first principles. Similar to the zincblende structure, the whole band dispersion of the valence and conduction bands consistently yields the band structure parameters required for device simulation [33], such as equivalent kp parameters or effective masses [18-20].

Because of their current high Seebeck value and electric conductivity, zinc oxide (ZnO) nanostructures are ideal photoelectric diodes [6]. It may transform waste heat flow into electrical energy or, conversely, electrical energy into cooling power because to this characteristic.

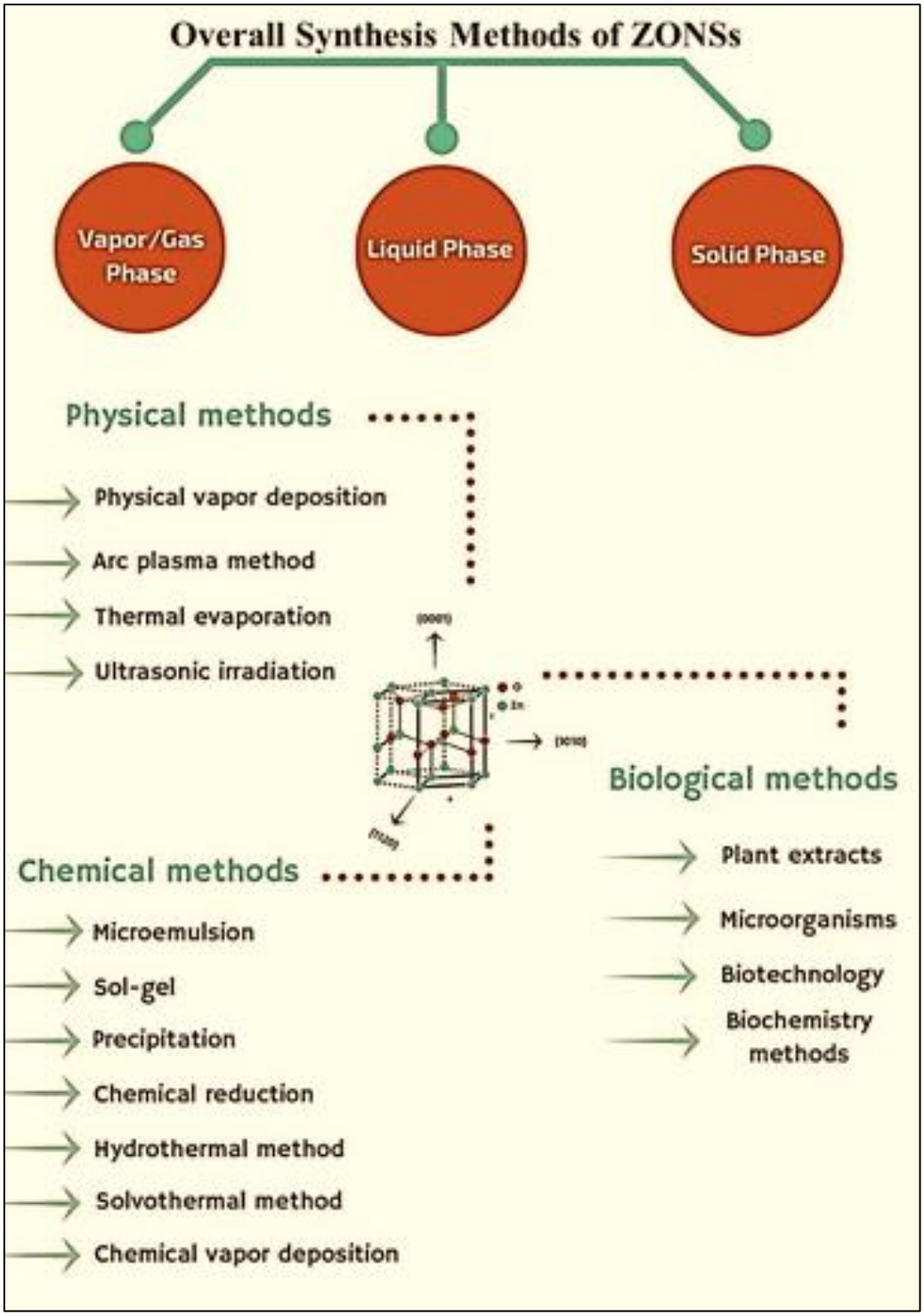


Fig.1. Overall Synthesis methods of ZnO nanostructures [35].

❖ Different properties of ZnSe:

Structural properties of ZnSe:

A.P. Samantilleke et al. (1998) found that (111) is the optimal orientation of ZnSe layers based on X-ray diffraction measurements [5]. The optimal orientation of ZnSe thin films electrodeposited onto a glass substrate coated with SnO_2 and previously cleaned was found to be along the (111), (100), and (222) planes, according to research done by R. Chandramohan et al. in 2005. They saw that the two most common type orientations in all of the deposits were (hhh) and (h00). It was discovered that the thin films had a cubic crystal structure and were polycrystalline in nature. The film grew uniformly and needle-like, as demonstrated by the SEM micrograph, with an estimated grain size of 0.002 microns. An increase in crystallite size as a result of annealing was seen in the Raman spectra of thin films that had been formed and annealed [21]. Through the examination of 2Θ values in the diffraction pattern, Mahalingam et al. (2007) verified that the ZnSe thin films that were electrodeposited had a polycrystalline nature and a cubic zinc blende structure. Their SEM investigations revealed that the film's surface was smooth and that the substrate was heavily coated in grains. Using the Debye-Scherrer formula [22], the crystalline size for the (111) plane of the ZnSe thin film was estimated to be 9.5 nm.

When A.R. de Moraes et al. (2002) investigated the structural characteristics of electrodeposited ZnSe-Fe thin films at 65^{o}C on a stainless steel substrate, they discovered an excess of Se close to the deposits' surface using XPS analysis. They asserted that electrochemical kinetics was the cause of this excess of Se. ZnSe-Fe thin film XRD examination revealed that ZnSe was linked with diffraction peaks at 2θ= 31.7^{o}, 53.2^{o}, 63 ^{o}. It may be concluded from this finding that the polycrystalline sample films that were deposited had a zinc blende structure, with the main (111) plane corresponding to the 2θ = 31.7^{o}. No diffraction peak corresponding to Fe was observed in XRD pattern. They claimed that this may be due to the small particle size of Fe and their intrinsic structural disorder.

K. R. Murali et al. [2009] examined the pulse electrodeposited ZnSe thin-film XRD pattern and came to a similar structural result as those made previously, namely that the films were cubic in shape and had a favored orientation of (111). They came to the conclusion that these films could be utilized in luminous devices since they could readily create a nanocrystalline thin film with a crystalline size of 15 nm using this technique [23].

Through the use of EDX, Raman, and UV reflectance spectroscopy, Sunyang Ham et al. [2008] demonstrated the photochemical deposition of CdZnSe thin films on Au substrate and discovered that the electrolyte composition could be used to adjust the Cd/Zn ratio inside the films [24].

ZnSe thin films produced by Charita Mehta et al. showed a combination of hexagonal and cubic phases [16]. When M. M. Ivashchenko et al. manufactured ZnSe thin films using the close-spaced vacuum sublimation (CSVS) process, they discovered that the films contained a low quantity of the hexagonal phase (wurtzite) and a zinc mix phase (sphalerite). The evaluated lattice constant was 0.56 nm, which is consistent with previous reports [25].

Optical properties of ZnSe:

When A.P. Samantilleke et al. measured the optical absorbance of ZnSe thin films produced electrochemically, they discovered that it peaked at 460 nm, indicating a 2.7 eV band gap.

According to T. Mahalingam et al. (2007), electrosynthesized ZnSe thin films in an aqueous solution of ZnSO4 and SeO2 have a low transmission of 40% at 400 nm and a high transmission of 90% in the infrared region. 2.66 eV was found to be the optical band gap value [22]. Using the pulse electroplating approach, the optical band gap of thin films was determined to be between 2.64 and 2.68 eV, which is reasonably similar to the previously reported value. There are peaks in the photoluminescence spectrum at 675 nm[23].

The PL emission peaks change to shorter wavelengths when the concentration of silicotungustic acid increases, possibly as a result of a band gap expansion. Band gap increases in the range of 2.7–3.1 eV as silicotungustic acid concentration rises. A direct band gap of 3.5 eV is present in the chemically produced ZnSe thin films [charita Mehta et al 2009].

After studying the transmission spectra of thermally evaporated ZnSe thin films, S. Chalina et al. asserted that the materials had a good visible light transmittivity. They also came to the conclusion that the transmission coefficient for the sample that had been heat-treated was higher than the value that had been obtained earlier. It was discovered that the preparation circumstances had a significant impact on the transmission spectra's shape. The energy gap that was estimated fell between 2.6 and 2.7 eV. Using the Swanpoel method, the refractive index was determined to be 2.658 at 505 nm and 2.487 at 756 nm [26].

Scientists	Methods	Optical band GAP (eV)
M. Öztaş *et al [2005]*	Spray Pyrolysis	2.63-2.70
S. Venkatachalam *et al* [2007]	Vaccum Evaporation	2.70-2.74
R. Chandramohan *et al* [2004]	Electrodeposition	2.82
K.R. Murali *et al* [2009]	Pulse Electrodeposition	2.64-2.68
S.Chaliha *et al* [2008]	Thermal Evaporation	2.60-2.70
S. Anatohe *et al* [2013]	Thermal Vacuum evaporation	2.70
F.I. Ezema *et al* [2006]	Chemical Bath Deposition	1.60-1.75
N.A. Olereke *et al* [2011]	Chemical Bath Deposition	2.70-2.75
P.C. Pingale *et al* [2013]	Chemical Bath Deposition	2.52-2.69

Table 2. Band gap energies of ZnSe by different synthesis method .

M. Öztaş et al. (2005) and Pandurang C. Pingale et al. (2013) discovered that the Zn:Se ratio affects the optical band gap. The optical band gap was estimated to be between 2.65 and 2.71 eV for unannealed thin films, and between 2.70 and 2.63 eV for annealed thin films that were heated to 400ºC for 60 minutes in an open air furnace, according to research done by M. Öztaş et al. in 2005. An increased blue-green response was seen upon annealing, and the estimated band gap shrank.

- **Electrical properties of ZnSe:**

The electrical characteristics of thermally evaporated ZnSe nanostructures were noted by S. Chalina et al. in 2008. The structures were found to have a conductivity of around 10^{-7} ohm-1 cm^{-1} at room temperature, despite their high resistivity. It was discovered that these ZnSe nanostructures exhibited unstable electrical activity. As the substrate temperature increased to 180^{0} c, the resistance of the films dropped, but the conductivity increased due to doping [26].

M. Öztaş and colleagues (2005) investigated the photoconductivity of ZnSe nanostructure with varying Zn:Se ratios. The photoconductivity was discovered to be in the order of 10^{-6} ohm^{-1}. As the Zn:Se ratio decreased, conductivity increased. Out of all the Zn:Se ratios measured, they discovered that 0.2:1 was the most conductive[27].

❖ Synthesis of ZnSe Nanostructures of Various Morphologies.

Generally speaking, ZnSe nanocrystal shape control was accomplished by adjusting the rate of precursor delivery to the reaction vessel at a far lower level using a syringe pump than was necessary for spherical nanocrystal formation. During precursor addition, the temperature was kept relatively constant, within ±2 °C. The reaction temperature, total volume of the stock solution, concentration, injection rate, and total volume all affected the nanocrystals' shape. We were able to rule out the possibility that the time-dependent phosphine ligand

content during the dropwise addition modality significantly changed the final particle shape in comparison to the one-pot injection modality by controlled syntheses carried out in amine/TOP (or TBA) as the starting mixes.

Injection Volume Experiments.

In all injection volume studies, a 0.35 M Zn/Se stock solution was rapidly injected at 290 °C in HDA or around 345 °C, which is the boiling point of ODA. A scaled-up synthesis was used to produce enough nanocrystals for examination. In four separate trials, 0.4 mL, 1, 2, and 8 mL of stock solution were injected in less than 0.4 seconds, and 28 g of amine was weighed in the flask for this purpose. After allowing the reaction to continue for two minutes, the heating source was quickly turned off, and cool TOP (5 mL) was added to further suppress development.

ZnSe Nanorods.

A 0.32 M Zn/Se solution with a set volume of 1.2 mL was dropwise injected into 14 g of ODA at 345 °C. By adjusting the injection rate from approximately 0.20 mL/min to approximately 0.05 mL/min, the aspect ratio of the nanorods could be adjusted from 2−3 to 7−8. On the other hand, greater aspect ratio nanorods were produced when the precursor volume was increased and the injection rate remained constant. When injecting dropwise at ∼0.20 mL/min, no more than 2 mL were supplied; however, when operating at an injection rate of ∼0.05 mL/min, up to 5−6 mL may be employed. This prevented the formation of branching nanostructures during growth. The flask was allowed to cool to room temperature following the addition.

Branched ZnSe Nanocrystals.

In order to create polypods, a 0.32 M Zn/Se precursor solution was injected at a rate of approximately 0.40 −0.30 mL/min into 14 g of ODA at a temperature of 330−290 °C. The main result of the relatively tiny precursor volume injection (2.5 mL) was tetra- and tripods with equally short arms. To create polypods with longer and different-looking arms, 5–7 milliliters of the same solution were injected. By injecting 5–7 mL of a 0.64 M Zn/Se precursor solution into 14 g of ODA (or HDA) at 290–270 °C, several branching point nanocrystals were produced. The heating source was removed to halt the reaction when the injection was finished [34].

References:

1. Ke, Qingqing, and John Wang. "Graphene-based materials for supercapacitor electrodes–A review." *Journal of Materiomics* 2.1 (2016): 37-54.
2. Huang, Jingsong, Bobby G. Sumpter, and Vincent Meunier. "A universal model for nanoporous carbon supercapacitors applicable to diverse pore regimes, carbon materials, and electrolytes." *Chemistry–A European Journal* 14.22 (2008): 6614-6626.
3. Simon, Patrice, and Yury Gogotsi. "Materials for electrochemical capacitors." *Nature materials* 7.11 (2008): 845-854.
4. Hashemi, Masumeh, et al. "The use of an electrocatalytic redox electrolyte for pushing the energy density boundary of a flexible polyaniline electrode to a new limit." *Nano energy* 44 (2018): 489-498.
5. González, Ander, et al. "Review on supercapacitors: Technologies and materials." *Renewable and sustainable energy reviews* 58 (2016): 1189-1206.
6. González, Ander, et al. "Review on supercapacitors: Technologies and materials." *Renewable and sustainable energy reviews* 58 (2016): 1189-1206.
7. Carignano, Mauro G., et al. "Energy management strategy for fuel cell-supercapacitor hybrid vehicles based on prediction of energy demand." *Journal of power sources* 360 (2017): 419-433.
8. Kötz, Rüdiger, and M. J. E. A. Carlen. "Principles and applications of electrochemical capacitors." *Electrochimica acta* 45.15-16 (2000): 2483-2498.
9. Deka, Biplab K., et al. "Recent development and challenges of multifunctional structural supercapacitors for automotive industries." *International Journal of Energy Research* 41.10 (2017): 1397-1411.
10. Hartmann, B., L. Prikler, and I. Varjasi. "Revealing technological possibilities of recovering braking energy of electric traction vehicles." *2017 IEEE Manchester PowerTech*. IEEE, 2017.
11. Raza, Waseem, et al. "Recent advancements in supercapacitor technology." *Nano Energy* 52 (2018): 441-473.
12. Ashar, Ambreen, et al. "Synthesis, characterization and photocatalytic activity of ZnO flower and pseudo-sphere: Nonylphenol ethoxylate degradation under UV and solar irradiation." *Journal of Alloys and Compounds* 678 (2016): 126-136.

13. Li, Xiuyan, et al. "Synthesis and comparison of the photocatalytic activities of ZnSe (en) 0.5, ZnSe and ZnO nanosheets." *Journal of Alloys and Compounds* 689 (2016): 287-295.

14. Park, Heeyeon, Haegeun Chung, and Woong Kim. "Synthesis of ultrathin wurtzite ZnSe nanosheets." *Materials letters* 99 (2013): 172-175.

15. Zhu, Zifan, et al. "ZnO/ZnSe heterojunction nanocomposites with oxygen vacancies for acetone sensing." *Journal of Alloys and Compounds* 906 (2022): 164316.

16. J. I. Pankove, Materials Research Society Symposia Proceedings Materials Research Society, Pittsburgh, 1990, Vol. 162, p. 515; B. Daudin, G. Feuillet, J. Hubner, Y. Samson, F. Widmann, A. Philippe, C. BruChevallier, G. Guillot, E. Bustarret, G. Bentoumi, and A. Deneuville, J. Appl. Phys. 84, 2295 (1998).

17. 7 T. Kogure and Y. Bando, J. Electron Microsc. 47, 135 (1998); M. Posternak, A. Baldereschi, A. Catellani, and R. Resta, Phys. Rev. Lett. 64, 1777 (1990); I. Vurgaftman, J. R. Meyer, and L. R. Ram-Mohan, J. Appl. Phys. 89, 5815 (2001).

18. D. C. Reynolds, C. W. Litton, and T. C. Collins, Phys. Rev. A 140, 1726 (1965).

19. D. G. Thomas, J. Phys. Chem. Solids 15, 86 (1960); J. J. Hopfield, ibid. 15, 97 (1960).

20. C. Priester and M. Lannoo, Phys. Rev. B 44, 10559 (1991); S. Z. Karazhanov, P. Ravindran, A. Kjekshus, H. Fjellvag, U. Grossner, and B. G. Svensson, J. Appl. Phys. 100, 043709 (2006).

21. Chandramohan, R., Mahalingam, T., Chu, J.P. & Sebastian, P.J., (2005), "Preparation and Characterization of Electrosynthesized Zinc Selenide Thin Films", Journal of New Material for Electrochemical Systems, Vol.8, pp.143-148.

22. Mahalingam, T., Kathalingam, A., Lee Soonil, Moon Sunghwan & Kim Deak Yong, (2007), "Studies of Electrosynthesized Zinc Selenide Thin Films", Journal of New Material for Electrochemical Systems, Vol. 10,pp.15-19.

23. Murali, K.R., Dhanapandiyana, S. & Manoharana, C., (2009), "Pulse electrodeposited Zinc Selenide films and their characterstics". Chalcogenide letters, Vol.6, no.1, pp.51-56.

24. Mehta, Charita, Saini, G.S.S., Abbas, Jasim M. & Tripathi, S.K., (2009), "Effect of deposition parameters on structural, optical and electrical properties of nano-crystalline ZnSe thin films", Applied Surface Science , Vol. 256, No. 3, pp.608-614 .

25. Ivashchenko, M. M., Opanasyuk, A. S. & Danilchenko., S. M., (2011), "Structure and substructure of zinc selenide films", Functional Materials, Vol. 18, No. 1, pp.18-23.

26. Chalina, S., Borah, M N, Sarmah, P C & Rahman, A, (2008), “Optical and electrical properties of thermally evaporated ZnSe thin films”, Indian Journal of Physics, Vol. 82, No.3, pp.303-310.

27. Pathak, R. K., and Shraddha Bais. "ZnSe thin films-a brief review." *International Journal of Advances in Engineering & Technology* 7.4 (2014): 1300.

28. Özgür, Ümit, et al. "A comprehensive review of ZnO materials and devices." *Journal of applied physics* 98.4 (2005).

29. Klingshirn, Chem. "ZnO: material, physics and applications." *ChemPhysChem* 8.6 (2007): 782-803.

30. Ellmer, Klaus, Andreas Klein, and Bernd Rech, eds. "Transparent conductive zinc oxide: basics and applications in thin film solar cells." (2007).

31. Gao, Pu Xian, et al. "Nanowire piezoelectric nanogenerators on plastic substrates as flexible power sources for nanodevices." *Advanced Materials* 19.1 (2007): 67-72.

32. Wang, Zhong Lin. "Zinc oxide nanostructures: growth, properties and applications." *Journal of physics: condensed matter* 16.25 (2004): R829.

33. Ashrafi, A. B. M. A., and C. Jagadish. "Review of zincblende ZnO: Stability of metastable ZnO phases." *Journal of Applied Physics* 102.7 (2007).

34. Cozzoli, P. Davide, et al. "Shape and phase control of colloidal ZnSe nanocrystals." *Chemistry of materials* 17.6 (2005): 1296-1306.

35. Ong, Chin Boon, Law Yong Ng, and Abdul Wahab Mohammad. "A review of ZnO nanoparticles as solar photocatalysts: Synthesis, mechanisms and applications." *Renewable and Sustainable Energy Reviews* 81 (2018): 536-551.

CHAPTER 4:

Instruments and Apparatus Used

In this chapter we discusses about the key apparatus and instruments used to characterize samples. A brief summary of their functioning principles has also been provided below.

4.1 Morphological Analysis:

4.1.1 FIELD EMISSION SCANNING ELECTRON MICROSCOPY (FESEM):

The scanning electron microscope (SEM) is a powerful tool for studying and analyzing microstructures. SEM uses a concentrated electron beam to scan the specimen's surface and generate several signals. These electron transmissions are finally transformed into a visual signal that appears on a cathode ray tube (CRT).

The electron beam can be generated by two ways:

- Thermionic emission
- Field emission.

In thermionic gun the anode receives an electrical potential that is positive. Heat is applied to the filament (cathode) until an electron stream forms. The positive potential then accelerates the electrons down the column.

In FEG, the single crystal tungsten wire with very sharp tip, usually prepared by electrolytic etching used as source. Strong electric field is formed on finely oriented tip to draw the electrodes towards the anode.

Sample Preparation

The specimens that can be analyzed must be compatible with high vacuum (~ 10-5 mbar) because the SEM operates at a high vacuum. This means that direct study is not possible for liquids or materials that contain water or other volatile components. In order to prevent contamination of the SEM specimen chamber, tiny powder samples must also be securely attached to a specimen holder substrate. Non-conductive materials must be mounted to a conductive specimen holder and coated with a thin conductive coating via sputtering or evaporation. Typical coating materials include Au, Pt, Pd, their alloys, and carbon also.

Components of FESEM

❖ Electron Guns:

Modern FESEM systems necessitate a steady electron beam from the electron gun with a high current, small spot size, customizable energy, and low energy dispersion. A FESEM system employs a variety of electron guns, and the quality of the electron beam produced by each varies significantly. The tungsten hairpin or lanthanum hexaboride (LaB6) cathodes employed in the early FESEM systems have been superseded by field emission sources, which give more current with less energy dispersion. The lifespan of the emitter is an important factor to consider when choosing electron sources.

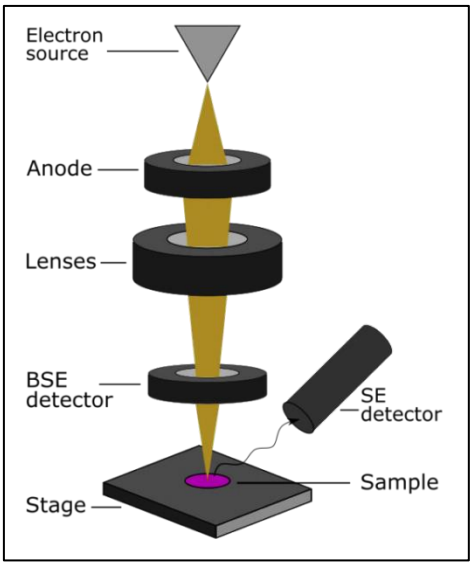


Figure 4. 1 Schematic Diagram of FESEM

❖ Electron Lenses

Electrostatic or magnetic fields can be employed to focus electron beams. However, because the aberration of an electron beam controlled by a magnetic field is minimal, the SEM system only uses a magnetic field. The electromagnets can change the paths taken by the electrons.

- ✓ **Condenser lens:**

After exiting the emission source through the anode plate, the electron beam will diverge. The electron beam is collimated and converged into a comparatively parallel stream using the condenser lens. Typically, a magnetic lens is comprised of two iron pole pieces that are symmetrical in rotation, with a copper winding inside to provide a magnetic field. The electron beam can pass through a hole in the middle of the pole pieces. The two pole pieces

are separated by a lens-gap, where the electron beam is affected by (focused) by the magnetic field. The condenser lens current can be changed to change the focal point's location.

- ✓ **The Objective Lens:**

The condenser aperture will be below the divergence of the electron beam. Using objective lenses, the electron beam is further de-magnified and centered into a probe point on the specimen surface. The fundamentals of Scanning Electron Microscopy and aperture size increase with decreasing spot size, or the diameter of the electron beam on the specimen surface, which determines image resolution.

- ✓ **Scan Coils :**

The electron beam is deflected over the item in a zigzag pattern by the scan coils. This scan movement and the generation of the image on the monitor happen simultaneously. The amount of noise in the image and the pace at which the screen refreshes are determined by the scan velocity. Often made comprised of upper and lower coils, scan coils stop a circular shadow from forming at low magnification.

- ✓ **Stigmator Coil:**

The stigmator coils correct anomalies in the beam's x and y deflection, resulting in a completely round form. When the beam is not circular but ellipsoidal, the image seems blurry and stretched.

- ✓ **Object Chamber:**

After being covered with a conductive coating, the object is placed on a specific holder. The object is inserted through an exchange chamber into the microscope's high vacuum section and secured on a moving stage. The secondary electron emission detector (scintillator) is situated behind the object holder in the chamber.



Figure 4. 2 FESEM (Hitachi S-4800) set up

- **Image Formation**

SEM electron beams interact with specimen surfaces, causing complex signals to be observed. Secondary electrons, BSEs (back scattered electrons), transmitted electrons, and specimen current may all be gathered and presented. To determine the composition of a specimen, excited x-ray or Auger electrons are studied. This section provides a basic overview of electron beam interactions with specimen surfaces and image creation using various signals.

4.1.2 ENERGY DISPERSIVE X-RAY SPECTROSCOPY (EDS/EDX):

The elemental composition of materials can be ascertained using an x-ray technique called Energy Dispersive X-Ray Analysis (EDX), often known as EDS or EDAX. EDX systems are add-ons for electron microscopes, namely scanning electron microscopy (SEM), which uses the microscope's image power to identify specimens of interest. The information produced by the EDX analysis consists of spectra with peaks that represent the constituent elements of the material under examination. It is also feasible to perform image analysis and elemental mapping of a sample.

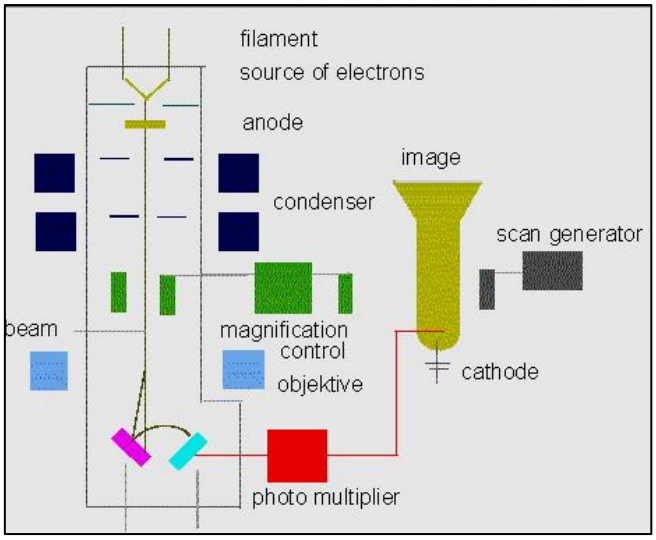


Figure 4. 3 Schematic Diagram of EDS

4.1.3 HIGH RESOLUTION TRANSMISSION ELECTRON MICROSCOPY (HRTEM):

Transmission electron microscope (TEM) is is an analytical tool allowing visualisation and analysis of specimens in realms of micro space ($1\mu=10^{-6}$ m) to nano space (1 nm $=10^{-9}$m). A beam of electrons is transmitted through an ultrathin specimen, interacting with the specimen as it passes through. An image is formed from the interaction of the electrons transmitted through the specimen; the image is magnified and focused onto an imaging device, such as a fluorescent screen, on a layer of photographic film, or to be detected by a sensor such as a CCD camera. TEMs are capable of imaging at a significantly higher resolution than light microscopes, owing to the small de Broglie wavelength of electrons.

- **Working Principle**
- The electron cannon, which emits a stream of monochromatic electrons, is represented by the "Virtual Source" at the top.
- This stream is concentrated into a narrow, thin, coherent beam using condenser lenses 1 and 2. The first lens (often adjusted by the "spot size knob") controls the "spot size"; the general size range of the final spot that strikes the sample. The "intensity or brightness knob" controls the second lens, which adjusts the size of the spot on the sample from wide to pinpoint.
- The condenser aperture, which is often user-selectable, limits the beam and eliminates high angle electrons, or those that are far from the optic axis, indicated by the dotted line down the centre.

- A portion of the specimen is transmitted when the beam strikes it.
- The objective lens focuses this transmitted component into an image.
- The beam can be restricted by optional metal apertures called the Selected Area and Objective. The Selected Area aperture allows the user to study the periodic diffraction of electrons by ordered arrangements of atoms in the sample, while the Objective aperture enhances contrast by obstructing high-angle diffracted electrons.
- The image is fully magnified as it travels down the column through the projector and intermediate lenses.
- The user can view the image because light is produced when the image hits the phosphor image screen.

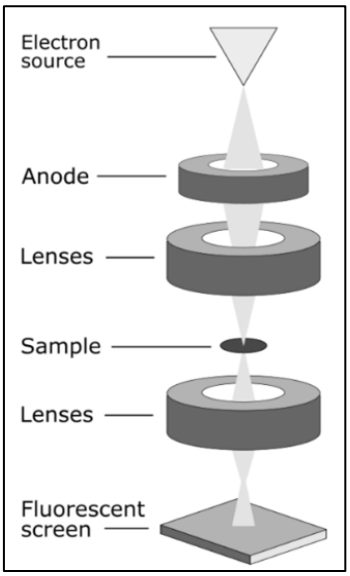


Figure 4. 4 Schematic diagram of TEM

- ## Restriction on samples

More time and expertise are often needed for sample preparation for TEM than for the majority of other characterisation techniques. A TEM specimen in the area of interest needs to have a thickness of at least 1000 A^o. The complete specimen must have a diameter of no more than 3 mm and a thickness of no more than 100 microns. Typically, the sample is thin and disc-shaped, with a hole in the centre and thin enough borders for transmission electron microscopy (TEM) viewing. The first disk is typically created by cutting and grinding bulk or thin-film/substrate material, with ion milling being used for the last stage of thinning. Using specialized tools like a tripod, grinding and polishing the specimen directly onto a TEM-thin substrate (Si3N4, carbon), dispersing powders directly onto the substrate, chemical etching

and electro-polishing, and lithographic patterning of walls and pillars for cross-section viewing are some other options for specimen preparation.



Figure 4. 5 HRTEM (JEOL-200 kV)

4.2 Crystal Structure Analysis:

Wilhelm Conrad Röntgen made the discovery of X-rays in 1895, right as the research on crystal symmetry was coming to an end. X-rays were first unknown to physicists, but it was quickly assumed correctly, in fact they were electromagnetic radiation waves, or simply another type of light. An X-ray incident beam interacts with itself when it exits a crystal due to the atomic planes of the crystal. X-ray diffraction is the term for the phenomena. Two primary applications of X-ray diffraction have been found: the identification of crystalline materials by fingerprint and the ascertainment of their structural composition. We can determine the size and the shape of the unit cell for any compound most easily using X-ray diffraction.

- ✓ **X-Ray Generation:**

X-rays are created when high-energy electrons from a heated filament typically tungsten bombard a metal target (commonly Cu or Mo). To interact with the electrons in the inner shell, the high energy electron needs to pass through the outer electron shells. An inner-shell

electron that receives more energy than a certain threshold is ejected, or it leaves the nucleus' attractive field, creating a hole in the inner shell and producing ionized electrons from the outer shells. It is this change that is accompanied by the emission of Auger atoms or X-rays. By adding electrons to the gap left by the lost electron, the ionized atom nearly returns to its lowest energy.

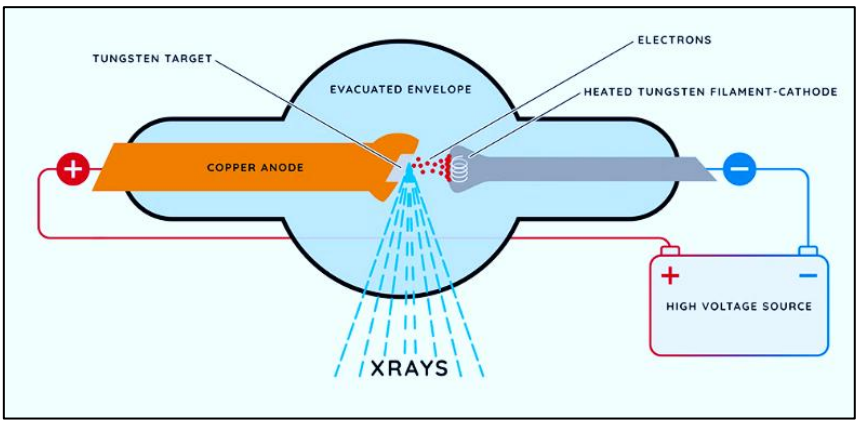


Figure 4. 6 X ray generation principle

✓ Basic Principle:

Electromagnetic radiation having wavelengths ranging from 0.01 to 10 nm is what is known as X-rays. X-rays are a type of electromagnetic radiation, and crystals are regular arrangements of atoms. X-ray rays are scattered by atoms, mostly by their electrons. An X-ray impacting an electron creates secondary spherical waves that emanate from the electron, much like an ocean wave striking a lighthouse produces secondary circular waves that emanate from the lighthouse. Elastic scattering is the term for this phenomena, and the scatterer is the electron, sometimes referred to as a lighthouse. A regular collection of spherical waves is produced by a regular collection of scatterers.

✓ Measurement of Interplanar Spacing:

Bragg's law is the fundamental law used in the structural analysis diffraction method. In θ-2θ mode, the diffraction traces were captured. Every atom in a crystal lattice contributes to scattering when monochromatic X-rays strike it. The lattice of crystals functions as a grid of parallel reflecting planes. When the path difference between two reflected waves from two separate planes is an integral multiple of λ, the intensity of the reflected beam at a given angle will reach its maximum. This requirement, known as Bragg's law, is provided by the relationship,

$$2d \sin\theta = n\lambda$$

Where n= order of diffraction

λ =wavelength of the x-rays

d=spacing between consecutive parallel planes

θ=the incident angle.

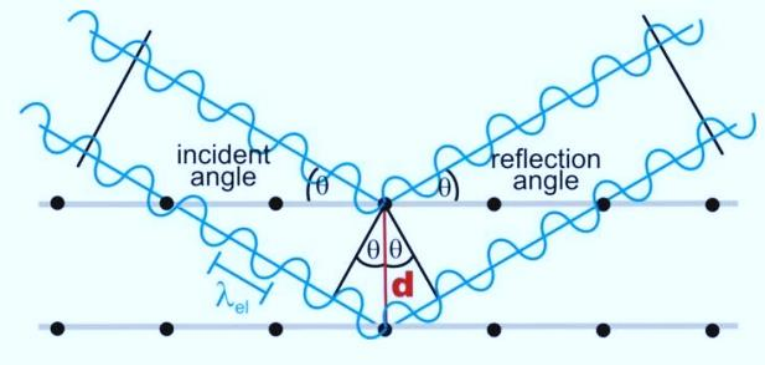


Figure 4. 7 X-ray diffraction from crystal planes satisfying Bragg's Law.

✓ Crystallite size determination:

The mean crystallite sizes of the powders are calculated using Scherrer formula:

$$D = \frac{0.9\,\lambda}{\beta\cos\theta}$$

Where D is the average crystallite size, λ =1.541 A° (X-ray wavelength), β is the full width of the diffraction peak at half maximum (FWHM) for the diffraction angle 2θ.

✓ Phase identification:

Following the aforementioned determination, the resulting XRD pattern is compared to the JCPDS card number kept in the JCPDS file. Different JCPDS cards are available for each organic and inorganic element. The obtained pattern is compared with those cards that fit the criteria. Using a D8 Advanced Bruker apparatus, phase identification of the generated samples was done using x-ray diffraction (XRD). The intensity vs. 2θ mode of the XRD pattern was recorded. Cu Kα (1.5406 Å) radiation from a highly stabilized Bruker X-ray generator (K 780) was passed via a germanium monochromator.

Method	Wave Length (λ)	Incident Angle (θ)
Laue Method	Variable	**Fixed**
Rotating Crystal Method	Fixed	**Variable (In part)**
Power Method	**Fixed**	**Variable**

4.3 Bond Structure Analysis:

4.3.1 FOURIER TRANSFORM INFRARED SPECTROSCOPY (FTIR):

The technique known as Fourier Transform Infrared Spectroscopy (FTIR) is used to examine the chemical makeup of a wide range of materials, including biological samples, inorganics, paints, coatings, adhesives, lubricants, semiconductor materials, coolants, and polymers. FTIR is able to applied for the analysis of a broad variety of materials in liquids, solids, pastes, powders, fibers, bulk or thin films, and other forms. When combined with appropriate standards, FTIR analysis can provide not only a qualitative (identification) study of materials but also a quantitative (quantity) analysis. An interferometer is used to first gather an interferogram of a sample signal, and then the interferogram is subjected to a Fourier Transform (FT) in order to obtain an infrared spectrum (also known as an FTIR, or Fourier Transform Infra-Red).

A Michelson Interferometer, which comprises of a beam splitter, a fixed mirror, and a mirror that accurately translates back and forth, is the foundation of an FTIR. A unique substance used to create the beam splitter allows it to transmit half of the energy that strikes it and reflect the other half. After hitting the beam splitter, the source's radiation splits into two beams. The stationary mirror receives the first beam sent through the beam splitter, while the moving mirror receives the second beam reflected off the beam splitter. The radiation is reflected back to the beam splitter by the stationary and moving mirrors. Once more, at the beam splitter, half of the reflected radiation is transmitted and the other half is reflected, sending one beam to the detector and the other back to the source.

- **Components of Interferometer:**

Various interferometers, including the Michelson, Lamellar grating, and Fabry-Perot interferometers, are used by various FTIR spectrometers. Because of its simple design and

operation, the Michelson interferometer is frequently preferred over the other two interferometers. The Michelson interferometer is used by the majority of FTIR spectrometers that are sold commercially. These are superior to the previous methods in several ways, including multiplexing, high energy throughput, and high frequency measurement precision.

The basic Michelson Interferometer consists of following components:

(a) a broad-band light source which emits light covering the mid-IR range.

(b) a beam splitter made of KBr or CsI.

(c) Two front surface coated mirrors : one moving and one fixed.

(d) a detector.

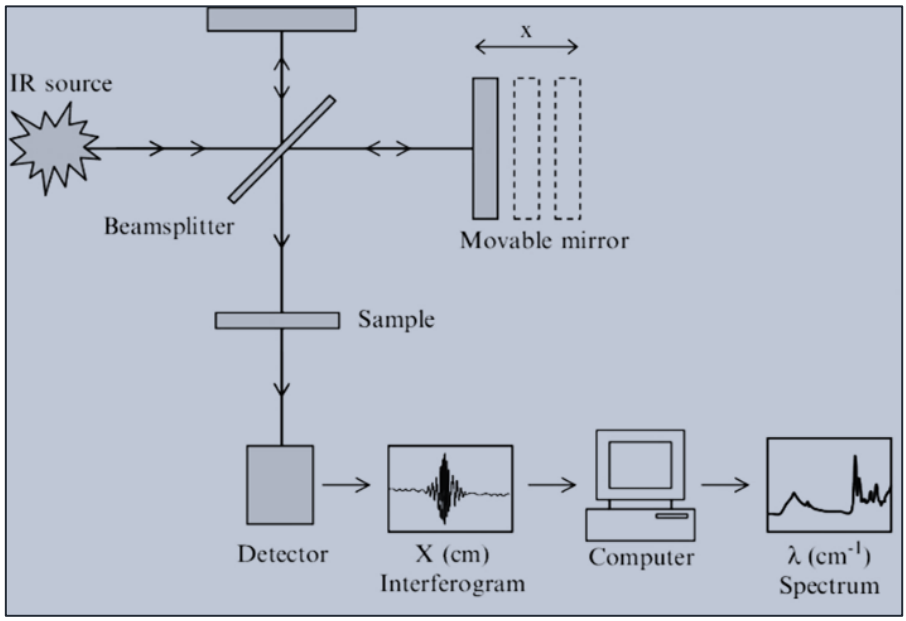


Figure 4. 8 schematic diagram of an FTIR.

Working principle of interferometer:

- The beam splitter receives light from the light source. Half of the light is transmitted, and the other half is reflected.
- The light that has been reflected travels to the stationary mirror and then back to the beam splitter. In addition to being directed towards the moving mirror, the transmitted light is also reflected back towards the beam splitter.

Each of the two beams from the moving and stationary mirrors is split into two at the beam splitter: one beam travels towards the detector, and the other beam returns to the source. As a result, the detector detects two beams: one coming from the fixed mirror and one from the moving mirror.

The two beams that arrive at the detector are identical in origin and have a fixed phase difference due to the optical path difference caused by the locations of the two mirrors. The two beams interfere as a result.

By situating the moving mirror, it is possible to cause constructive or destructive interference between the two beams for a specific frequency. An interferogram is produced when the moving mirror is scanned throughout a range; the maximum intensity of the interferogram corresponds to constructive interference, and the least intensity to destructive interference.



Figure 4. 9 FTIR spectrometer experimental set up

4.4 Optical Property Analysis:

4.4.1 UV-VIS near Infrared Spectroscopy:

UV-Vis near Infrared (UV-Vis-NIR) Spectrophotometer: This instrument measures the UV-visible spectral region's optical transmittance, absorbance, and reflectance. UV-Vis near Infrared (UV-Vis-NIR) Spectrophotometer: This instrument measures the UV-visible spectral region's optical transmittance, absorbance, and reflectance. The percentage of radiation that is absorbed, transmitted, or reflected at each wavelength is determined using UV-Vis absorption spectroscopy. This is usually accomplished by taking a wavelength range scan and noting the absorbance. Investigating the degree of multiple bond or aromatic conjugation within molecules is a common application in organic chemistry. The method can be extended to measure reflected light instead of transmitted light, and it can also be extended to gases and solids.

Light absorption can be described by two fundamental laws as,

Lambert's Law- As long as there are no additional physical or chemical changes to the transparent medium, the percentage of incident light absorbed by the material is independent of the light's intensity. Consequently, an equivalent amount of the incoming energy will be transmitted by subsequent layers of equal thickness.

Lambert's law can be expressed by,

$$I/Io = T$$

where I is the intensity of the transmitted light, Io is the intensity of the incident light, and T is the Transmittance.

Beer's Law- The thickness of the medium in the light path and the concentration of the absorbing medium are directly correlated with the absorption of light.

A combination of the two laws (Beer-Lambert Law) describes the relationship between absorbance (A) and transmittance (T).

$$A = \log Io/I = \log 100/T = \varepsilon\, c\, b$$

Where, A is absorbance (no unit of measurement)

ε is molar absorptivity ($dm^3\ mol^{-1}\ cm^{-1}$)

c is molar concentration ($mol\ dm^{-3}$)

b is path length (cm)

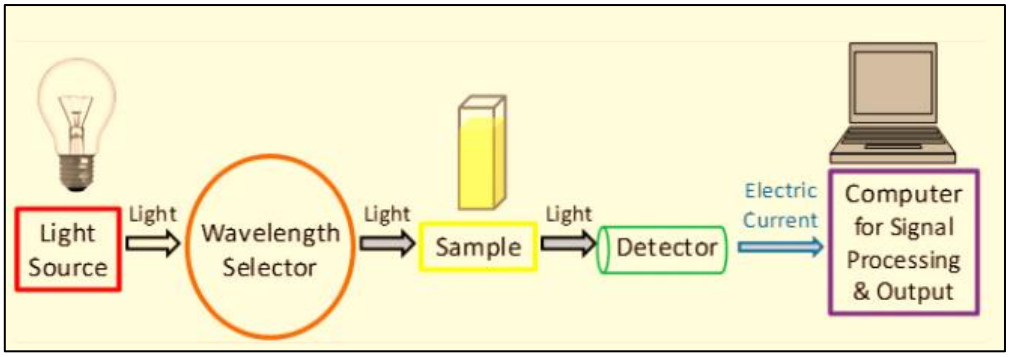


Figure 4. 11 Basic Principles of UV-VIS Spectroscopy

✓ Light reflection and reflectance spectra

The spectrometer beam must be focussed in order to project diffuse reflectance into the sample, where it will be reflected, scattered, and transmitted through the material (shown on

the right). The accessory then gathers and directs the diffusely scattered, back-reflected light some of which is absorbed by the sample to the detection optics. Diffuse reflection refers only to the portion of the beam that is scattered within a sample and returns to the surface.

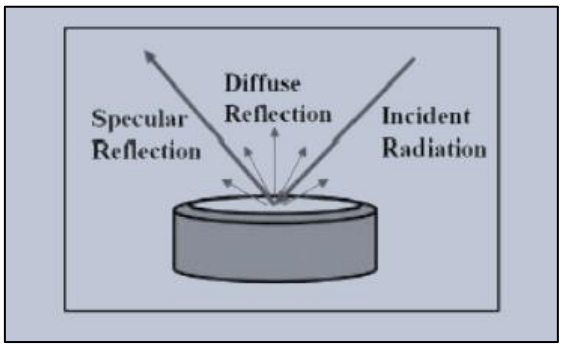


Figure 4. 12 Diffuse and Specular Reflectance

✓ Kubelka-Munk Function

$$F(R) = \frac{(1-R)^2}{R} = \frac{k}{s}$$

R is the absolute reflectance of the sampled layer.

k is the molar absorption coefficient.

s is the scattering coefficient.

This spectrum conversion for ibuprofen, obtained using diffuse reflectance, is displayed in the spectra above. Using a library search of a transmission spectrum database, it is simple to find the Kubelka-Munk converted spectrum for ibuprofen, which compares well with the transmission spectrum.

✓ Components UV-Vis Spectrophotometer

Spectrophotometer consists of the following components

- Source of radiation of appropriate wavelengths.
- Monochromator and optical geometry.

- filter Sample compartment.
- Detector, Photomultiplier, Measuring system, computer.

The UV VIS spectra carried out by Shimadzu UV 3600 spectrophotometer.



Figure 4. 13 UV-VIS-NIS (SHIMADZU UV-3600) Spectrophotometer

4.5 Cyclic Voltammetry:

The most popular method for gathering qualitative data and knowledge about electrochemical reactions is cyclic voltammetry. It provides a quick way to find the electroactive species' redox potentials. Cyclic voltammetry is a technique for determining how a redox active solution's current responds to a linearly cycled potential sweep between two or more pre-set values. It is a useful method for rapidly learning about the energy levels of the analyte, the kinetics of electronic-transfer reactions, and the thermodynamics of redox processes. Like other voltammetry techniques, cyclic voltammetry uses a three-electrode setup: a working electrode, a reference electrode, and a counter electrode. Initially, cyclic voltammetry is carried out in an electrochemical cell by introducing the three electrodes, the reference solution, and the electrolyte solution.



Fig 4.14. Cyclic Voltammetry setup

CHAPTER 5:

Synthesis, Characterization of ZnSe/ZnO Nanocomposite.

5.1 Introduction:

Energy crisis and depleting energy resources have triggered into plentiful efforts for the development alternative ways to cope up with the energy deficiency. Supercapacitor is one such energy storage device that plays an essential role in constant energy supply. Transitional metal selenides and their composites have undergone research in the recent times as potential candidates of supercapacitor devices due to their astounding physical, chemical and electrical property.

A large number of studies have been done to synthesize II-VI semiconducting materials because of its interesting physical, chemical, optical properties including size quantization, catalytic properties etc. These semiconductors include oxides, selenides, sulfides and so on. ZnO has been the subject of much research due to its inexpensive cost and relatively high photocatalytic and energy storage activity, owing to its wide band gap energy of 3.37 eV. In a similar vein, ZnSe, another significant semiconductor, has a band gap of 2.67 eV. ZnSe nanostructure materials have garnered significant attention recently due to their beneficial characteristics in organic material degradation [2-4].

As we know, the morphologies of nanoscale ZnO or ZnSe have a significant impact on their uses. For potential future uses, a great deal of work has gone into creating nanoscale ZnO or ZnSe in a variety of morphologies with unique or improved characteristics. The solvothermal method is one of the most used synthesis techniques due to its ease of use and environmental sociability. $ZnQ(en)_{0.5}$ (Q= S, Se, or Te) is a common organic-inorganic composite that has been created as nanocrystals using the solvothermal technique . ZnSe was produced by heat treatment into a variety of morphologies, including nanosheets , nanoparticles , nanobelts , nanoflowers, nanoplates and nanoribbons. Nevertheless, there haven't been many studies on the ZnSe(en)0.5 composite's thermal breakdown in an air environment. The topotactic transformation from $ZnS(en)_{0.5}$ complex to porous ZnSe and ZnO nanoflakes was reported when $ZnSe(en)_{0.5}$ was heated under air atmosphere [6].

This study describes the preparation of precursor $ZnSe(en)_{0.5}$ nanosheets by a solvothermal process with en-water (v/v = 2:1) as reactant solvent. Thermal treatment of the $ZnSe(en)_{0.5}$ composite yielded porous ZnO and ZnSe nanoflakes. To describe the composition and morphology of the as-prepared samples, various analytical techniques including XRD, SEM, TEM were utilized. An investigation was conducted on the form and

dimension relationship between $ZnSe(en)_{0.5}$ and ZnSe or ZnO. The suggested process involved the topotactic conversion of ZnSe(en)0.5 composite to either ZnSe or ZnO [1].

Because of its stability and tunable morphological features, ZnSe/ZnO, a famous II–VI wide bandgap semiconductor material, has been employed in sensors, photodetectors, energy storage devices and optoelectronic devices [5].

5.2 Experimental Section

5.2.1 Synthesis:

ZnSe/ ZnO nanoparticles were created using a straight forward solvothermal technique. In this example synthesis,

- Forty milliliters of ethylenediamine were used to dissolve two millimoles of selenium powder.
- Two mmol Zinc nitrate hexahydrate ($Zn(NO_3)_2.6\ H_2O$) were dissolved in twenty millilitre of deionized water.
- The both solutions were stirred for forty minutes individually.
- These two solutions were then combined to another beaker and agitated for thirty minutes.
- As a result, the combined solution was put into an 80 ml Teflon-lined autoclave and heated to one eighty degree centigrade for twelve hours.
- The solution was naturally cooled to room temperature before being repeatedly cleaned with ethanol and deionized water for several times.
- Then the sample was dried at sixty degree centigrade for five to seven hours.
- The samples are found by annealing the as synthesized $ZnSe(en)_{0.5}$ composite at 350, 400 and 450^0C for two hours under air atmosphere were termed as Z350, Z400, Z450 respectively [1].

2 mmol Se powder = 0.157 gm. Ethylenediamine = 20 ml.

2 mmol $Zn(NO_3)_2.6\ H_2O$ = 0.594 gm. Deionized water = 40ml.

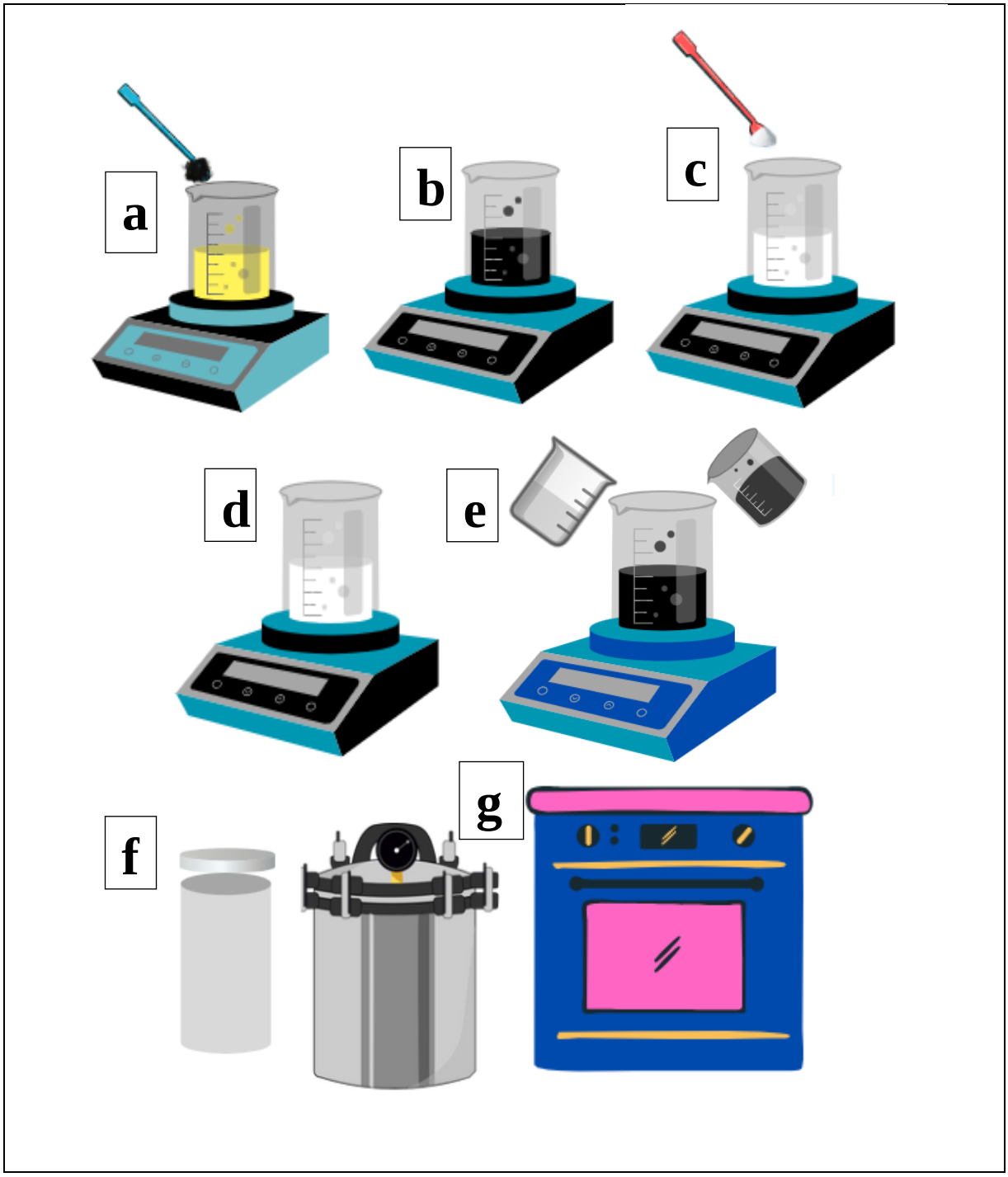


Figure5. 1: Schematic diagram of the synthesis process of ZnSe/ZnO.

(a) Ethylenediamine + Se Powder, (b) Stirrer for 40 minutes, (c) $Zn(NO_3)_2.6\ H_2O$ + DI water, (d) Stirrer for 40 minutes, (e) Both solution was mixed in another beaker and stirred for 30 minutes, (f) The mixture was kept into an 80 ml Teflon-lined autoclave, (g) Heated to 180^0C for 12 hours.

5.3 Characterizations:

X-ray diffraction (XRD), Transmission electron microscopy (TEM), Field emission scanning electron microscopy (FESEM), and Fourier transform infrared spectroscopy (FTIR) were used, in that order, to characterize the structure and morphology. Cyclic voltammetry (CV), and galvanic charge-discharge (GCD) were used to characterize the electrochemical performances.

5.3.1 XRD (X-ray diffraction)

A flexible non-destructive analytical method for examining the phase composition, crystal structure, and orientation of powder, solid, and liquid samples is called X-ray diffraction (XRD).It also indicates the physical and chemical properties of the sample.

❖ Bragg's Law:

From Bragg's diffraction law, $2d\sin\theta = n\lambda$ [d= inter planar spacing, θ = incident angle of light, λ = incident wavelength, n= integer].

❖ Lattice parameter determination:

$$d\sqrt{h^2 + k^2 + l^2} = a$$

Where d= inter planar distance, (hkl) = Miller Indices of crystal plane, a=lattice parameter.

❖ Scherrer Equation:

Utilizing the Scherrer equation, crystallite size can be verified. It is employed to establish a connection between the broadening of a peak in a diffraction pattern and the size of sub-micrometer particles, or crystallites, in a material. Paul Scherrer is honored in the name when the sample is in powder form. When the XRD curve is triangular shape, it's written as,

$$t = \frac{0.9\,\lambda}{\beta\cos\theta_B}$$

Where t = crystallite size β= Full Width Half Maxima at the highest peak, θ_B = angle at which FWHM is taken. λ= incident wavelength.

XRD Analysis:

The XRD patterns of $ZnSe(en)_{0.5}$, ZnO, ZnSe and 3 wt% ZnSe/ZnO heterostructure are shown in fig. 2. Here the strong and sharp diffraction peaks recommend good crystallinity and good particle sizes of $ZnSe(en)_{0.5}$.The XRD patterns of the synthesized samples are found by annealing of $ZnSe(en)_{0.5}$ composite at different temperature in air atmosphere. The pure ZnO is wurtzite and the diffractive peaks at 2Θ of 31.82^0, 34.3^0, 36.24^0, 47.53^0, 56.68^0,

62.88^0, 68.04^0 are corresponding to (110), (002), (101), (102), (110), (103) and (112) crystal planes containing to JCPDS card no 36-1451 [7]. For pure ZnSe, the sample has the diffractive peaks at 2Θ of 26.02^0, 27.46^0, 29.42^0, 38.2^0, 45.48^0, 49.46^0, 53.66^0 are corresponding to the lattice planes of (110), (002), (101), (102), (110), (103) and (112). Now ZnSe/ZnO nanocomposite shows the diffractive peaks of ZnO and ZnSe. The intensity of the diffractive peaks of ZnSe is lower than ZnO. In Fig. 2 Z350, Z400, Z450 represented the XRD patterns of ZnSe, ZnSe/ZnO and ZnO respectively [8].

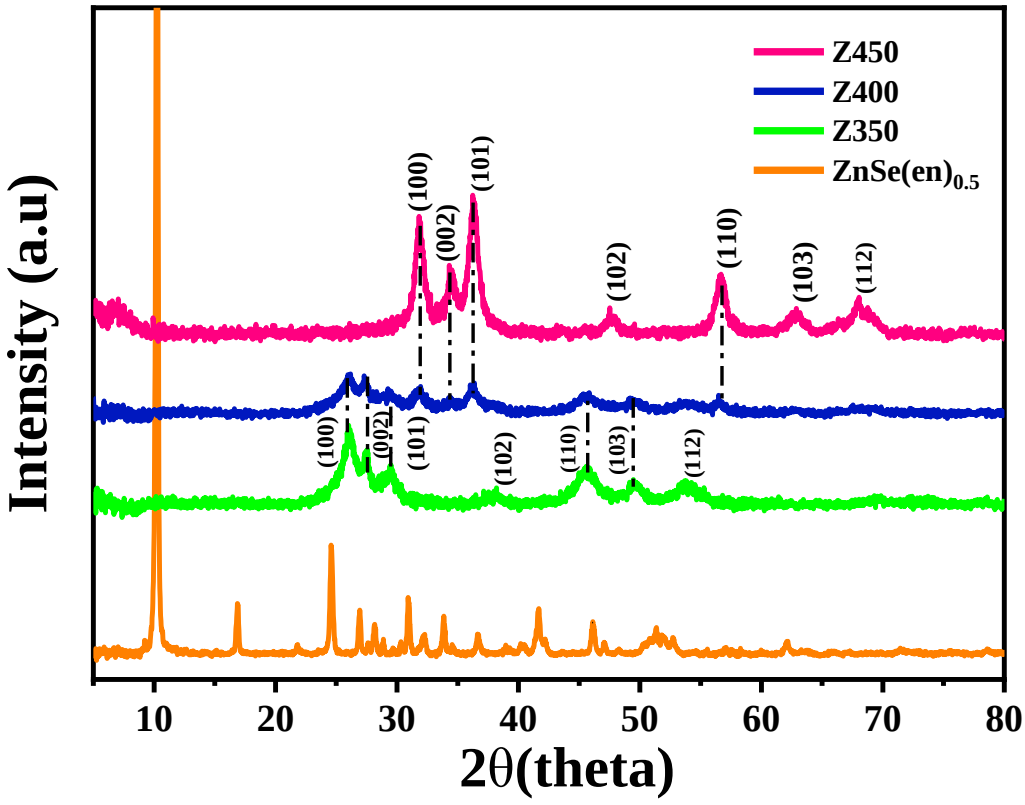


Fig 5.2 XRD patterns of ZnO, ZnSe and 3 wt% ZnO/ZnSe composite.

5.3.2 FESEM analysis

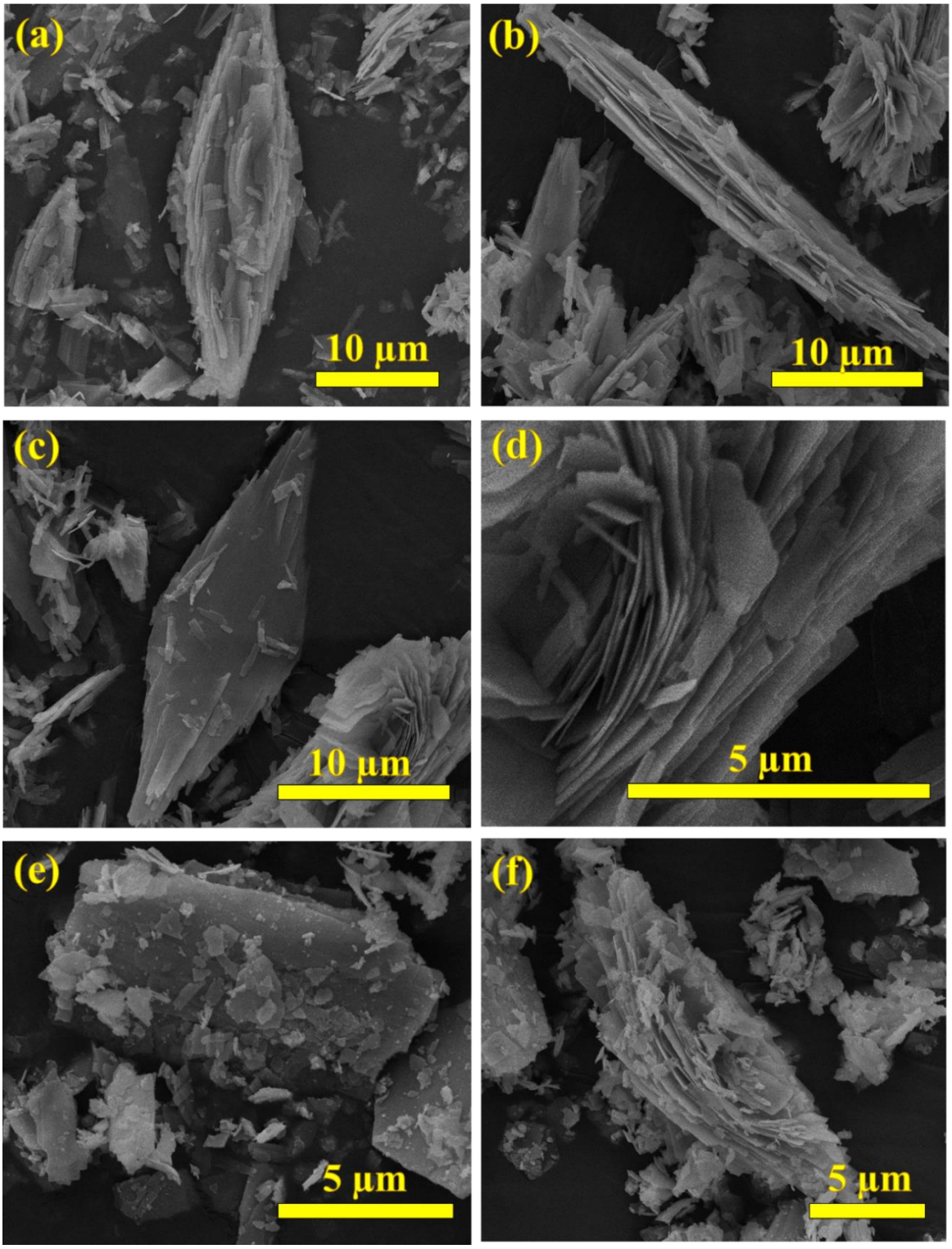


Fig. 5.3. Low and high-magnification SEM images of Z350 (a, b), Z400(c, d), Z450 (e, f).

Fig. 5.3 displays the SEM images of all prepared samples. The low magnification SEM image in Fig. 5.3(c) shows that a diamond-like structure of the prepared $ZnSe(en)_{0.5}$ composite. These nanoflakes actually vary in size; their lateral dimensions fall between 5 and 10 μm[1]. The $ZnSe(en)_{0.5}$ composite's surface is flawlessly smooth, and the high-magnification SEM picture in Fig. 5.3(c) demonstrates that the thickness of Z400 is approximately 80 nm. Fig. 5.3(b), (d) and (f) show the low magnification and Fig. 5.3(a), (c) and (e) shows high magnification SEM images. It displays the large number of uniformly dispersed, randomly oriented nanoflake formations over the surface [9]. The nanoflake's average width was between 50 and 70 nm. In Fig. 5.3(a) and (b), the pure ZnSe displayed an uneven flaky structure with some holes. In Fig. 5.3 (e), the ZnO nanoparticles were uniformly distributed on ZnSe nanoflakes and had shortened in size. This further demonstrated the effective blending of ZnO nanoparticles and ZnSe nanoflakes, as evidenced by the more pronounced morphologies and structures that showed the homogeneous dispersion of ZnO nanoparticles on ZnSe nanoflakes [8]. The SEM and selected area of EDS mapping images in ZnO/ZnSe composites in confirmed the existence of Zn, Se and O elements without any impurities. In addition, the number of bright spots in proportional to the atom concentration,was consistent with the ZnO/ZnSe composites, which indicated ZnO/ZnSe composites to be successfully prepared from the three elements scattered area.

5.3.3 FTIR analysis:

The FTIR spectrum revealed that the produced nanoparticles' functional groups ranged from 4500 to 500 cm^{-1}.FT-IR is typically utilized to find the samples' molecular vibrational information. The FT-IR spectra of ZnO nanostructure, ZnSe/ZnO nanocomposites, and bare ZnSe are displayed in Figure 7. There have been FTIR spectra. The FTIR peaks and their positions are determined by the crystalline structure, chemical composition, and shape of the materials. The O–H stretching vibration is correlated with the broad absorption band that spans 3302 to 3349 cm^{-1}. Zn–OH's distinctive peak was measured at 744 cm^{-1}.Zn-Se vibration modes exhibit characteristic bending, which is represented by the peaks at 727cm^{-1}. The C-H bond may be seen at the 2916 to 2920 cm^{-1} peaks. The intense peak at 2021 cm^{-1} is due to the existence of the C=O stretching and the band at 1251 cm^{-1} is an indication of the presence of C–O stretching [11-14].

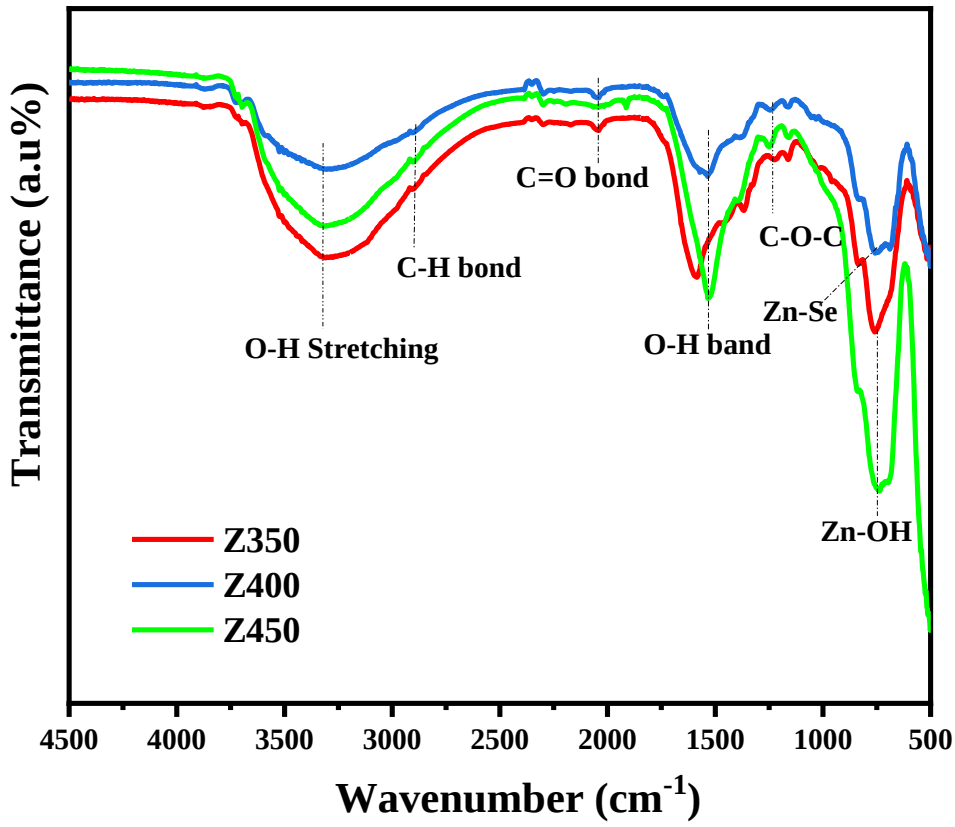


Figure 5.4 FTIR spectra of Z350, Z400 and Z450.

References:

1. Li, Xiuyan, et al. "Synthesis and comparison of the photocatalytic activities of ZnSe (en) 0.5, ZnSe and ZnO nanosheets." *Journal of Alloys and Compounds* 689 (2016): 287-295.
2. A.Ashar, M. Iqbal, I.A. Bhatti, M.Z. Ahmad, K. Qureshi, J. Nisar, I.H. Bukhari,Synthesis, characterization and photocatalytic activity of ZnO flower andpseudo-sphere: nonylphenol ethoxylate degradation under UV and solar irradiation, J. Alloys Compd. 678 (2016) 126e136.
3. W.W. Xia, C. Mei, X.H. Zeng, G.K. Fan, J.F. Lu, X.D. Meng, X.S. Shen, Nanoplatebuilt ZnO hollow microspheres decorated with gold nanoparticles and theirenhanced photocatalytic and gas-sensing properties, ACS Appl. Mater. Interfaces 7 (2015) 11824e11832.
4. N. Huang, J.X. Shu, Z.H. Wang, M. Chen, C.G. Ren, W. Zhang, One-step pyrolytic synthesis of ZnO nanorods with enhanced photocatalytic activity and high photostability under visible light and UV light irradiation, J. Alloys Compd. 648(2015) 919e929.
5. Yi, Ting-Feng, et al. "ZnS nanoparticles as the electrode materials for high-performance supercapacitors." *Solid State Ionics* 343 (2019): 115074.
6. A. Tayyebi, M. Outokesh, M. Tayebi, A. Shafikhani, S.S. S¸ engc¸or, ZnO quantumdots-graphene composites: formation mechanism and enhanced photocatalytic activity for degradation of methyl orange dye, J. Alloys Compd. 663(2016) 738e749.
7. Y. He, Y. Wang, L. Zhang, et al., High-efficiency conversion of CO2 to fuel over ZnO/g-C3 N4 photocatalyst, Appl. Catal. B 168 (2015) 1–8.
8. Zhang, Shuangfang, Xiaohong Yin, and Yinan Zheng. "Enhanced photocatalytic reduction of CO2 to methanol by ZnO nanoparticles deposited on ZnSe nanosheet." *Chemical Physics Letters* 693 (2018): 170-175.
9. Tiwari, Satyam, Sushmitha Veeralingam, and Sushmee Badhulika. "ZnSe nanoflakes/ZnO quantum dots heterojunction-based bandgap engineered, flexible broadband photodetector on paper substrate." *Materials Research Bulletin* 166 (2023): 112374.

10. X.M. Liu, Q.Y. Zhong, W.M. Guo, W.K. Zhang, Y.Y. Ya, Y.Q. Xia, Novel Platycladus orientalis-shaped Fe-doped ZnO hierarchical nanoflower decorated with Ag nanoparticles for photocatalytic application, J. Alloy. Compd. 880 (2021) 160501.
11. Saikia, K., P. Deb, and E. Kalita. "Sensitive fluorescence response of ZnSe (S) quantum dots: an efficient fluorescence probe." *Physica Scripta* 87.6 (2013): 065802.
12. Haghighatzadeh, Azadeh, et al. "Facile synthesis of ZnS–Ag2S core–shell nanospheres with enhanced nonlinear refraction." *Journal of Materials Science: Materials in Electronics* 31.2 (2020): 1283-1292.
13. Vivek, C., B. Balraj, and S. Thangavel. "Structural, optical and electrical behavior of ZnO@ Ag core–shell nanocomposite synthesized via novel plasmon-green mediated approach." *Journal of Materials Science: Materials in Electronics* 30.12 (2019): 11220-11230.
14. Patel, Jayesh D., Frej Mighri, and Abdellah Ajji. "A facile route towards the preparation of ZnSe nanocrystals." *Materials Letters* 131 (2014): 366-369.
15. Shaikh, Asiya F., et al. "ZnSe/ZnO Nano-heterostructures for enhanced solar light hydrogen generation." *ChemistrySelect* 2.28 (2017): 9174-9180.
16. G. Duchateau, A. Yamada, K. Yabana, Electron dynamics in α-quartz induced by two-color 10-femtosecond laser pulses, Phys. Rev. B 105 (16) (2022), 165128.

CHAPTER 6:

Electrochemical Study

6. Electrochemical Study:

Three electrode cyclic voltammetry has been used in detail to explore the electrochemical characteristics of ZnSe/ZnO in energy storage devices.

- **Details of 3-electrode setup:**

All electrochemical measurements for the supercapacitor electrodes as constructed were performed using a three electrode cell. In the setup, Z350 (ZnSe), Z400 (ZnSe/ZnO nanocomposite), Z450 (ZnO) coated on Ni foam acted as working electrode. Platinum wire acted as the counter electrode and Ag/AgCl electrode was chosen to be as the reference electrode. The Ni foam was coated with samples, polyvinylidene fluoride (PVDF) and carbon black in the ratios of 40 mg, 5 mg, and 5 mg. The electrolyte was a 1M KOH solution. Every measurement was done at room temperature without the use of any outside gases. We conducted cyclic voltammetry (CV) at various scan rates ranging from 5 to 100 mV/s. Galvanostatic charge/discharge experiments were performed to assess the specific capacitance, power density, and energy density at different current densities, ranging from 0.1 to 1 A/g. While measuring CV, a potential window between 0 and 0.6 V was employed.

- **CV Performance of ZnSe, ZnSe/ZnO, ZnO coated Ni electrode:**

Three factors affect CV performance and electrochemical measurements of an electrode: the type of electrolyte, mass loading onto the electrode, and the area under the plotted CV curve. In this work, the nature of CV measurements has been studied using base electrolyte (KOH). From their plots for each sample electrode, the active area under the CV curve (total current) for each scan rate has been determined. Here specific capacitance has been calculated and the formula is given bellow.

Specific capacitance: $$\frac{\textbf{Area under CV curve } (\int I\, dv)}{\textbf{Scan rate} \times \textit{Potential window} \times \textbf{mass loaded}}$$

❖ Z350 electrode performance and different capacitance:

For Z350 electrode, the CV has been performed at different scan rates such as 5 mV/s, 10 mV/s, 20 mV/s, 30 mV/s, 40 mV/s, 50 mV/s, 60 mV/s, 70 mV/s, 80 mV/s, 90 mV/s and 100 mV/s. The mass loaded into the electrode is 3.2 g.

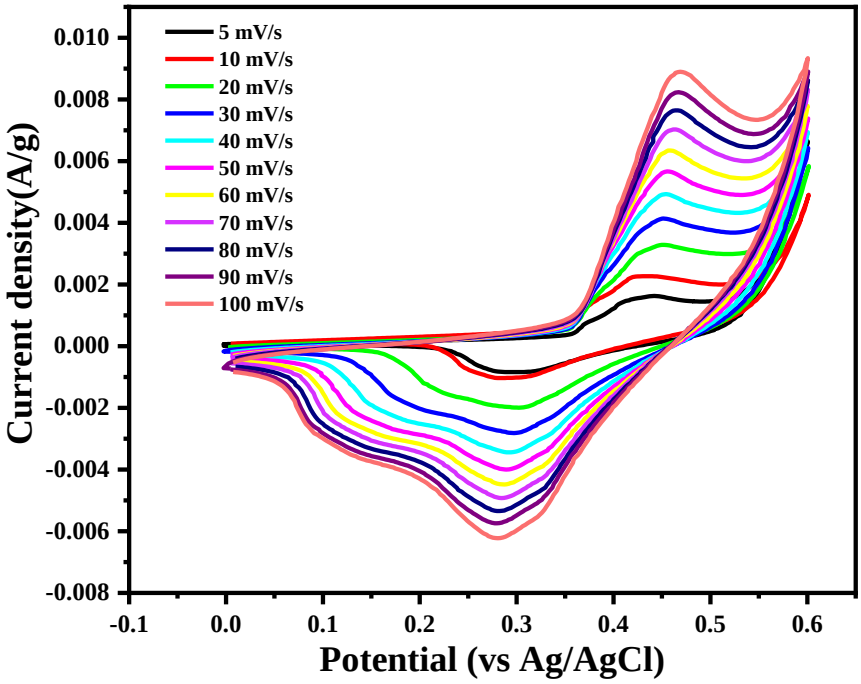


Fig 6.1. CV curve of Z350 at different scan rates.

Scan rate (mV/s)	5 mV/s	10 mV/s	20 mV/s	30 mV/s	40 mV/s	50 mV/s	60 mV/s	70 mV/s	80 mV/s	90 mV/s	100 mV/s
Specific Capacitance ($F\ g^{-1}$)	93.617	52.8	36.69	31.34	28.003	25.721	23.77	22.37	21.12	20.19	19.3

Table 6.1. Details of scan rates and specific capacitance value of Z350.

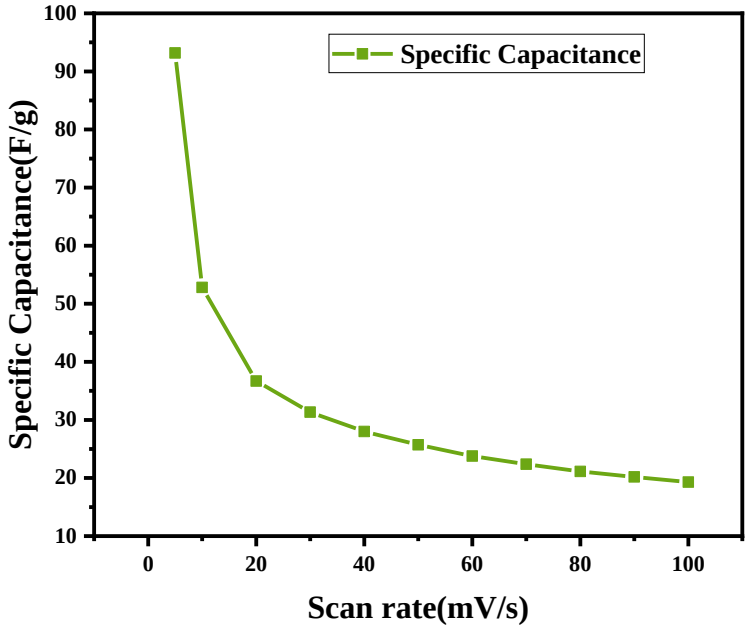


Fig 6.2. Specific Capacitance vs Scan rate plot of Z350.

❖ Z400 electrode performance and different capacitance:

For Z400 electrode, the CV has been performed at different scan rates such as 5 mV/s, 10 mV/s, 20 mV/s, 30 mV/s, 40 mV/s, 50 mV/s, 60 mV/s, 70 mV/s, 80 mV/s, 90 mV/s and 100 mV/s. The mass loaded into the electrode is 2.4 g.

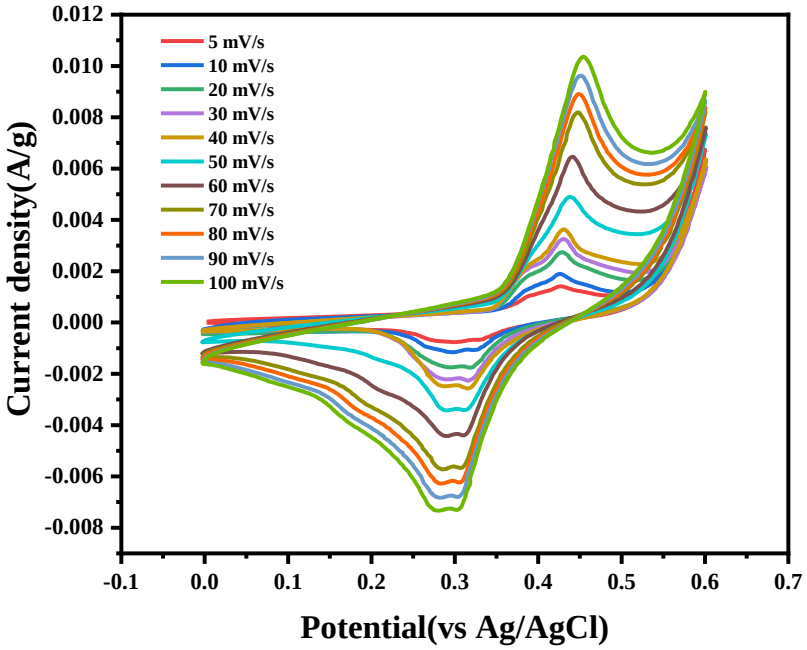


Fig 6.3. CV curve of Z400 at different scan rates.

Scan rate (mV/s)	5 mV/s	10 mV/s	20 mV/s	30 mV/s	40 mV/s	50 mV/s	60 mV/s	70 mV/s	80 mV/s	90 mV/s	100 mV/s
Specific Capacitance ($F\ g^{-1}$)	126.95	83.68	61.03	44.15	38.00	30.68	30.61	30.54	28.98	26.7	26.29

Table 6.2. Details of scan rates and specific capacitance value of Z400.

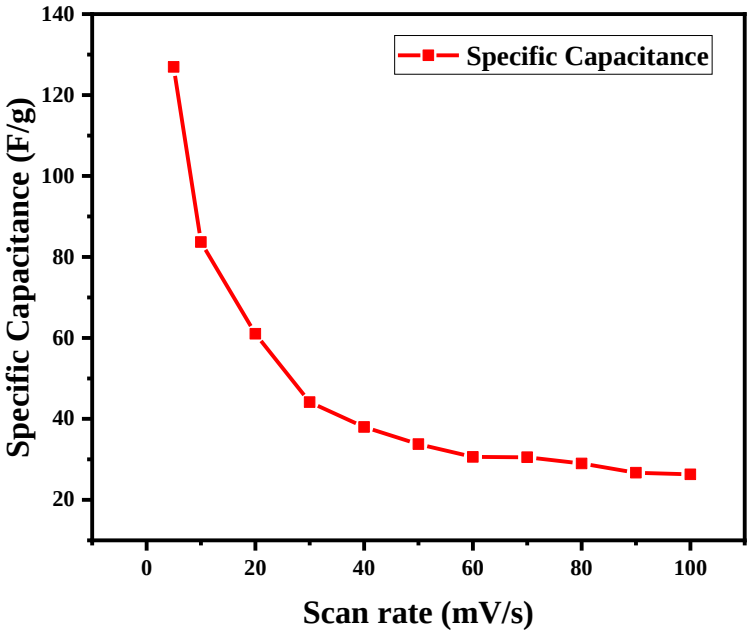


Fig 6.4. Specific Capacitance vs Scan rate plot of Z400.

❖ Z450 electrode performance and different capacitance:

For Z450 electrode, the CV has been performed at different scan rates such as 5 mV/s, 10 mV/s, 20 mV/s, 30 mV/s, 40 mV/s, 50 mV/s, 60 mV/s, 70 mV/s, 80 mV/s, 90 mV/s and 100 mV/s. The mass loaded into the electrode is 4.0 g.

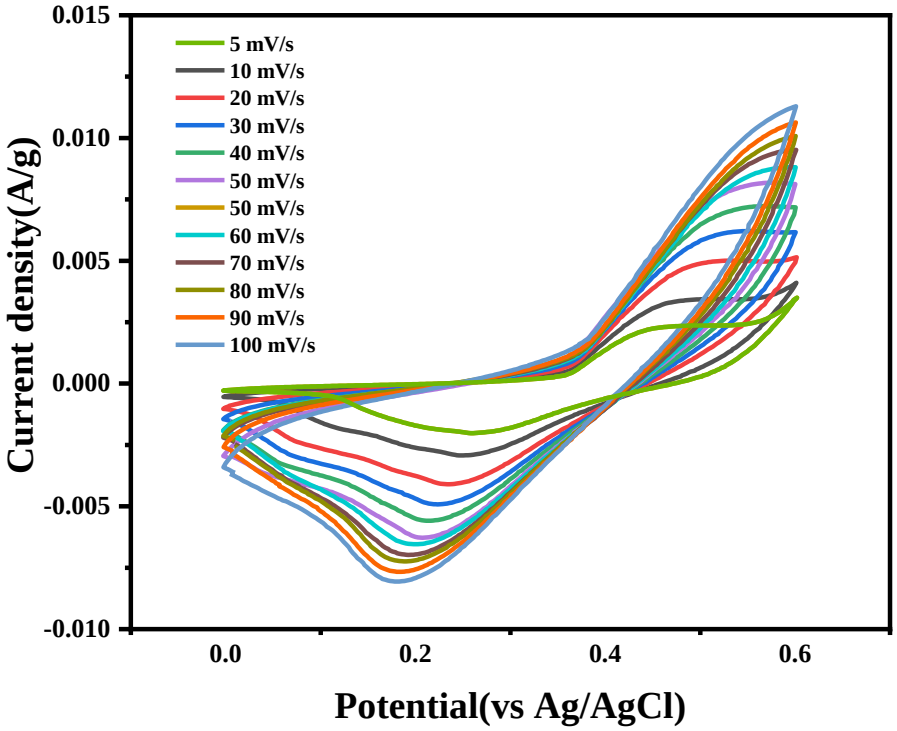


Fig 6.5. CV curve of Z450 at different scan rates.

Scan rate (mV/s)	5 mV/s	10 mV/s	20 mV/s	30 mV/s	40 mV/s	50 mV/s	60 mV/s	70 mV/s	80 mV/s	90 mV/s	100 mV/s
Specific Capacitance ($F\ g^{-1}$)	99.16	72.53	51.53	41.27	35.46	32.57	26.75	24.50	22.05	20.92	20.42

Table 6.3. Details of scan rates and specific capacitance value of Z450.

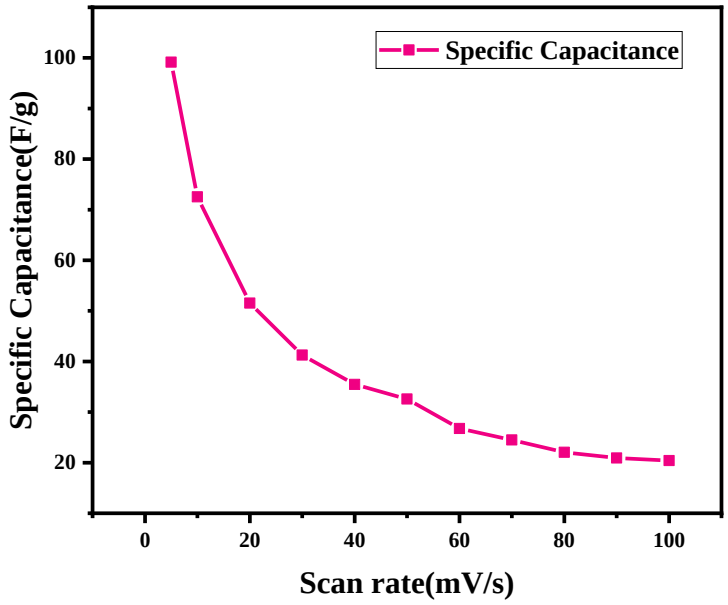


Fig 6.6. Specific Capacitance vs Scan rate plot of Z450.

In Z350 and Z400, there is an appearance of double-peaking, which is very prominent in Z400. The CV structure of Z450 is a little bit different; there is an appearance of a single peak.. Although the currents are observed to increase with scan rate, the voltammograms retain their characteristic "double-peaked" appearance. The latter can be explained by the fact that, first of all, there is very little current since the voltage is at a range that does not promote the reactant's forward reaction. The current rises as the voltage is swept up because the reaction quickens. Eventually, though, the reaction at the electrode surface depletes the reactant concentration. The rate-determining process then shifts, causing the current to be regulated by the reactant's diffusion to the surface and eventually falling off once more.

Because the diffusion layer is produced over a shorter distance by a faster scan, there is an increase in current density with scan rate. Since the concentration changes over a shorter distance from bulk to zero, the diffusive flux and current are both higher. In order to ensure that the measurement has not been tainted by physical factors other than diffusion, it is customary to verify experimental data by comparing the peak current to the square-root of the scan rate [3].

Strong faradaic electron transport was confirmed by a clearly visible redox peak in the CV profile [1].An increase in scan rate was found to be associated with an apparent increase in peak current and the area of the CV curve. As the active species diffusivity becomes stable, a higher scan rate will cause the slope to rise. The specific capacitance of the resultant

product is dependent on the scan rate; as the scan rate increases, the corresponding current density rises and the specific capacitance falls. Because more ions can interact with the electrode and electrolyte contact at this scan rate, a higher specific capacitance was achieved with a lower scan rate. For both anodic and cathodic peaks, the corresponding peaks are moved towards the positive and negative potential side as scan rate increases. There may be indications of some diffusional restrictions and it could be the result of the material's internal resistance [2].

❖ Charge-Discharge Characteristics:

To ensure that supercapacitors are operating at optimal efficiency, it is crucial to examine their charge-discharge characteristics. A super capacitor would ultimately be assessed based on how quickly it charges and how slowly it discharges. In addition, this curve can be used to experimentally determine the materials' power and energy densities. Here, charge-discharge tests were performed for several samples at varying current densities.

Energy density can be expressed as $E_s = 1/2\ C_s\ (V)^2$

Power density can be expressed as $Ps = E/t$

where t is the discharge duration in that potential window, v is the potential window, E_s is the energy density, P_s is the power density, and C_s is the specific capacitance from the charge-discharge plot.

Galvanostatic charging/discharging (GCD) was used to investigate the efficiency and discharge behavior of the electrode material. The resulting plotted curves, at current densities of 0.1–1.0 A g−1 and potentials ranging from 0.0 to 0.6 V, are shown in Fig. 6.6 - 6.8. All prepared electrodes of ZnSe, ZnO, and ZnSe/ZnO exhibit typical charging/discharging curves that demonstrate their non-linearity, long discharge times, and pseudocapacitive characteristics. This electrode-electrolyte interaction is influenced by the porous structure of activated carbon (AC), with the high specific area of carbon increasing the charge storage capacity. It has been observed that when current density rises, charging and discharging periods go shorter.

The specific capacitance of the nonlinear GCD pattern were calculated using the following relations:

$$C_{sp} = \frac{I\Delta t}{m \times \Delta v}$$

Where I is the constant current density, Δt is the area of discharge GCD pattern, m is the mass of the active material of a single electrode, Δv is the potential window. The Ohmic drop is the sudden voltage drop during the discharge cycle, arising from the contact resistance between the electrode and the electrolyte interface; this voltage drop increases with the increasing number of charging-discharging cycles.

❖ Charge-Discharge curve

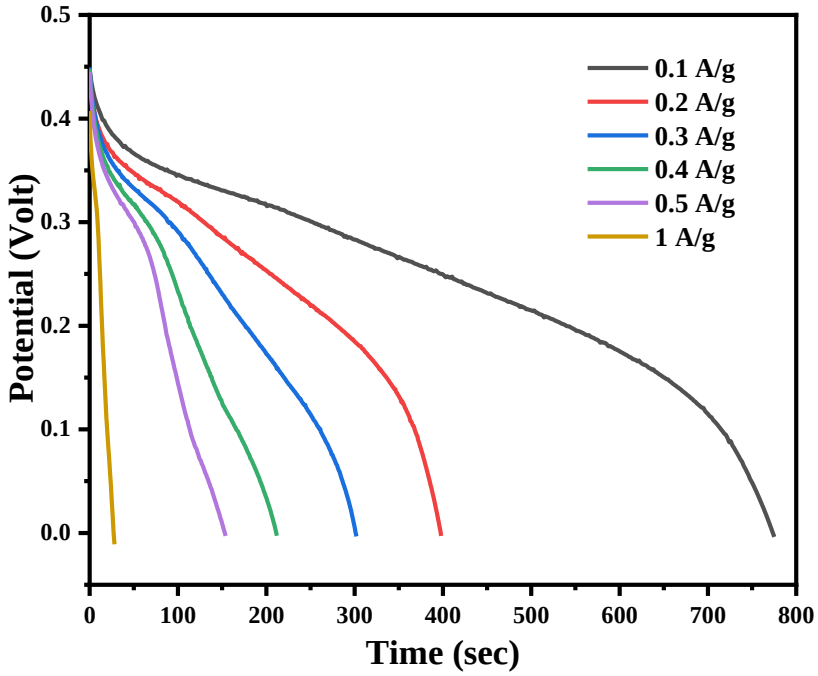


Fig 6.6. GCD curves for Z350.

Current density (A g^{-1})	0.1	0.2	0.3	0.4	0.5	1.0
Specific Capacitance (F g^{-1})	55.16	62	63.5	60.6	55.83	46.6

Table 6.5. Details of Current density and specific capacitance value of Z350.

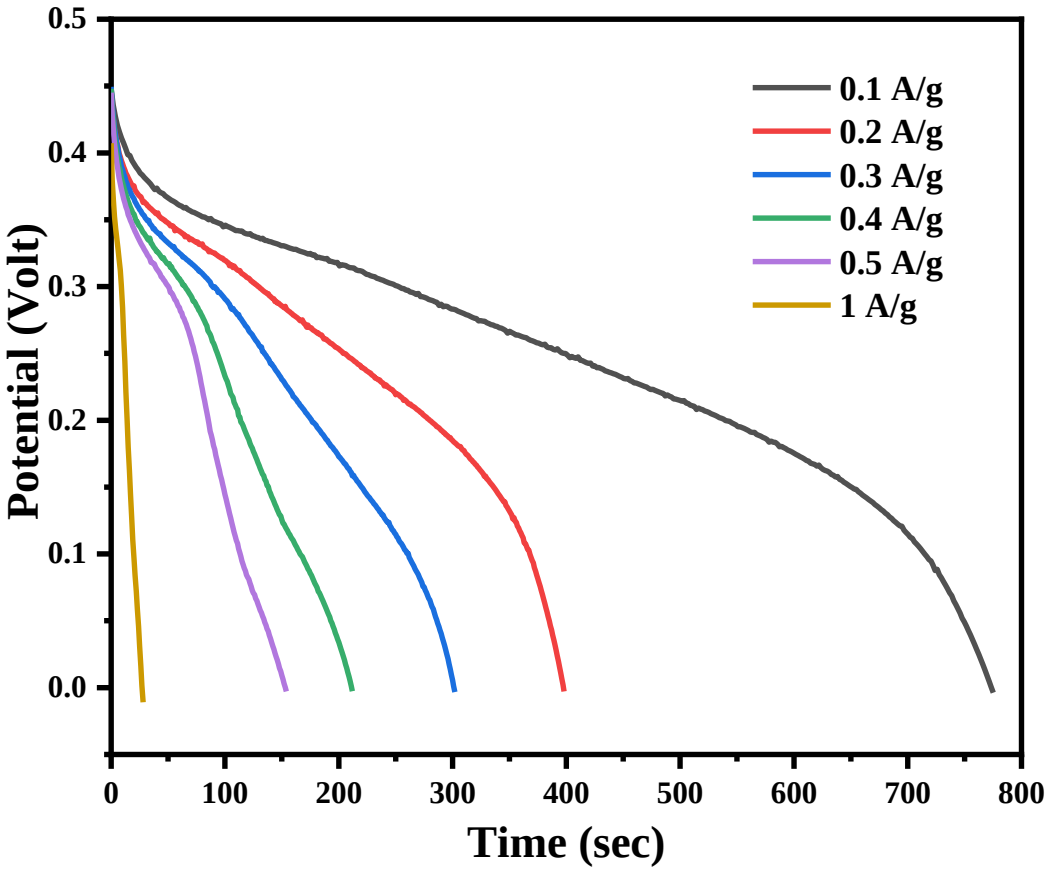


Fig 6.7. GCD curves for Z400.

Current density (A g^{-1})	0.1	0.2	0.3	0.4	0.5	1.0
Specific Capacitance (F g^{-1})	131.6	136	155	148	140.83	51.66

Table 6.4. Details of Current density and specific capacitance value of Z400.

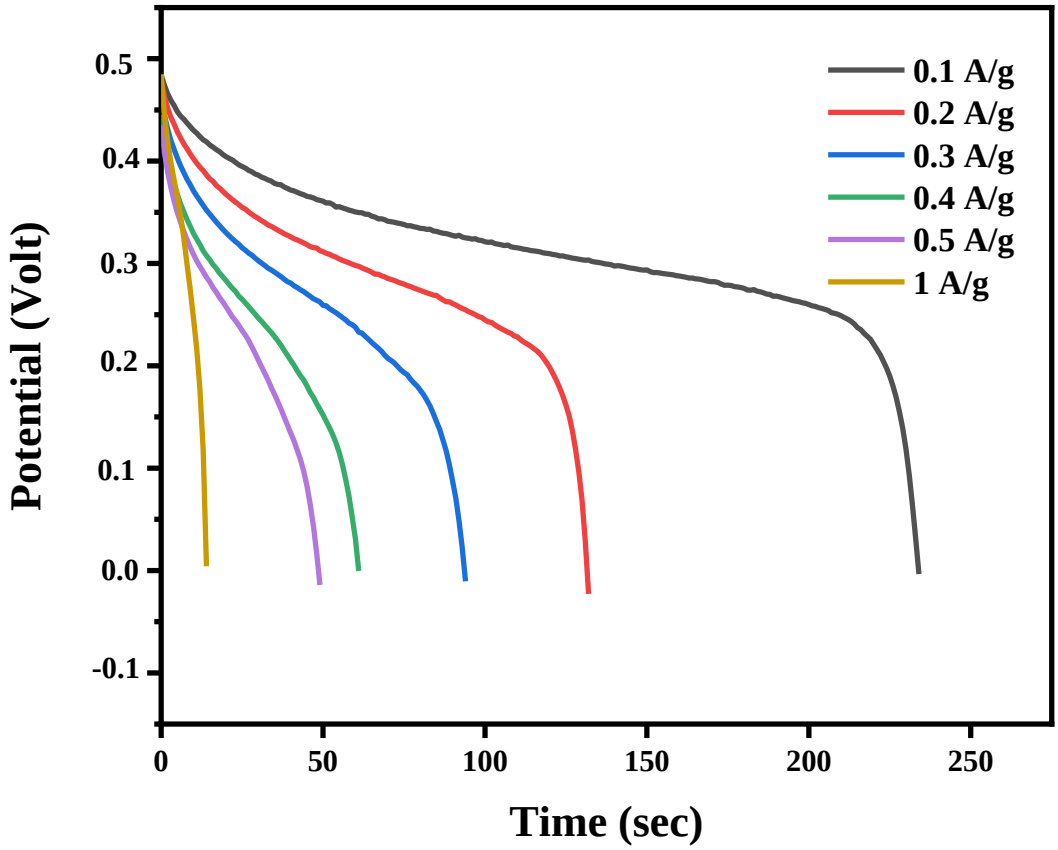


Fig 6.8. GCD curves for Z450.

Current density (A g^{-1})	**0.1**	**0.2**	**0.3**	**0.4**	**0.5**	**1.0**
Specific Capacitance (F g^{-1})	**39.5**	**44**	**48**	**42**	**40**	**23.3**

Table 6.6. Details of Current density and specific capacitance value of Z450.

The measurement of Coulombic Efficiency was done for over 3000 cycles at a current density of 1.5 A/g in a voltage range of 0-2 V.

There are various possible reasons for this initial capacitance decline. First, it can be the consequence of small-pore blockage in the activated carbon (AC) electrode during the initial charge and discharge operations of ion insertion and dis insertion. Second, pore regions and ion diffusion channels may be blocked as a result of the potential irreversible reactions of ions and redox elements absorbed on the surface of the AC electrode, which could consume charge.

Thirdly, deterioration of the electrodes and electrolyte breakdown may result in an increase in interfacial resistance. Finally, the absorption of different byproducts during the early galvanostatic charge-discharge (GCD) cycles may cause the effective pore area to decrease. The specific capacitance stabilized after a few cycles, showing reversible charge-discharge behavior, despite these initial difficulties. It's interesting to note that every cell seemed to fade almost exactly at first. Using the formula Coulombic efficiency (%) = (t_{charge} / $t_{discharge}$) × 100%, the cells' Coulombic efficiency was determined. Within the potential range of GCD experiments, t_{charge} and $t_{discharge}$ correspond to the charging and discharging times, respectively. The cyclic stability of an ASC device is critical to its practical application. At a current density of 1.5 A g^{-1}, the ASC device's cycle dependability was further confirmed over 3000 cycles.

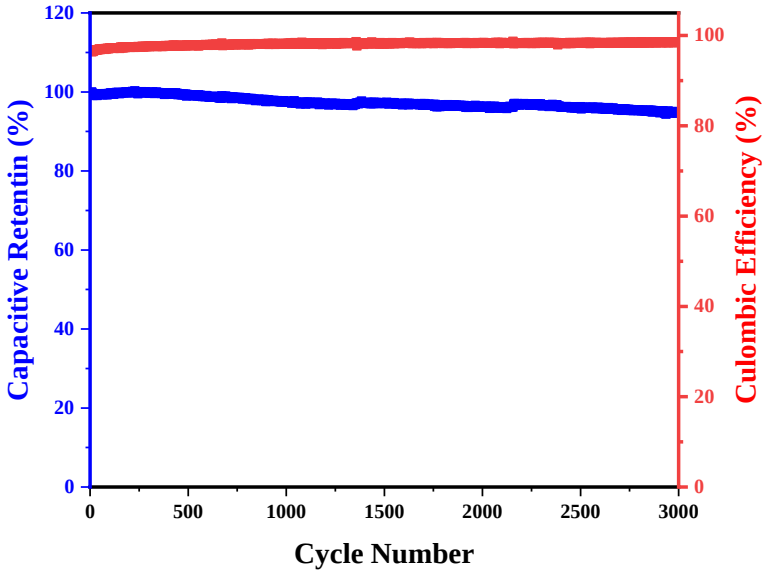


Fig 6.9. retention capacity and coulombic efficiency vs. cycle number; inset shows a Nyquist plot of the Z400 electrode after 3000 cycles.

The produced supercapacitors show a good stability factor in terms of Coulombic Efficiency. Consequently, it was seen that the sample could maintain 95.5% of its capacitance even after 3000 cycles, which was a good accomplishment for the system as built. Following the lengthy operation cycle, the sample's Coulombic efficiency similarly stayed nearly constant, indicating that it is a viable option for related applications.

➢ Electrochemical Impedance Spectroscopy (EIS):

Moreover, an investigation into the part that ionic conductivity plays in the electrochemical properties of the electrodes was conducted using Electrochemical Impedance Spectroscopy (EIS). The investigation utilizing Electrochemical Impedance Spectroscopy (EIS) was carried out in a frequency range of 10 MHz to 1 MHz, providing valuable information about the bulk and interfacial properties of the supercapacitors. In a Nyquist plot, the imaginary component of impedance (Z″) is plotted against the real component of impedance (Z′) of Z350, Z400 and Z450. The significant increase in impedance at low frequencies is ascribed to ion diffusion across the electrode, but this resistance is mostly formed at the interface between the electrolyte and electrode surface. The ASC device's EIS curves show almost comparable behaviour in the low-frequency region before and after a 3000-cycle operation, showing the same Warburg impedance in both scenarios.

These plots show the equivalent series resistance (RESR) in the high frequency range, which is made up of the inherent resistance of the electrode material, the contact resistance between the active material and the current collector, and the electrolyte resistance.

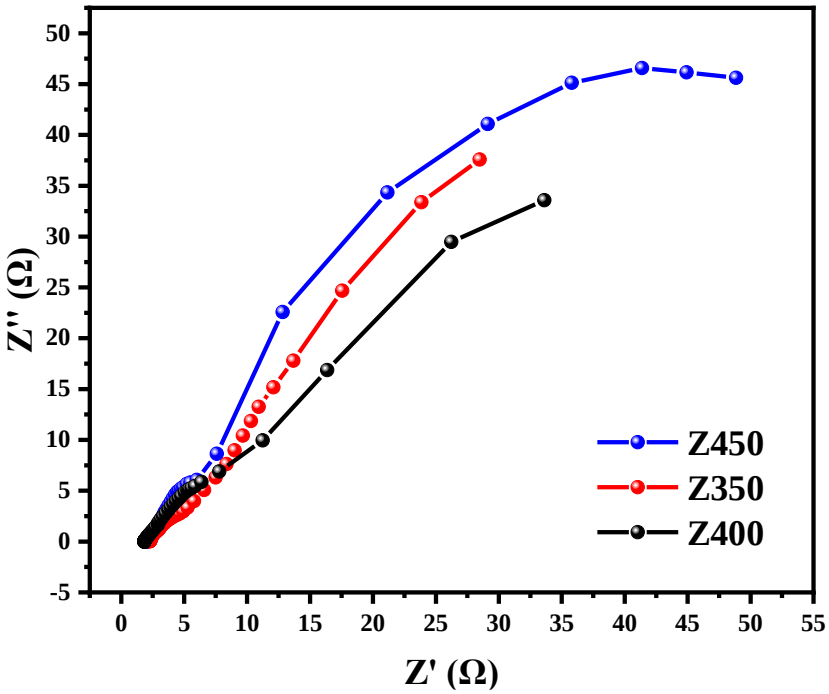


Fig 6.10. Nyquist plots of Z450, Z350 and Z400.

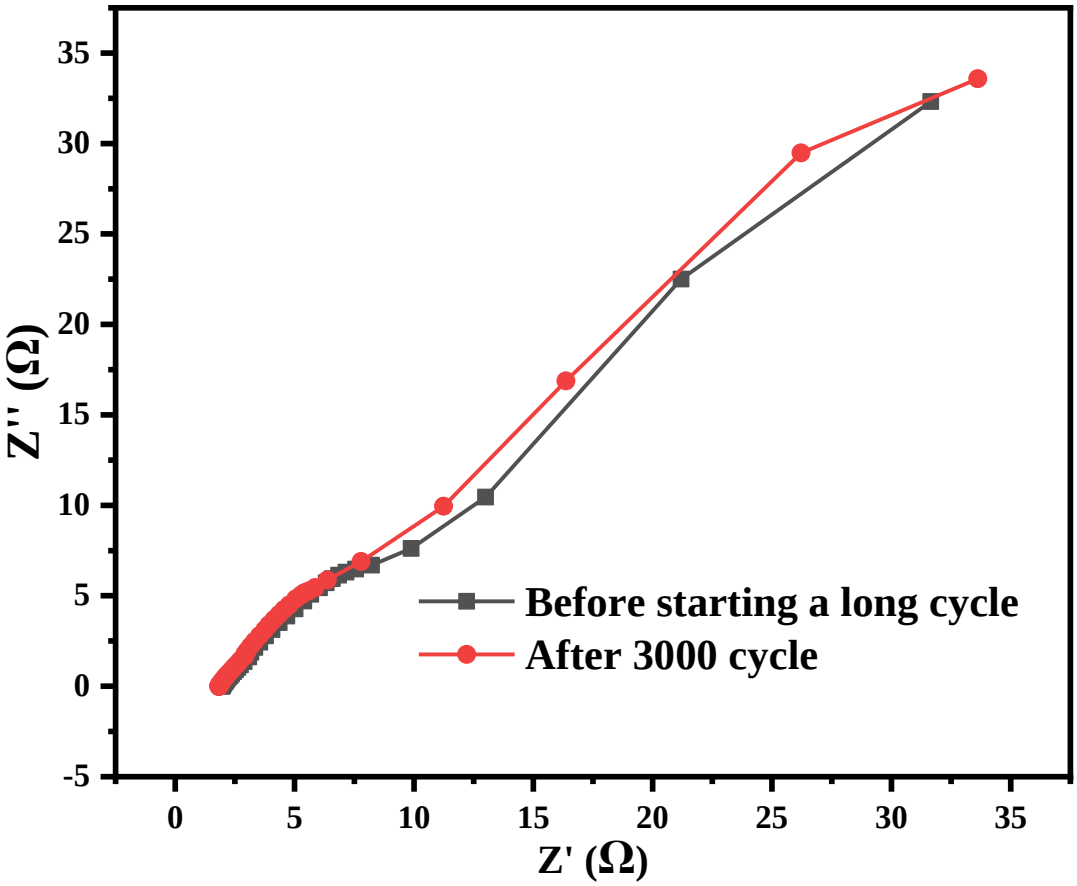


Fig 6.11. Nyquist plots before and after 3000 cycles.

References:

1. Samuel E, Joshi B, Kim Y, Aldalbahi A, Rahaman M, Yoon SS (2020) ACS Sustain Chem Eng 8:3697–3708. https:// doi. org/ 10.1021/ acssu schem eng. 9b067 96
2. Sangeetha Vidhya, M., et al. "Recent progression of flower like ZnSe@ MoSe2 designed as an electrocatalyst for enhanced supercapacitor performance." *Topics in Catalysis* 65.5 (2022): 684-693.
3. Dickinson, E. "Modeling Electroanalysis: Cyclic Voltammetry." (2013).
4. Das, Pulok, et al. "Morphology tuned electrochemical properties of CuBO2 nanostructures." *Materials Chemistry and Physics* 301 (2023): 127642.
5. Ivanishchev, A. V.;Gridina,N. A.;Rybakov,K.S.;Ivanishcheva,I. A.; Dixit, A. Structural and electrochemical investigation of lithium ions insertion processes in polyanionic compounds of lithium and transition metals. J. Electroanal. Chem. 2020, 860, 113894. (64) Park, J.; Kim, B.; Yoo, Y.-E.; Chung, H.; Kim
6. Zhang, J.; Jiang, J.; Li, H.; Zhao, X. A high-performance asymmetric supercapacitor fabricated with graphene-based electrodes. Energy Environ. Sci. 2011, 4 (10), 4009−4015.
7. Ghamouss, F.; Brugere, A.; Jacquemin, J. Physicochemical Investigation of Adiponitrile-Based Electrolytes for Electrical Double Layer Capacitor. J. Phys. Chem. C 2014, 118 (26), 14107−14123.
8. Fan, L.-Q.; Zhong, J.; Wu, J.-H.; Lin, J.-M.; Huang, Y.-F. Improving the energy density of quasi-solid-state electric double-layer capacitors by introducing redox additives into gel polymer electrolytes. J. Mater. Chem. A 2014, 2 (24), 9011−9014.
9. Yadav, N.; Singh, M. K.; Yadav, N.; Hashmi, S. A. High performance quasi-solid-state supercapacitors with peanut-shell derived porous carbon. J. Power Sources 2018, 402, 133−146.
10. Ivanishchev, A. V.; Lee,S.-H.; Kim,J.-J.; Ivanishcheva, I. A.; Nam, S.-C.; Song, J.-H. Li-ion diffusion characteristics of surface modified Ni rich NCM cathode material. J. Electroanal. Chem. 2023, 932, 117242.
11. Sardar, K., et al. "Synthesis of different manganese tungstate nanostructures for enhanced charge-storage applications: theoretical support for experimental findings." *Physical Chemistry Chemical Physics* 24.46 (2022): 28271-28282.

Chapter 7:

Application of ZnSe/ZnO Nanocomposite in Photo-Catalysis

5.3.4 UV-VIS spectroscopy:

Figure 4 shows the UV-Vis absorption spectra of ZnO and ZnO/ZnSe nano-heterostructures that were produced and had varying ratios of ZnSe to ZnO. Solid sample attachment was used to quantify this UV-visible absorbance. The conventional formula, $E= hc/\lambda$, was used to do the band gap calculations. The optical absorption characteristics of the ZnO and ZnSe/ZnO nano-heterostructures differ significantly from one another. Strong and wide absorptions in the UV were seen in the ZnO, with the band edge appearing at 390 nm. Nonetheless, the ZnSe/ZnO nano-heterostructures as produced exhibited absorption peaks in both the visible and ultraviolet regions. As the amount of ZnSe in the generated ZnSe/ZnO nano-heterostructures increases, the absorbance in the visible range increases. When the initial weight ratio of ZnSe is increased, the visible light absorption capability of ZnSe/ZnO nanocomposites is much better than that of pure ZnO nanostructure. The two band edges, 390 and 472 nm, attributable to ZnO and ZnSe semiconductors, are visible in the produced ZnSe/ZnO nano-heterostructures. The band gap values that correlate are 2.67 and 3.18 eV. ZnSe's enhanced absorption of visible light contributes to increased charged carrier generation [15].

- **Photocatalytic Test:**

There was a 50 ml quartz beakar stolen. Quartz beaker is a clear choice for UV photocatalysis because glass absorbs UV light. To create a solution with a concentration of 10^{-5} M, 40 ml of water and the required amount of MB solution were added to the beaker. 30 mg of the sample was added to the mixture and swirled for one hour in the dark using a magnetic bead after ten minutes of stirring. The beaker was then placed beneath a 40W UV lamp, which emitted light at a maximum wavelength of 256.4 nm. We keep stirring. Five milliliters of the solution were sampled at predetermined intervals, and filter paper was used to remove the catalyst. Next, UV-Visspectroscopy was used to test the declining MB solution and demonstrate its degradation.

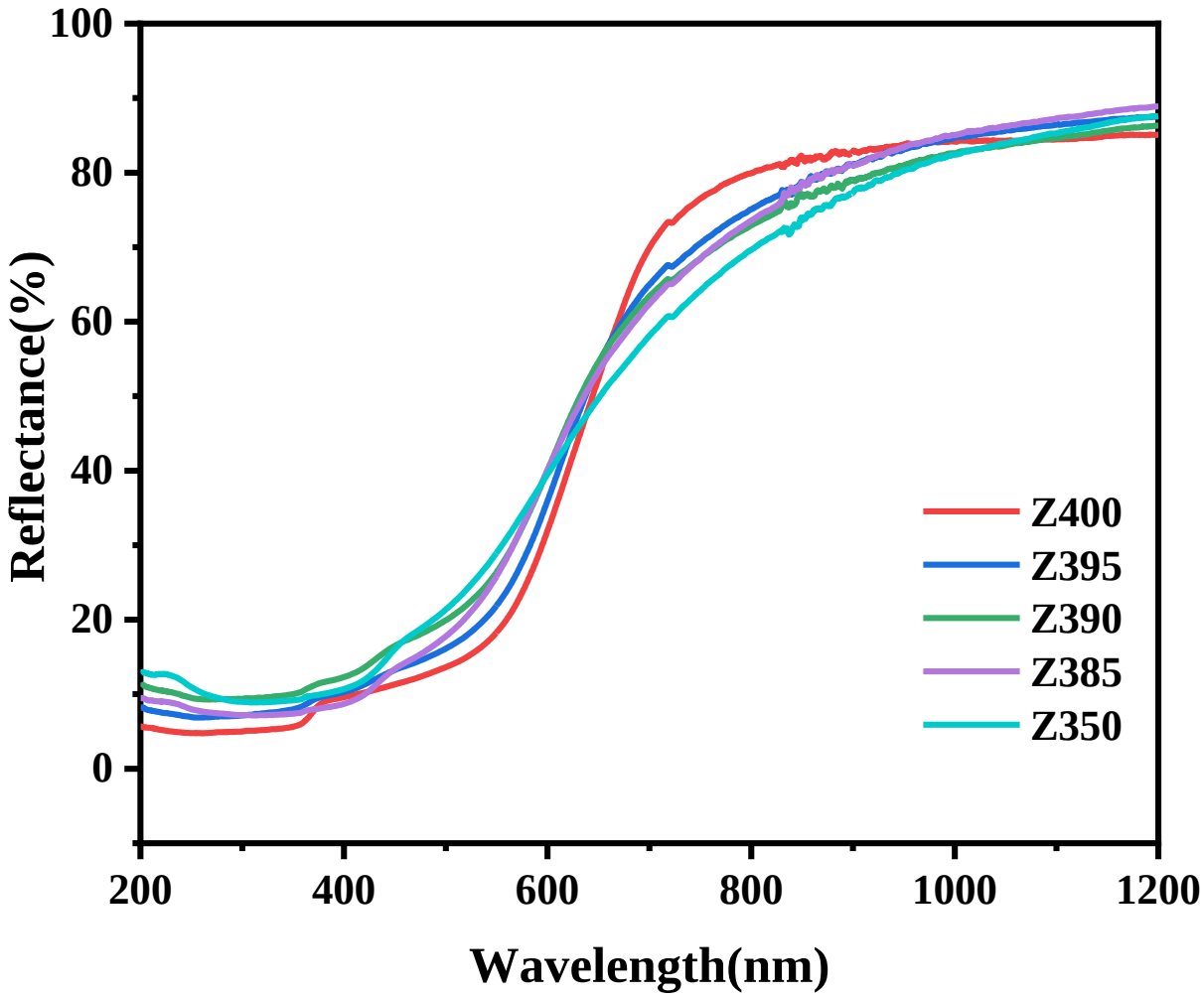


Figure 7.1 Reflectance spectra of Z450, Z425, Z400, Z375, Z350.

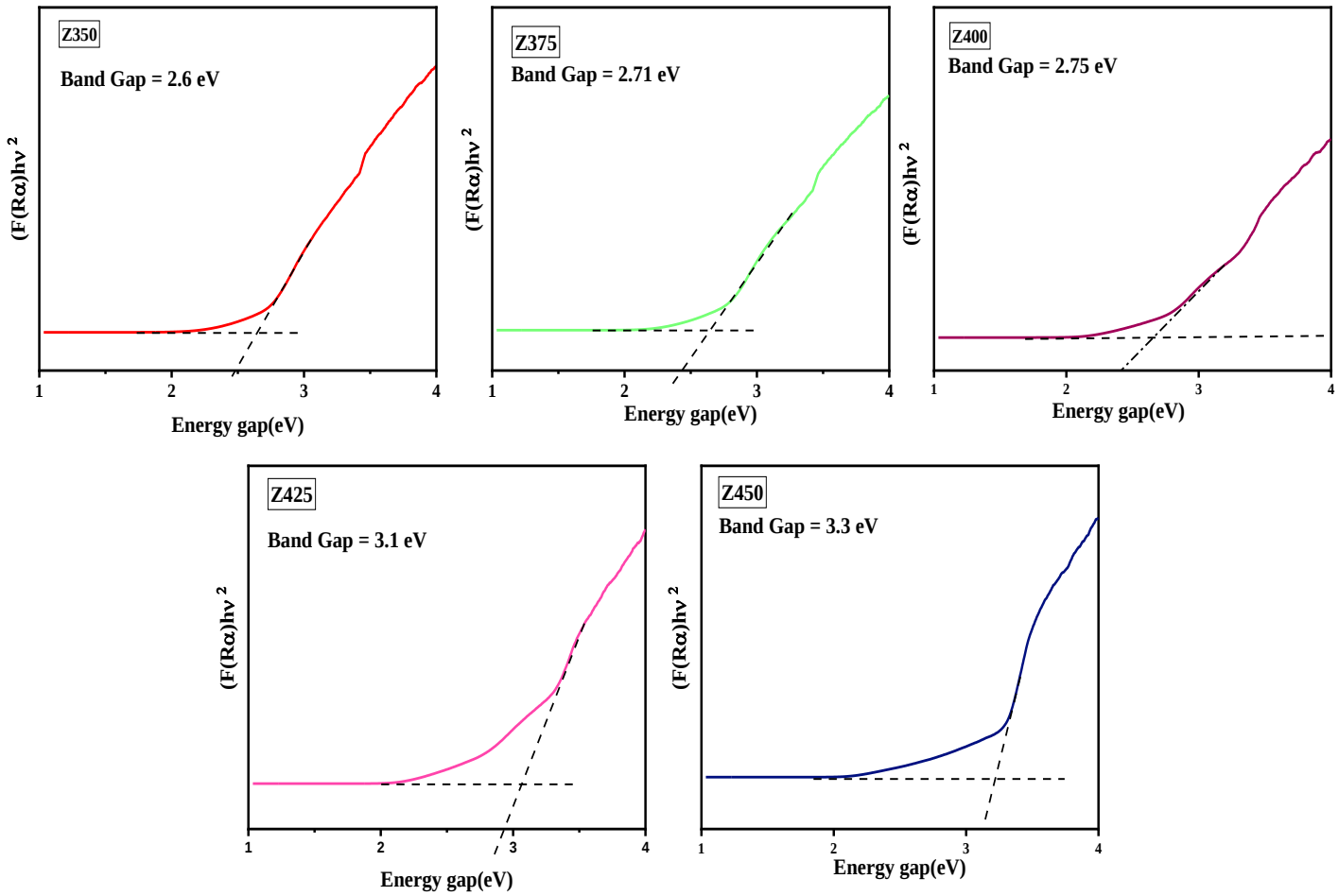


Figure 7.2 Bandgap Calculation of Z450, Z4255, Z400, Z375, Z350.

The Kubelka-Munk formula is used to calculate f(R), where R is the solid solution reflectance. Plotting of $(f(R)\ h\upsilon)^2$ vs $h\upsilon$ follows. The band gap value is obtained by extrapolating the curve's linear zone to the $h\upsilon$ axis and finding the axis' intercept. It is noted that the bandgap energy map only shows one slop, indicating that only a direct permitted transition is possible. Based on the measured bandgap value, ZnO's bandgap was calculated using an absorbance graph that showed an absorption of 3.3 eV, as shown in Fig. 4(a). The absorption was more pronounced in the UV spectrum. Excellent absorption in the broadband spectrum can be attributed to the absorption of ZnO in the UV and ZnSe in the visible range. At 380 nm, a notable excitation peak for ZnSe was seen at high energy, which was obviously different from the spectra of ZnSe nanoflakes that had previously been published. Its bandgap is 2.6 eV, as indicated by the plot of photon energy ($h\upsilon$) on the x axis and $(\alpha h\upsilon)^2$ on the y axis. While ZnSe is capable of absorbing photons, its absorption coefficient is not as high as it is in the long-wavelength band. This is because there are fewer accessible states in the conduction band as photon energy increases, which reduces the likelihood of electron excitation [16]

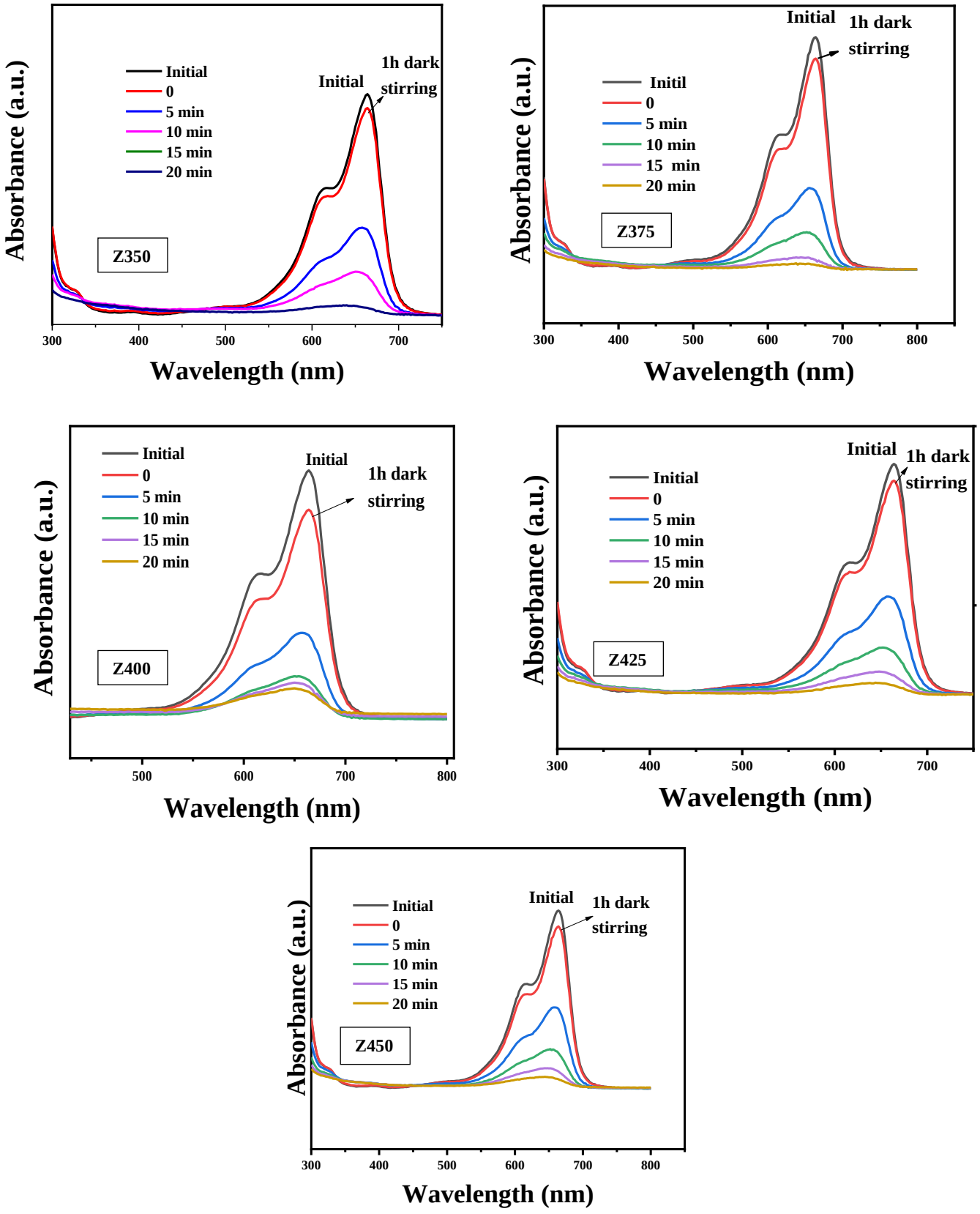


Fig. 7.3 UV–Vis absorption spectra of MB after different time intervals in the Presence of Z350, Z375, Z400, Z425, Z450.

➢ UV light driven Photocatalysis:

As the UV range is between 200 nm to 400 nm, samples were taken for photocatalysis under UV light when x=1, 0.8, 0.6. It's clear from the characteristic absorbance spectra of MB that under UV irradiation the absorption peak gradually decreases in presence of photocatalyst (x=1, 0.8, 0.6) and it disappears almost completely after 20 min for ZnSe, ZnSe/ZnO and ZnO.

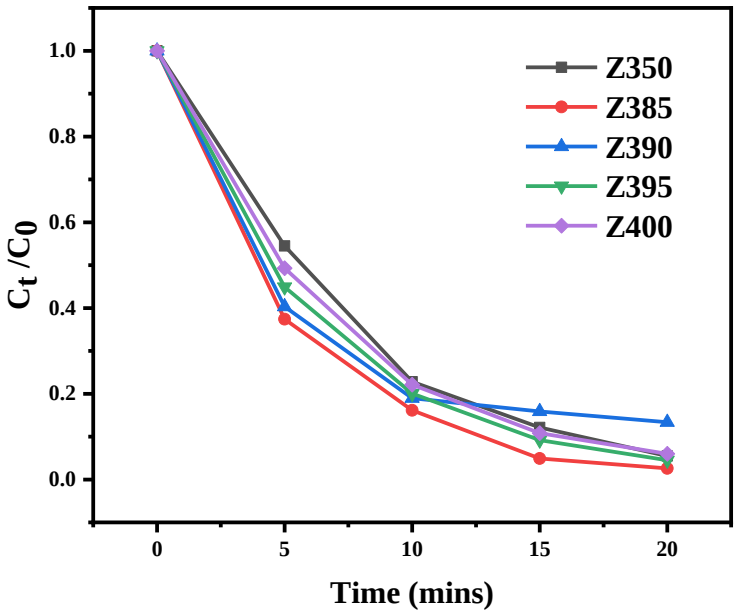


Fig. 7.4 Comparison of degradation of MB dye in presence of different catalysts.

Ct/C0 vs time (min) is plotted in Figure 5.7 which denotes that in 20 min almost 99.95 % of MB dye is degraded in presence of ZnSe whereas for other two samples it takes more time. Excitation of the semiconductor ZnSe by UV or visible light results in the creation of valence-band holes and conduction-band electrons. Generally speaking, surface active sites and imperfections on semiconductors can be blamed for the photocatalytic activity. Large ZnSe nanoflakes' surface area, which is the second structure of the as-synthesised ZnSe microspheres, has been shown to enhance photocatalytic reaction sites and improve electron-hole separation efficiency.

References:

1. Vadivel, S., et al. "Graphene oxide–BiOBr composite material as highly efficient photocatalyst for degradation of methylene blue and Rhodamine-B dyes." *Journal of Water Process Engineering* 1 (2014): 17-26.

2. Hu, Limin, et al. "Facile synthesis of BiOF/Bi 2 O 3/reduced graphene oxide photocatalyst with highly efficient and stable natural sunlight photocatalytic performance." *Journal of Alloys and Compounds* 633 (2015): 256-264.

3. Xia, Jiexiang, et al. "Solvothermal synthesis and enhanced visible-light photocatalytic decontamination of bisphenol A (BPA) by gC 3 N 4/BiOBr heterojunctions." *Materials Science in Semiconductor Processing* 24 (2014): 96-103.

4. Mukhlish, MZ Bin, et al. "Photocatalytic degradation of different dyes using TiO2 with high surface area: a kinetic study." *Journal of Scientific Research* 5.2 (2013):301-314.

5. Rahman, Mohammed Mastabur, et al. "A Comparative study on the photocatalytic degradation of industrial dyes using modified commercial and synthesized TiO2 photocatalysts." *Journal of Chemical Engineering* 27.2 (2014): 65-71.

6. Mittal, Manish, Manoj Sharma, and O. P. Pandey. "Fast and quick degradation properties of doped and capped ZnO nanoparticles under UV–Visible light radiations." *Solar Energy* 125 (2016): 51-64.

7. Shukla, Sheifali, et al. "Surfactant functionalized tungsten oxide nanoparticles with enhanced photocatalytic activity." *Chemical Engineering Journal* 288 (2016): 423-431.

8. Wang, Lu, et al. "Enhanced photocatalytic hydrogen evolution under visible light over Cd 1− x ZnxS solid solution with cubic zinc blend phase." *International Journal of Hydrogen Energy* 35.1 (2010): 19-25.

9. Garaje, Sunil N., et al. "Template-Free Synthesis of Nanostructured Cd x Zn1–x S with Tunable Band Structure for H2 Production and Organic Dye Degradation Using Solar Light." *Environmental science & technology* 47.12 (2013): 6664-6672.

10. Yao, Wei-Tang, et al. "Flexible Wurtzite-Type ZnS Nanobelts with Quantum-Size Effects: a Diethylenetriamine-Assisted Solvothermal Approach."*small* 1.3 (2005): 320-325.

CHAPTER 8:

Conclusion & Future Scope

8.1. Conclusion:

The insufficiency of energies is a major disadvantage for growing of proficient supercapacitor and this is more necessary to pull a strong attention to use the materials as innovative materials.Selenium possesses an electronegativity lower than that of oxides and sulfur.This makes the chemical bond between the atom and the binding electrons weaker resulting in higher electrochemical activity that metal oxides or hydroxides. ZnSe and ZnO were created by solvothermal synthesis of $ZnSe(en)_{0.5}$ nanoflakes in air, which was accomplished by heating the nanosheets to a specific temperature. ZnSe and ZnO shared the same hexagonal wurtzite structure, and the $ZnSe(en)_{0.5}$ composite maintained its size and form throughout the conversion process. The SEM verified the XRD patterns' findings that the heterostructures were made of wurtzite ZnO and ZnSe. ZnSe was the strongest photocatalyst, followed by ZnO, and $ZnSe(en)_{0.5}$ was the weakest, according to a study of the photocatlytic characteristics of all the samples. It was deduced that the photocatalytic activity was influenced by the electron–hole separation rate and the density of the defects, and the photocatalysis mechanism of the ZnO/ZnSe heterostructures was systematically illuminated. Type II heterostructures are created in order to increase the carrier lifetime and improve photodetection. Under varying light intensities, it exhibits outstanding photoresponsivity and detectivity. The remarkable photocatalytic activities of ZnO/ZnSe heterostructures determined their promising potentials in relevant photoconversion applications. The prepared ZnSe/ZnO nanoparticles with uniform size verifies their enormous potential application as a prominent candidate for high-performance energy storage device.

8.2. Future Scope:

At the forefront of science and technology research today is the creation of high-potential energy storage (ES) devices using cutting-edge technologies. Supercapacitors (SCs), also known as electrochemical capacitors, have demonstrated extended durability and faster charge storage capabilities, making them promising prospects in the energy sector. For practical purposes, however, SCs are not a practicable alternative to batteries and fuel cells. Numerous materials, each with unique benefits and drawbacks, have been researched for use as SCs electrodes. Novel materials that show promise for increasing the capacitance of SCs include metal oxides, selenides, carbides, and sulfides that have surfaced in recent years. Due

to presence of large pores and it's moderate band gap, it shows a very good capacitive nature compared to the other two dimensional materials. It's composite with other materials possibly show good charge/discharge property where capacitance can vary from 100 F to 1000 F within a voltage range of 2-5 Volts.

As our composite material shows photo-catalytic nature, it can also be used as photodetector to detect wide range of spectral light. Finally we can say the heterostructure of ZnSe/ZnO shows different chemical properties in different aspect of modern day technology and it could be a promising candidate of material in near future of advancement.